Effects of ionizing radiation on organotypic slice cultures

Dissertation

zur Erlangung des Doktorgrades
der Naturwissenschaften

vorgelegt beim Fachbereich Physik
der Johann Wolfgang Goethe-Universität
in Frankfurt am Main

von
Dipl.-Phys. Mareike Hildegard Müller
aus Seeheim-Jugenheim

Frankfurt am Main 2013
(D30)

Vom Fachbereich Physik der Johann Wolfgang Goethe-Universität Frankfurt am Main als Dissertation angenommen.

Dekan:	Prof. Dr. Joachim Stroth
Gutachter:	Prof. Dr. Dr. h. c. Horst Stöcker
	Prof. PhD Marco Durante

Datum der Disputation: 24.06.2013

Für Robert und Sebastian

Believe that the sun will shine tomorrow

(Bon Jovi)

Zusammenfassung

Krebs ist nach Herz-Kreislauf-Erkrankungen die zweithäufigste Todesursache in Deutschland. Zu den Krebsarten mit den schlechtesten Prognosen gehören Leber- und Pankreaskrebs, trotz stetiger Weiterentwicklung der Therapiemöglichkeiten. Die Behandlung von Krebserkrankungen erfolgt durch Operation, Chemotherapie und/oder Strahlentherapie bzw. aus einer Kombination dieser drei Therapieformen. In den meisten Fällen wird die Strahlentherapie konventionell, d.h. mit Röntgenstrahlen durchgeführt. In den letzten 20 Jahren hat jedoch die Bestrahlung mit Schwerionen, speziell ^{12}C, größere Aufmerksamkeit und Erfolge in der Tumortherapie erlangt. 2009 wurde die an der GSI entwickelte Kohlenstofftherapie mit ihrer auf der Welt einmaligen aktiven Strahlführung am HIT (Heidelberger Ionenstrahl-Therapiezentrum) in Heidelberg in die klinische Routine eingeführt.

Röntgenstrahlen sind energiereiche Photonen. Sie wechselwirken mit Materie im therapierelevanten Energiebereich (bis zu einigen MeV) über Photoeffekt, Compton-Effekt und Paarbildung. Dieses Wechselwirkungsverhalten resultiert in einem exponentiellen Abfall der Dosis im Gewebe. ^{12}C-Ionen hingegen sind massebehaftete Atomkerne, die hauptsächlich über inelastische Stöße mit dem Targetmaterial wechselwirken. Bei hohen Energien kommt es zu wenigen Stößen, bei denen jedoch verhältnismäßig viel Energie übertragen wird. Dies führt dazu, dass das ^{12}C-Ion nach jedem Stoß etwas langsamer weiterfliegt und somit in immer kürzeren Abständen mit den Atomen des Targetmaterials zusammenstößt. Den größten Teil ihrer Energie geben Ionen auf relativ kurzer Strecke am Ende ihrer Bahn ab, im sogenannten Bragg-peak. Da dieses Tiefendosisprofil im Gegensatz zu dem exponentiell abfallenden Dosisprofil der konventionellen Röntgenstrahlen steht, nennt man es auch inverses Tiefendosisprofil. Ionen eignen sich aufgrund dieses inversen Tiefendosisprofils besonders zur Bestrahlung von tiefliegenden Tumoren. Das umliegende Gewebe wird durch die geringere Dosis im Eingangskanal geschont, hierdurch kommt es zu geringeren Nebenwirkungen.

Treffen Ionen (außer Protonen) auf das Targetmaterial, geben sie neben mehreren inelastischen Stößen ihre Energie durch Fragmentierung ab. Dabei fragmentieren nicht nur die Ionen, sondern auch die Kerne des Targetmaterials. Je weiter die zurückgelegte Strecke im Material, desto niedriger ist der Anteil der ursprünglichen Ionen und desto höher ist der Anteil der Fragmente. Diese haben ein eigenes, energieabhängiges

Tiefendosisprofil, welches das der ursprünglichen Ionen überlagert. Da leichtere Ionen eine höhere Reichweite haben, verursachen diese Fragmente einen charakteristischen Schwanz geringer Dosis hinter dem Bragg-peak der ursprünglichen Ionen.
Für die Patientenbestrahlung müssen genaue Daten belegen, wieviele Teilchen und Fragmente im Target ankommen und wie hoch die Dosis an einer gegebenen Stelle im Target ist. Direkt gemessen werden kann dies nur exemplarisch an einem Phantom-Versuchsaufbau. Dieser besteht aus einem Wassertarget variabler Tiefe, hinter dem Ionisationskammern die Energie der ankommenden Teilchen messen. Zur Erstellung beispielsweise eines Therapiebestrahlungsplans kann dann auf die gemessenen Daten zurückgegriffen werden und die applizierte Dosis (sowohl im Tumorvolumen als auch im umliegenden Gewebe) berechnet werden. Dafür werden spezielle Simulationsprogramme verwendet.
Bei den diesen Programmen zugrundeliegenden Berechnungsmethoden haben sich zwei unterschiedliche Vorgehensweisen etabliert: die deterministischen und die Monte-Carlo (MC)-Berechnungen. Deterministische Programme basieren auf Messwerttabellen, aus denen Gleichungen zur Energieabgabe hergeleitet werden. Mit diesen Gleichungen kann die applizierte Dosis im Patienten berechnet werden. MC-Simulationsprogramme wiederum basieren auf gemessenen Wirkungsquerschnitten, welche die Wechselwirkungswahrscheinlichkeit eines jeden Ions mit dem umgebenden Targetmatieral angibt. Neben der deponierten Energie können sie auch die produzierten Fragmente sowie weitere physikalischen Prozesse (z.B. Positronen-Emission) realistisch berechnen.
Bevor Ionen jedoch in der Patiententherapie angewendet werden, müssen ihre aus den physikalischen Eigenschaften abgeleiteten vermeintlichen Vorteile in biologischem Material überprüft werden. In der medizinisch angewendeten Strahlenforschung gibt es vorwiegend zwei biologische Testsysteme: Zelllinien oder primäre Zellkulturen (sog. *in vitro*-Kulturen) oder lebende Versuchstiere (*in vivo* Experimente). Primäre Zellkulturen werden direkt aus Gewebe gewonnen, Zelllinien entstehen aus primären Zellkulturen und können mitunter über Jahrzehnte in Kultur gehalten werden. In beiden Fällen handelt es sich um Zellen eines bestimmten Zelltyps, die meist als Monolayer kultiviert werden und sich begrenzt (primäre Zellkultur) oder aufgrund von genetischen Mutationen während des Zellteilungsprozesses unbegrenzt (sog. unsterbliche Zelllinien) teilen können.

Die Vorteile vor allem der Zelllinie liegen in ihrer einfach Handhabbarkeit. Eine Zelllinie zu kultivieren bedeutet relativ geringen Arbeitsaufwand, das biologische Material kann nach Belieben vervielfältigt werden, bei Nichtgebrauch kann sie sogar zur späteren Verwendung eingefroren werden. Zudem können Zellkulturen aus humanen Zellen hergestellt werden. Diese eliminieren experimentelle Unsicherheiten basierend auf speziesspezifischen Unterschieden.

Jedoch haben Untersuchungen an diesen leicht handhabbaren Zellkulturen auch Nachteile. Die gesamte Kultur enthält nur einen Zelltyp. Ein natürliches Gewebe besteht aber aus verschiedenen Zelltypen, der extrazellulären Matrix und einem Immunsystem. Typischerweise wachsen Zellkulturen als Monolayer. Die ursprünglich dreidimensionale Umgebung der Zellen wird auf eine zweidimensionale reduziert, es kommt zum Informationsverlust einer kompletten Dimension. Zusammenfassend stellt die Zellkultur also ein einfach zu handhabendes, aber auch stark vereinfachtes, biologisches Testsystem dar.

Demgegenüber steht das Tierversuchsmodell. Vorteil des Tiermodells ist, dass sich die zu untersuchenden Gewebe zum Zeitpunkt des Experiments in ihrer nativen Umgebung befinden. Durch gezielte genetische Manipulationen lassen sich diverse Mausmodelle mit bestimmten Eigenschaften züchten. Nachteile des Tiermodells sind die hohe Zahl der pro Experiment benötigten Versuchstiere, speziesabhängige, nicht auf den Menschen übertragbare Versuchsergebnisse sowie interindividuelle Unterschiede.

Ein Zwischenmodell, welches die Vorteile der beiden vorher genannten Modelle miteinander verbindet, stellen die sogenannten organotypischen Slicekulturen dar. Es handelt sich dabei um Gewebeschnitte, die aus verschiedenen Organen eines Versuchstiers gewonnen und anschließend kultiviert werden. In diesen Slicekulturen verbleiben die verschiedenen Zelltypen eines Gewebeverbandes in ihrer ursprünglichen dreidimensionalen Anordnung und die extrazelluläre Matrix bleibt erhalten. Zudem können aus einem Organ mehrere Gewebeschnitte gewonnen werden. Die Anzahl der benötigten Versuchstiere wird daher reduziert und verschiedene Versuchsparameter können an demselben Individuum erforscht werden. Gewebeschnitte können zudem aus humanem Material gewonnen werden, somit können speziesabhängige Unterschiede eliminiert werden. An pathologischem Gewebe können Krankheitsbilder und Therapien erforscht werden, gesundes Gewebe dient als physiologisches Modell zur Untersuchung von Nebenwirkungen und zur Erforschung grundlegender molekularer Prozesse.

Bestrahlungstherapien werden häufig von vielfältigen – akuten wie späten – Nebenwirkungen begleitet (z.B. Müdigkeit, Übelkeit, Durchfall, Erbrechen, Hautschädigung). In gravierenden Fällen kann dies zum Abbruch einer Therapie führen. Die Minimierung der Nebenwirkungen ist deshalb für den Erfolg einer Strahlentherapie von sehr großer Bedeutung. Daher ist es zwingend erforderlich, die Dosis im gesunden Gewebe so gering wie möglich zu halten. Dieses kann – wie eingangs beschrieben – durch eine Ionenbestrahlung erreicht werden. Eine weitere Möglichkeit, die Nebenwirkungen einer Strahlentherapie zu verringern, könnte darin bestehen, die Therapie zu einem Zeitpunkt durchzuführen, an dem gesundes Gewebe möglichst wenig durch die Strahlenbehandlung geschädigt wird. Einige Studien haben bereits gezeigt, dass der Zeitpunkt einer Bestrahlung das Ausmaß der therapiebegleitenden Nebenwirkungen günstig bzw. nachteilig beeinflussen kann. Die zeitabhängigen Unterschiede in der Strahlenempfindlichkeit normaler Gewebe dürften durch circadiane molekulare Uhrwerke bedingt sein, die in allen Geweben ticken und durch eine Zentraluhr im Gehirn (Nucleus suprachiasmaticus) koordiniert und an den Tag-Nacht Rhythmus angepasst werden.

Entscheidend dabei ist, dass das gesunde Gewebe weiterhin dem normalen Rhythmus des Organismus unterliegt, während das Tumorgewebe häufig jegliche Rhythmizität verloren zu haben scheint. Therapierelevant kann dies ausgenutzt werden, um Nebenwirkungen, welche zu einem Abbruch oder einer Unterbrechung der Therapie führen könnten, einzudämmen und die Therapie für den Patienten erträglicher zu machen.

Zur Bestrahlung der biologischen Proben wurde mit dem GSI-eigenen Programm ein Tiefendosisprofil eines ausgedehnten Bragg-peaks erstellt. Das erst Ziel dieser Arbeit war, dieses Tiefendosisprofil mit drei anderen Simulationsprogrammen zu reproduzieren und zu vergleichen. Weiterhin sollten die Effekte ionisierender Strahlung auf Zellteilungsrate, Apoptoserate und Rate der DNA-Doppelstrangbrüche in Schnittkulturen gesunder Maus-Lebern und Explantatkulturen gesunder Maus-Pankreata untersucht werden, um Nebenwirkungen ionisierender Strahlen abzuschätzen. Zusätzlich wurden diese Parameter nach ^{12}C-Bestrahlung in neoplastischem Lebergewebe bestimmt. Die Untersuchung der Wirkung von Strahlung auf das molekulare Uhrwerk erfolgte an Leberschnitten und Explantatkulturen von Pankreas und Nebenniere, die von transgenen $Per2^{luc}$-Mäusen gewonnen wurden. Im Gewebe

dieser Tiere kann die Expression von *Per2*, einem wichtigen Uhrengen, über mehrere Tage „online“ verfolgt werden.

Material und Methoden

Für die Simulationen zur deponierten Dosis der ^{12}C-Ionen im biologischen Material wurden die vier Programme MCHIT, TRIM, TriP98 und ATIMA verwendet. Der angegebene Versuchsaufbau entsprach dem für die eigentliche Bestrahlung nach Austritt der Ionen aus dem Strahlrohr. Die biologischen Proben, die Gewebeschnitte und Explantatkulturen, wurden wie bei einer Therapieplanberechnung durch Wassertargets simuliert. Bestrahlt wurde mit einem ausgedehnten Bragg-peak zu Dosen von 2Gy, 5Gy und 10Gy. Bei den Berechnungen wurde der lineare Energietransfer (LET) von ^{12}C-Ionen für insgesamt 26 verschiedene Energien berechnet. Die einzelnen Bragg-peaks wurden im post-processing superpositioniert und ergaben somit das Dosisprofil des ausgedehnten Bragg-peak. Das Dosisprofil eines ausgedehnten Bragg-peaks zeichnet sich durch eine konstante Dosis über eine bestimmte Strecke aus. Zusätzlich zu diesem Tiefendosisprofil wurde mit MCHIT die Menge der auftretenden Fragmente simuliert.

Gewebeschnitte zur Bestrahlung wurden aus drei unterschiedlichen Mausstämmen hergestellt. Für die Referenzexperimente mit Röntgenstrahlen wurde Leber und Pankreas aus gesunden C3H-wildtyp (wt) Mäusen präpariert. Die Präparate der C3H wt-Mäuse dienten zur Analyse der Nebenwirkungen von Strahlung auf gesundes Gewebe. Für die Bestrahlung mit ^{12}C-Ionen ergab sich die günstige Gelegenheit, transgene c-myc/TGF-α Mäuse zu verwenden, welche einen induzierbaren Lebertumor aufweisen. Von diesen Tieren konnten Leberschnitte sowohl aus gesundem Gewebe (OHLSC – organtypic healthy liver slice cultures) als auch aus neoplastischem Gewebe (ONLSC – organotypic neoplastic liver slice cultures) hergestellt werden. Zur Untersuchung der Wirkung von Strahlung auf die innere Uhr wurden Leberschnitte und Explantatkulturen von Pankreas und Nebenniere von transgenen Per2^{luc}-Mäusen präpariert. Per2^{luc}-Mäuse exprimieren das Enzym Luziferase unter der Kontrolle des Promoters von *Per2*, einem wichtigen Bestandteil des circadianen Uhrwerks. Diese Schnitte wurden nur mit Röntgenstrahlen behandelt.

Unabhängig des genetischen Hintergrunds der Spendermaus wurden für alle Experimente Gewebeschnitte und Explantatkulturen zu zwei unterschiedlichen

Tageszeiten präpariert: zur Mitte des subjektiven Tages und zur Mitte der subjektiven Nacht. Dadurch sollte eine tageszeitabhängige Reaktion des Gewebes auf Bestrahlung analysiert werden.
Nach der Präparation wurden die Proben für mehrere Tage auf einer Membran an einer Grenzschicht von Flüssigkeit und Luft kultiviert. Nach 24h erfolgte die Bestrahlung mit unterschiedlichen Dosen. Als Kontrolle dienten unbestrahlte Proben. Alle Proben wurden 1h bzw. 24h nach der Bestrahlung fixiert und immunhistologisch auf Marker für Proliferation (Zellteilung, Marker: Ki67), Apoptose (programmierte Selbsttötung der Zelle, Marker: Caspase3) und DNA-Doppelstrangbrüche (Marker: γH2Ax) quantitativ untersucht.

Ergebnisse und Diskussion

Die ^{12}C-Bestrahlung der Leber- und Pankreasproben wurde mit dem GSI-eigenen Simulationsprogramm TRiP98 berechnet. Dieses berechnete Tiefendosisprofil, nach welchem die biologischen Proben bestrahlt wurden, diente als Referenz für die Ergebnisse der anderen drei Programme (ATIMA, MCHIT, TRIM). ATIMA und TRIM sind allgemeine Programme für den Energieverlust von Ionen in Materie. Sie können das von TRiP98 berechnete Tiefendosisprofil nur ungenügend reproduzieren. ATIMA berechnet aufgrund fehlender Fragmentierung ein linear ansteigendes Tiefendosisprofil. TRIM lässt im Grunde das gleiche Muster vermuten. Allerdings zeigt TRIM bei der Berücksichtigung des diskret implementierten ripple filters (ein Bauteil im Strahlengang zur künstlichen Strahlaufweitung) aufgrund interner Binningprozesse gravierende Abweichungen vom typischen Dosisprofil. Das MC-Programm MCHIT, welches speziell für die Wechselwirkung von Ionen mit Materie in medizinischer Anwendung entwickelt wurde, zeigt die beste Übereinstimmung mit der TRiP98-Referenzkurve. Bis auf eine leicht höhere Durchschnittsdosis um 0.1 Gy konnte das Tiefendosisprofil nahezu exakt reproduziert werden.
Während die Pankreas-Präparate im Hinblick auf die untersuchten Parameter leider keine auswertbaren Ergebnisse ergaben, zeigten die untersuchten Parameter im gesunden Lebergewebe dosisunabhängig deutliche Tag-Nacht-Unterschiede: die Proliferationsrate war zur Mitte des subjektiven Tages signifikant höher als zur Mitte

der subjektiven Nacht. Umgekehrt waren die Raten für Apoptose und DNA-Doppelstrangbrüche zur Mitte der subjektiven Nacht signifikant erhöht. Diese Tag-Nacht-Unterschiede ließen sich im neoplastischen Lebergewebe nicht nachweisen. Unabhängig von der Art der Bestrahlung konnte bei der Variation der Dosis im gesunden Lebergewebe kein Einfluss auf die untersuchten Parameter festgestellt werden. Im neoplastischen Lebergewebe hingegen wird die Rate der DNA-Doppelstrangbrüche durch eine Bestrahlung dosisabhängig erhöht.

Die Auswirkungen ionisierender Strahlen auf das circadiane Uhrwerk wurden in den Gewebeproben transgener $Per2^{luc}$-Mäuse analysiert. Die Analyse dieser Tiere erlaubt, den circadianen Rhythmus des molekularen Uhrwerks in Leber und anderen Geweben durch Messung der Luziferase-Aktivität in Echtzeit aufzuzeichnen. Wie in Leberschnitten und Explantatkulturen von Nebennieren dieser Tiere gezeigt werden konnte, behalten diese Präparate ihren circadianen Rhythmus in Kultur bei. Sie zeigen außerdem, dass ionisierende Strahlen dosisabhängig zu einem Phasenvorsprung des circadianen Uhrwerks unter Beibehaltung der Periodizität führen.

Fazit

Die Ergebnisse der Dosissimulationen von ^{12}C-Ionen in Wasser zeigen, dass deterministische und MC-Programme fast identische Ergebnisse liefern. MC-Programme tun dies unter gleichzeitiger Berechnung von Fragmententstehung. Beim heutigen Stand der Computertechnologie sind MC-Programme aufgrund der zeitaufwändigen Berechnungen noch nicht für den alltäglichen Klinikgebrauch verwendbar. Dennoch kann davon ausgegangen werden, dass diese Programme bei sich entsprechend weiterentwickelnder Rechnerleistung auch zur Therapieplanberechnung im Klinikbetrieb verwendet werden können.

In dieser Arbeit wurden zum ersten Mal organotypische Gewebeschnittkulturen ionisierender Strahlung ausgesetzt und deren Wirkung in Bezug auf Zellteilungsrate, Apoptoserate und Anzahl der DNA-Doppelstrangbrüche analysiert. Das Modell der Gewebeschnitte liefert reproduzierbare Ergebnisse in Bezug auf diese untersuchten Parameter. Es eignet sich als Testmodell zur Erforschung von Gewebereaktionen auf ionisierende Strahlung und stellt eine attraktive Ergänzung zu Zellkultur und Tierversuchen dar. Die Ergebnisse der Gewebeschnittanalyse nach Bestrahlung von bis zu 10Gy weisen auf eine dosisunabhängige hohe Reparaturkapazität gesunden

Lebergewebes hin. Im Tumorgewebe kommt es jedoch dosisabhängig zu gehäuften DNA-Doppelstrangbrüchen. Dies lässt auf eine geringere Reparaturkapazität des neoplastischen Gewebes schließen. Im Zusammenhang mit der zeitabhängigen Reaktion der gesunden Leber kann geschlussfolgert werden, dass die Berücksichtigung der Tageszeit, zu der Leber bestrahlt wird, einen positiven Einfluss auf die Nebenwirkung der Bestrahlung haben kann.

Contents

Zusammenfassung v
Material und Methoden ix
Ergebnisse und Diskussion x
Fazit xi
1 Introduction 16
1.1 Radiotherapy 17
1.1.1 X-ray therapy 18
1.1.2 Particle therapy 21
1.2 Circadian clock 26
1.2.1 Circadian rhythms in peripheral tissues 27
1.2.2 Circadian rhythm in oncology 29
1.3 Organotypic slice cultures 31
1.4 Aims of this thesis 35
2 Simulations of nuclear beams in matter 37
2.1 Codes to calculate energy loss in matter 38
2.1.1 TRiP98 38
2.1.2 ATIMA 38
2.1.3 TRIM 39
2.1.4 MCHIT 39
2.2 Beamline setup at GSI 40
2.3 Results and discussion 41
3 Materials and Methods 48
3.1 Animals 48
3.1.1 C3H wildtype mice 48
3.1.2 Transgenic mice 48
3.1.3 Housing of animals prior to organotypic slice/explant culture preparation 48
3.2 Preparation of organotypic slice/ explant cultures 49
3.2.1 Preparation of organotypic liver slice cultures for irradiation experiments 49
3.2.2 Preparation of OLSC for bioluminescence experiments 50
3.2.3 Preparation of organotypic pancreas explant cultures 50
3.2.4 Preparation of organotypic adrenal gland explant cultures 51
3.2.5 Perfusion of Bmal1-wt mice 51
3.3 Irradiation of tissue cultures 51
3.3.1 X-ray irradiation 51
3.3.2 Heavy ion (^{12}C) irradiation 52
3.4 Histological and immunofluorescent staining 52
3.4.1 Cryosectioning 52
3.4.2 Histological staining – Hematoxylin-Eosin 53
3.4.3 Immunofluorescent staining 54
3.5 Recording tissue-specific circadian rhythms via luminometry 55
3.6 Microscopes and data acquisition software 58
3.6.1 Zeiss light microscope 58
3.6.2 Confocal microscope 58
3.7 Image processing and evaluation 59
3.8 Statistical analysis 62
3.8.1 Irradiation data 62
3.8.2 Circadian data 64

4 Results 66
4.1 X-ray irradiation 66
4.1.1 Proliferative data in OLSC 66
4.1.2 Apoptotic data in OLSC 70
4.1.3 DNA DSB data in OLSC 73
4.2 ^{12}C irradiation 75
4.2.1 OHLSC from c-myc/TGF-α mice showed very few proliferative cells *in vitro* 75
4.2.2 ONLSC showed an increased proliferation rate *in vitro* 76
4.2.3 OHLSC showed very few apoptotic cells *in vitro* 77
4.2.4 ONLSC showed an increased apoptosis rate *in vitro* 79
4.2.5 OHLSC showed very few DNA DSB sites *in vitro* and post-irradiation 80
4.2.6 ONLSC showed an increased DNA DSB rate *in vitro* 81
4.3 Comparison of X-ray- and ^{12}C-data 82
4.3.1 Proliferation rate 82
4.3.2 Apoptosis rate 84
4.4 C3H pancreas did not show immunohistochemical reaction 85
4.5 c-myc /TGF-α pancreas explant cultures showed immunohistochemical reaction in vitro in non-fibrotic areas 87
4.6 Immunohistochemistry in liver ex vivo 88
4.6.1 Proliferation rates ex vivo in C3H-liver 88
4.6.2 Apoptosis rate and DNA DSB rate *ex vivo* in wt-liver 88
4.7 Immunohistochemistry in pancreas ”ex vivo” 89
4.7.1 Proliferation rate 89
4.7.2 Apoptosis rate and DNA DSB rates *ex vivo* in wt-pancreas 91
4.8 Morphological assessment of organotypic slice and explant cultures 92
4.8.1 Liver 92
4.8.2 Pancreas 95
4.9 Bioluminometric studies 98
4.9.1 OLSC showed a distinct circadian rhythm even after irradiation *in vitro* 98
4.9.2 Pancreas showed a distinct circadian rhythm *in vitro* 100
4.9.3 Adrenal glands showed a distinct circadian rhythm in vitro 103
4.9.4 Irradiation with X-rays did not lead to a change in period length 105
4.9.5 Irradiation with X-rays lead to a phase-shift 106
5 Discussion 108
5.1 Effect of X-rays on OLSC 109
5.1.1 Proliferation 109
5.1.2 Apoptosis 111
5.1.3 DNA double-strand breaks 112
5.2 Effect of ^{12}C radiation on healthy and neoplastic transgenic liver OSC 113
5.2.1 Proliferation 113
5.2.2 Apoptosis 115
5.2.3 DNA DSBs 116
5.3 Comparison X-rays to ^{12}C 117
5.4 OSC of murine liver and OEC of murine pancreas stay viable and functional in vitro 119
5.4.1 Liver 119
5.4.2 Pancreas 123
5.5 Ionizing radiation leads to a phase-shift in circadian rhythm 125
5.6 Clinical relevance 128
6 Summary 129
6.1 Background 129
6.2 Goals 132

6.3 Materials and methods 132
6.4 Results and discussion 133
6.5 Conclusion 134
Bibliography 136
Glossary 169
List of Abbreviations 171

1 Introduction

Cancer is the cause for the second highest death rate in Germany and the Western world each year. In 2010, it was the cause of 25.5% of all reported deaths in Germany, only to be exceeded by cardiovascular disease, which accounts for 41.1% of all reported deaths [StatBund2010]. The cancers focused on in this thesis, liver cancer and pancreatic cancer, have a low occurrence. Each year, about 7600 patients in Germany are diagnosed with liver and/or gall bladder cancer, whereas about 15000 patients were diagnosed with pancreatic cancer in 2008 [RKI2012]. However, due to their usually late diagnosis, the chance at a cure is rather low for both tumor types. The 5-year survival rate for patients with liver cancer is about 10%, the prognosis for patients with pancreatic cancer in Germany is even poorer at 5-8% [RKI2012].

Cancer of the liver

The most common type of primary liver cancer is the hepatocellular carcinoma, followed by the cholangiocarcinoma. The hepatocelluar carcinoma is the cancerous malformation of hepatocytes, the parenchymal cells of the liver. The cholangiocarcinoma refers to the malignancies of epithelial cells from the bile ducts in the liver, which transfer the bile produced in the liver into the small intestine. In addition to these primary tumors, the liver is also a frequent target for metastases due to its detoxifying function in the organism. Up to 75% of the blood supplied to the liver comes from the hepatic portal vein, in which blood from the pancreas, spleen, and gastrointestinal tract gets directed to the liver for detoxification. Therefore, the liver is especially prone to metastases from the gastrointestinal tract.

There are various ways to treat liver cancer. The most common treatment, surgery (including organ transplant), is only applicable in less than 20% of all liver cancer patients [Krishnan2008, Hawkins2006, Tse2008]. Next to radiation and surgery, other treatments include chemotherapy (a variation of which is transarterial chemoembolization especially for the treatment of hepatocellular carcinoma), radiofrequency ablation, and percutaneous ethanol injection. Historically, irradiation of the liver was discarded as a practical therapy due to a serious side-effect called radiation-induced liver disease (RILD). The liver as a whole can only be irradiated up to a (therapeutically ineffective) dose of about 30-35 Gy before being severely damaged [GasentBlesa2008, Krishnan2008, Matsuzaki1999, Tse2008]. RILD is characterized by the so-called veno-occlusive disease, which is a congestion of the central veins of the liver lobules, leading to fibrosis/sclerosis and a

degeneration of the hepatocytes. RILD occurs between 2 weeks to 4 months after irradiation or chemotherapy and can eventually lead to liver failure. However, several studies [GasentBlesa2008, Greco2004, Tse2008] have shown that partial irradiation of the liver allows the dose to be increased up to therapeutically relevant doses of 90Gy, making radiation an attractive alternative therapy for inoperable liver cancers [Ask2005, GasentBlesa2008, Hawkins2006, Krishnan2008, Matsuzaki1999, Mayahara2005, Tse2008].

Pancreatic cancer

The majority of all pancreatic cancers, comprising about 95% of the incidences, are adenocarcinomas, which are neoplasms of epithelial cells of the exocrine pancreas. Tumors of the endocrine pancreas are rather rare, being only a part of the residual 5% pancreatic cancers which include other cancer types originating in the exocrine pancreas. Pancreatic cancers have the bleakest prognosis, with a 5-year survival rate of roughly 5%.

Treatment options for pancreatic cancer consist of surgery, chemotherapy and radiation therapy. Normally, radiation therapy is combined with chemotherapy for pancreatic cancers before surgery, so as to reduce the size of the tumor which needs to be resected. Doses applied to pancreatic tumors usually range between 40-70Gy [Ceha2000, Edgar2004, Kokubo2000, Shinchi2002, Wanebo2000]. Via this procedure, the probability of successfully resecting all of the neoplastic tissue is increased and patients have an increased median survival time [Edgar2003, Lockhart2005, Shinchi2002]. In case of unresectable tumors, chemoradiotherapy has been shown to increase the median survival time by 100% compared to the median survival time of patients receiving only radiation treatment [Li2004], but the essential role of radiation remains unclear as other studies do not show a significant improvement in adjuvant (chemo)radiotherapy [Lockhart2005, Neoptolemos2004]. In cases where no cure is expected, radiation is applied for palliative treatment, pain relief having been reported for 50-85% of patients [Minsky1988]. Overall, the prognosis for patients diagnosed with pancreatic cancer are bleak and call for ongoing research in radiotherapy in combination with cytotoxic and biological agents [Crane2001].

1.1 Radiotherapy

Besides surgery and chemotherapy, radiotherapy is the most frequently applied form of cancer treatment. Ever since Röntgen's discovery of X-rays in 1895, their application for medical services has vastly expanded. Today, ionizing radiation is not just used in radiooncology for the primary treatment of benign and malignant tumors, but also for diagnostic purposes, such as in the well-known X-ray photograph, computer tomography and scintigraphy (for example of the thyroid gland) as well as for palliative, anti-

inflammatory, or immunesuppressing treatment [Kauffmann2006]. Specifically for radiooncology, the objective of radiotherapy has been driven by two main optimization strategies: (1) optimizing the conformity of applied dose to the actual tumor tissue whilst sparing normal surrounding tissue and (2) increasing the biological effectiveness of the applied radiation in the neoplastic region [Kraft2000]. In addition to conventional X-ray radiotherapy, current optimization has brought clinical application of stereotactic radiotherapy, intensity-modulated radiotherapy as well as proton and hadron therapy.

1.1.1 X-ray therapy

X-rays are electromagnetic radiation of energies ranging from approximately 100 eV to 100 keV. They are produced when electrons interact via Coulomb scattering with electrons of the atomic shell and are usually of lower energy than γ-rays. These are produced during the deexcitation process of an excited atom to an energetically lower state and typically have energies of more than 100 keV.

When photons interact with matter, depending on their energy, they interact in one of the following ways: via elastic scattering, photoelectric effect, inelastic (Compton) scattering, pair production, and photonuclear interactions. For medical purposes, only the photoeffect, Compton scattering, and pair production are relevant interaction effects.

The photoelectric effect describes the process of the incident X-ray photon being absorbed by an electron of the target material, whereby the electron is emitted from the atomic shell. Depending on the kinetic energy of this electron, it can either travel a

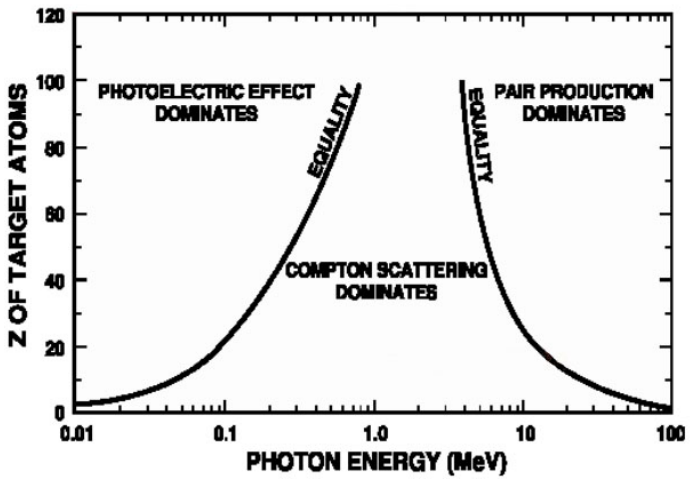

Figure 1 Energy and atomic number dependence of photon interaction with matter The schematic shows the prevailing interaction of photons depending on the energy of the photons and the atomic number of the target material. For low energies and high atomic number, the photoeffect dominates, for low atomic number, the Compton scattering is most likely for a wide energy range, and at high energies and high atomic numbers, pair production is the dominant effect. For therapy conditions, the atomic number is low, the prevailing effect during X-ray radiotherapy being Compton scattering. (Courtesy of V. Patera)

certain range in the target material and take part in further interactions, or it gets reabsorbed by its original atom. Usually, the atom having lost an electron by photoelectric effect will deexcite by electrons falling from higher energetic levels to lower levels, emitting characteristic γ-rays or by emitting an Auger electron, also from an energetically higher shell.

Inelastic scattering, also known as Compton scattering, describes the process of the incoming X-ray photon emitting an electron of a target atom from its shell, whilst being scattered in a different direction with respect to mass-energy and momentum conservation. Finally, if the photon energy exceeds 1.022 MeV (twice the energy at rest of an electron), the photon can interact with a nucleus (for matters of energy and momentum conservation) and produce an electron-positron pair. These again react with the surrounding material, for example via Compton scattering or positron-electron annihilation, which produces two γ-quants.

The probability of X-ray photons to interact with matter in one of the above mentioned ways depends on the energy and on the atomic number Z of the target material (Figure 1). For low atomic numbers, Coulomb scattering is the most dominant interaction, at high atomic numbers and low photon energies, the photoelectric effect is dominant, and for high atomic numbers and high photon energies, pair production is the most dominant effect. As can be seen, in energy ranges common for radiotherapy and at low atomic numbers, the most common interaction is Compton scattering.

The probabilities for each of the above mentioned interactions to take place per unit length can be added up to produce the so-called attenuation coefficient μ [1/m]:

$$\mu = \tau + \sigma + \kappa \,, \tag{1.1}$$

where τ is the probability (or cross section) for photoeffect, σ is the probability for Compton effect, and κ is the probability for pair production. The interaction of photons with matter is an all or nothing event: either a photon reacts with matter and energy is released, or it does not react, whereupon no energy is released into matter. The intensity of a photon beam after having traversed matter of a certain length x is thus given by the exponential attenuation law

$$I_x = I_0 \exp(-\mu x) \,, \tag{1.2}$$

in which I_x is the intensity of photons after matter of length x, I_0 is the incident intensity of photons, and μ is the attenuation coefficient of equation (1.1). The exponential decay of photon energy release in matter means that most of the energy deposition occurs at the beginning and decreases exponentially (Figure 2).

For radiotherapy, this means that most of the dose (defined as the energy deposited in mass) is deposited at the surface of the target, i.e. the patient. This is beneficial for skin tumors or tumors located directly underneath the skin. For deep-seated tumors, however, irradiation with X-rays from one direction would mean an unacceptable high dose in the normal tissue in front of the tumor.

Optimizations regarding the dose application with X-rays have resulted in the development of various dose application techniques using several radiation fields to minimize the dose deposited in surrounding normal tissue while delivering the maximum dose inside the tumor volume. Next to the usual conformal radiotherapy, stereotactic radiotherapy, radiosurgery, and intensity modulated radiation therapy (IMRT) have improved the dose application in the last few years. Stereotactic radiotherapy and radiosurgery ("gammaknife") refer to a very precise dose application in several or single fractions, respectively, with a constant energy flux and are usually applied to rather small tumor volumes. IMRT on the other hand is a so-called dynamic radiotherapy. Here, the irradiation field is divided into several smaller fields which can be irradiated from different directions each with a different intensity. This is particularly advantageous for tumor irradiation in close proximity to sensitive anatomical structures or tissues. However, due to the increased number of irradiation fields from different directions, typically more non-tumorous tissue is irradiated (with a lesser dose) than in conventional conformal radiotherapy. This has to be considered especially in pediatric radiotherapy for risk of radiation-induced tumors. For all of these clinical application techniques, the main disadvantage for the treatment of deep-seated tumors is the underlying physical principle of the exponentially decreasing dose-deposition of X-rays. An advantageous alternative to this has been achieved by changing from photons to charged particles as ionizing radiation type.

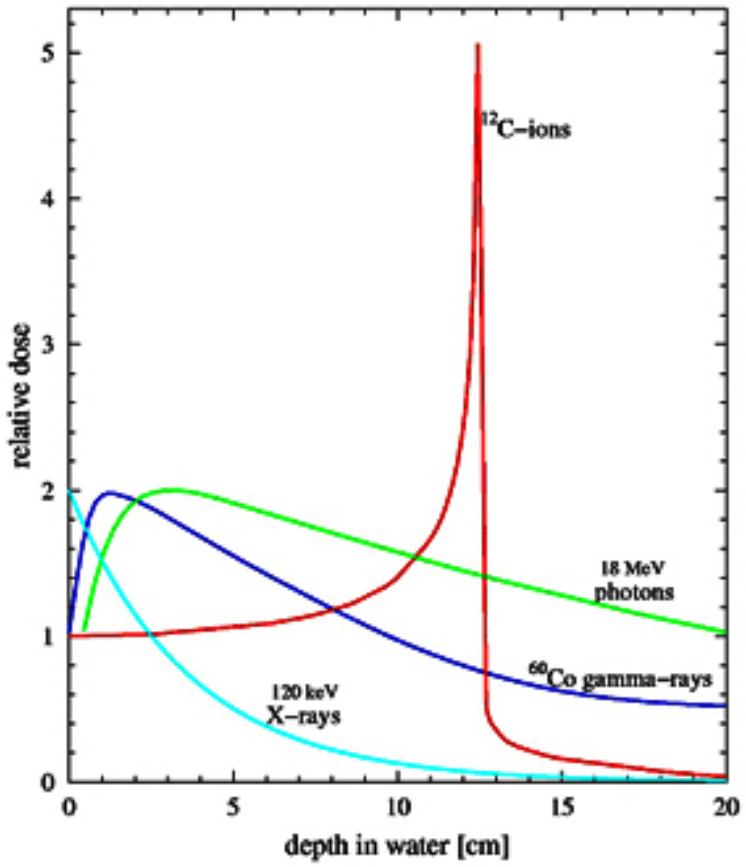

Figure 2 Relative dose of ^{12}C ions and photons in water The energy deposition of photons of various energy and ^{12}C ions are shown in a water phantom. The dose of 120 keV X-rays decreases exponentially immediately after hitting the target. Higher energetic photons (from ^{60}Co and 18 MeV photons) have a build-up effect shortly after the target surface, but also show the characteristic exponential decrease in energy loss thereafter. ^{12}C ions show a low dose in the entrance channel and a sharp peak, the so-called Bragg peak, at the distal part of the track. Courtesy of U. Weber.

1.1.2 Particle therapy

Particle therapy was first proposed by Robert Wilson in 1946 [Wilson1946], who proposed to use protons due to the superior depth-dose profile compared to X-rays for deep-seated tumors. Whereas X-rays show an exponential decrease in energy deposition in matter, the depth-dose profile for particles is characterized by relatively low energy transfer at the beginning of the track with a sharp peak of energy release at the very end of the particle track (Figure 2). This peak at the end of the track is called Bragg peak (named after William Henry Bragg, who first described this peak energy loss for α-particles in 1905

[Bragg1905]). The depth-dose profile of particles is also known as inverse depth-dose profile.

The energy loss of particles in matter is described by the Bethe-Bloch formula [Bethe1930, Bloch1933a, Bloch1933b]:

$$\frac{dE}{dx} = \frac{4\pi e^4 Z_{eff}^2 Z_t N}{m_e v^2} \ln \frac{2mv^2}{I} + relativistic\ \ terms\,, \tag{1.3}$$

where dE/dx is energy loss per length, e is the electron charge, m_e is the mass of the electron, $v = \beta c$ is the projectile velocity, Z_t is the atomic number of the target material and N is the electron density of the target. It does not suffice to give the charge of the projectile with Z_p, as the charge of the projectile depends on its velocity. At high velocities, the projectile is stripped of its electrons and Z_p is given by the atomic number of the projectile. However, as the particle slows down in matter, it recollects electrons, decreasing its effective charge. The effective charge of a projectile is therefore dependent on the projectile velocity, a circumstance taken into account by the Barkas formula [Barkas1963]:

$$Z_{eff} = Z_p(1 - \exp(-125\beta Z_p^{\frac{2}{3}}))\,. \tag{1.4}$$

The energy loss described by the Bethe-Bloch formula is proportional to $1/v^2$, which in principle describes the increasing energy loss at lower projectile velocity very well.

In addition to the inverted depth-dose profile, particle traversal through matter differs from X-ray interaction with matter by nuclear fragmentation and lateral scattering. Due to collisions with the target material, heavier particles than protons can fragment.

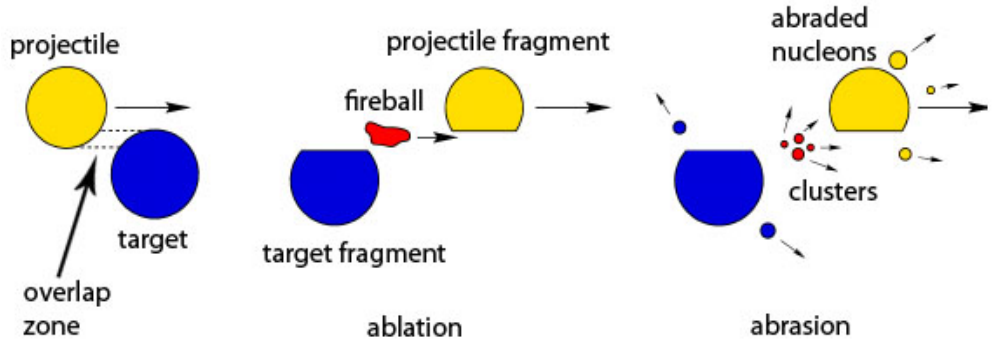

Figure 3 Schematic of ablation and abrasion process. Modified from [Gunzert-Marx2004].

Fragmentation is a two-step process: in the first step, i.e. abrasion, nucleons in the overlap zone are abraded and produce a lighter fragment. In the second step, i.e. ablation, the excited remaining target and projectile fragments deexcite by further emitting individual or clustered nucleons (Figure 3).

These fragments usually have a greater range in the target material and form a characteristic tail for heavier nuclei. Hence, more dose is deposited behind the distal part of the original projectile track. This is a negative side-effect of heavy ion therapy and has to be accounted for in treatment planning. However, particularly for ^{12}C ions, fragmentation offers the advantage of producing the instable isotopes ^{11}C and ^{10}C. Both isotopes are positron-emitters ($T_{1/2}(^{11}C) = 20\,min$, $T_{1/2}(^{10}C) = 19\,s$). Emitted positrons react with an electron in the surrounding target material and annihilate into two γ-quants, each with a characteristic energy of 511 keV. As the range for ^{11}C and ^{10}C is approximately the same as it is for ^{12}C, detecting the photons produced by positron emmission via positron emission tomography (PET) allows for an accurate monitoring of local beam delivery.

Apart from inflicting additional dose behind the original particle Bragg peak due to fragmentation, further dose uncertainties are brought about by lateral scattering. Lateral scattering is mainly due to Compton scattering of the projectiles by the target nuclei. Lateral scattering is characterized very well by Molière [Molière1948], who describes an increasing Gaussian spread of the initial pencil beam. For protons, the lateral scattering can be so high that the incident particle beam is scattered much more than photons [Kraft2000]. Contrary to that, carbon ions are much less subject to lateral scattering. This is a major advantage in clinical application as the carbon beam has a local uncertainty of ~1 mm, making it possible to treat neoplastic tissue in close proximity to sensitive tissue, such as, for example, the optic nerve or chiasma.

The absorbed dose is defined as energy per mass unit, the unit of dose is Gray [Gy]. One Gray is defined as 1 Joule per kilogram. For particle therapy, in which fluence is measured as a dose indicator, the following equation is used to calculate the absorbed dose:

$$D[Gy] = 1.6 \cdot 10^{-19} \cdot \frac{dE}{dx}\left[\frac{keV}{\mu m}\right] \cdot F\left[cm^{-2}\right] \cdot \frac{1}{\rho}\left[\frac{cm^3}{g}\right], \tag{1.5}$$

where *dE/dx* is the energy loss of the particles per unit length, *F* is the number of particles per cm² (fluence), and ρ is the mass density of the absorber material.

This holds true for a parallel beam of particles that passes through a thin volume of matter. For tumor irradiation though, where the target is a macroscopically extended volume, particles of one energy do not suffice. Rather, the energy of the primary particles has to be varied, allowing the Bragg peaks of the particles to be placed across the range of the target volume, ensuring a maximum dose deposition distributed homogeneously in the tumor. Making the dose calculation inside an extended tumor volume even more elaborate are the nuclear fragments, which add to the absorbed dose. Overall, the dose in an extended target

volume is the sum of the energy loss of particles of different energy and different atomic number [Kraft2000].

A pronounced advantage of particle therapy in comparison to X-ray irradiation is an enhanced biological effectiveness. The relative biological effectiveness is defined as the ratio of X-ray dose and particle dose needed to produce the same effect:

$$RBE = \frac{D_X}{D_p} \tag{1.6}$$

A common model used to characterize radiation damage is clonogenic survival of cells. Cells that divide into colonies of 50 or 100 cells after a certain period of time post-irradiation are considered to have clonogenically survived. Typical survival curves done with X-rays show a shouldered curve when plotted semilogarithmically, whereas cell survival after particle irradiation can be linear (Figure 4). The data points are fit with the linear quadratic model, in which survival is modeled according to the following formula:

$$S(D) = \exp(-\alpha D - \beta D^2) \quad . \tag{1.7}$$

S is the measured survival of dose D, α and β are experimentally determined parameters. The ratio α/β describes the shoulder of the survival curve. Linear survival curves acquired with particle irradiation are only described by α.

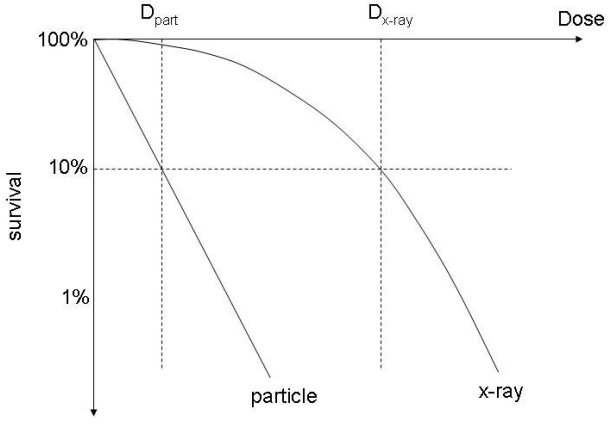

Figure 4 Definition of relative biological effectiveness (RBE) The RBE is defined as the ratio of doses from X-rays and particles to produce a similar biological effect. Shown are schematic survival curves of cell lines, the RBE is calculated at the biological effect of 10% survival post-irradiation.

Apart from being dependent on the dose [Weyrather1999, Furusawa2000], the RBE is dependent on linear energy transfer (LET) [Belli1998, Tsuruoka2005], atomic number of the projectile [Blakely1979, Tsuruoka2005], and on the repair capacity of the irradiated cells [Weyrather1999, Suzuki2000b].

Theoretical explanations for the higher biological effectiveness of particles mainly focus on the microscopic track structure of particles [Khvostunov2010, Nikjoo1994, Nikjoo1999]. The track structure of a particle is governed by the particle interactions with electrons of the target material. These electrons are emitted via Coulomb interaction and in the further course, these electrons interact with the surrounding target material. At the beginning of a particle track, interaction incidents are rather seldom, but when they do happen, the emitted electrons receive a rather large portion of energy and thus can travel a large range before stopping in the material. As the projectile slows down, the interaction probability increases and more electrons are emitted into the surrounding material, however, with less energy. At the end of the particle track, many electrons are emitted and stay in close proximity to the original track, causing a lot of dose to be deposited in a small volume of material. The electron emission is radially symmetric, the range which the electrons travel in matter can be approximated by $1/r^2$, r being the length of the particle track. As the dose distribution in matter resembles the radial electron emission, the dose distribution is also proportional to $1/r^2$. This is contrary to X-ray radiation, where the dose is distributed homogeneously in the tissue.

This effect has to be taken into account in particle treatment planning, as deep-seated tumors are irradiated with a spread out Bragg peak (SOBP). In an SOBP, the tumor region is divided into several slices in longitudinal direction. Each of these slices corresponds to a specific primary particle energy, so that the Bragg peak from particles of one particular energy is located in the corresponding slice. To cover the whole of the tumor, each slice is scanned in the lateral plane. The dose deposited in each slice has to be corrected by the expected relative biological effectiveness. This is done for carbon treatment, but not for proton therapy, where an overall RBE of 1.1 is applied to the whole radiation field [Paganetti 2002].

In summary, due to the inverted depth-dose profile of particles with mass, for deep-seated tumors they pose a superior irradiation technique to X-rays, which display an exponentially decreasing energy loss in matter. In addition, further physical processes such as fragmentation and lateral scattering are favorable for carbon ions, although current research emphasis is put on the evaluation of using other particles in therapy, such as helium or oxygen [Sommerer2009, Winkelmann2009, Winkelmann2012].

1.2 Circadian clock

All organisms are subject to rhythms, last they only seconds or years. The most prominent rhythm for mammals is the day-night rhythm, which corresponds to a sleep-wake-cycle. The astrophysical solar day, indicated through sunrise and sunset, is a powerful external stimulus, also called *zeitgeber*, which forces its rhythm onto almost all organisms. If this *zeitgeber* is removed (organisms are kept in constant darkness), then this external rhythm is replaced by an inner circadian rhythm characteristic of each species, which lasts about one day (latin "circa" about, "dies" day). Mice, for example, have a circadian rhythm lasting about 23 hours, whereas humans have a circadian rhythm lasting about 25 hours [Aschoff1971].

External light stimuli are passed via the retinohypothalamic tract to the suprachiasmatic nuclei (SCN), two areas located above the optic chiasma, which are known to function as the master clock of an organism. Information on light/dark is passed via the intrinsically photosensitive retinal ganglion cells, the axons of which project into the optic nerve, optic chiasma, and SCN. According to the external light information transmitted by this retinohypothalamic tract, the SCN orchestrates all other temporal functions of an organism [Schibler2003, vonGall2000, Yoo2004].

This is realized by approximately 20 000 neurons in the SCN, which adjust to an external *zeitgeber* by a complex transcription/translation negative feedback loop [Reppert2001]. The circadian rhythm is intrinsic and cell-autonomous, consisting of a primary and an auxiliary negative feedback loop (Figure 5). The primary transcription/translation negative feedback loop consists of the transcription factors CLOCK and BMAL1, which form heterodimers that bind to an E-box so as to initiate the transcription of Period (*Per1*, *Per2*, and *Per3*) and Cryptochrome (*Cry1* and *Cry2*) genes. The translated PERs and CRYs accumulate in the cytoplasm, form heterodimers there, then translocate back into the cell nucleus, acting on the CLOCK:BMAL1 heterodimers there to suppress their E-box mediated transcription until their levels have decreased in order for CLOCK:BMAL1 transcription to start anew.

In addition to this primary negative feedback loop, CLOCK and BMAL1 heterodimers also initiate the transcription of Rev-erbα and RORα. These two nuclear receptors act conversely on the RRE transcription factor binding site within the Bmal1 promoter, Rev-erbα repressing transcription of Bmal1, RORα activating Bmal1 transcription.

One cycle of the primary and auxiliary feedback loop takes about 24h. The molecular components of the circadian clock influence the expression level of other, so-called clock controlled genes (CCG). The circadian clock residing in the SCN generates a circadian

oscillation of the whole organism via these CCG, generating rhythmic physiological outputs, some of which are temperature, heart rate, blood pressure, and metabolism.

The circadian system has been modeled as a set of coupled self-sustained (Becker-Weimann2004, Geier2005) or dampened (Bernard2007) harmonic oscillators. The equations these models are based on focus on the negative and positive feedback loop of the molecular clock and describe the experimental data very well.

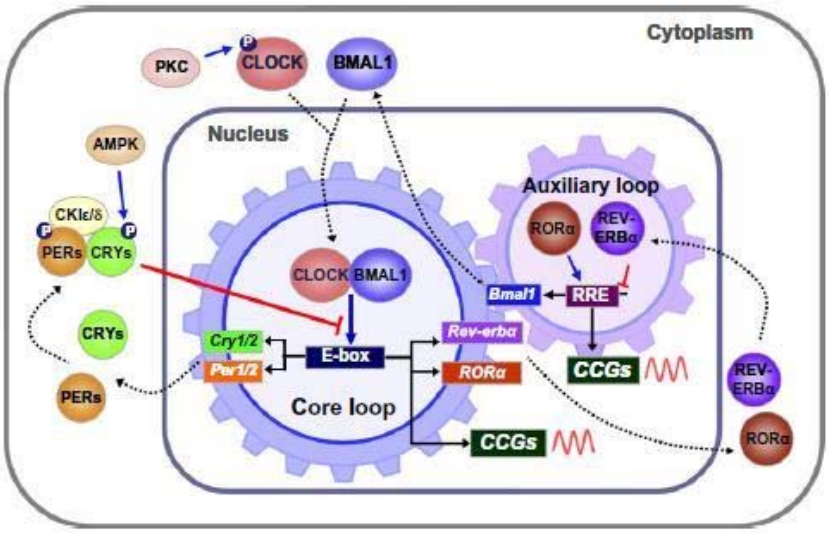

Figure 5 Negative translational/transcriptional feedback loop of the circadian clock The primary core loop consists of CLOCK and BMAL1, which form heterodimers that bind to an E-box, which initiates the transcription of Period and Cryptochrome genes. The translated PERs and CRYs form heterodimers in the cytoplasm. These translocate back into the nucleus, where they suppress their own E-box mediated transcription by acting on the CLOCK:BMAL1 heterodimers. When the levels of PER:CRY heterodimers have decreased below a certain threshold, the CLOCK:BMAL1 transcription reinitiates. In an auxiliary loop, CLOCK:BMAL1 heterodimers initiate the transcription of nuclear receptors Rev-erbα and RORα. They act conversely on the RRE transcription factor binding site within the Bmal1 promoter, Rev-erbα repressing transcription of Bmal1, RORα activating Bmal1 transcription. Both the core loop and auxiliary loop influence the expression levels of other clock controlled genes (CCGs), which generate a physiologic output. Courtesy of [Son2011]

1.2.1 Circadian rhythms in peripheral tissues

After the SCN had been identified as the master clock of mammals, it was hypothesized that the SCN generates and orchestrates all other rhythmic physiologic functions. Experiments with explant cultures or SCN lesioned laboratory mice, however, have shown that

peripheral tissues such as liver, heart, lung, pancreas, kidney, and adrenal gland are capable of sustaining an own circadian oscillation [Yoo2004]. A hypothesized second circadian clock, located somewhere in the periphery and not inside the brain, was not to be found. Instead, it seems that there are non-SCN cyclic cells in the periphery, which need synchronizing stimuli to oscillate in phase with the organism. These synchronizing stimuli are hypothesized to come mainly from the SCN [Moore1972, Ralph1990, Stephan1972], but it has also been shown in several studies that peripheral oscillators can be entrained by non-photic stimuli such as feeding-fasting cycles or variations in body temperature [Buhr2010, Damiola2000, Kornmann2007]. Peripheral oscillators are rather thought to be controlled by various humoral and neural signals via the hypothalamus-pituitary-adrenal gland axis [see review Son2011]. Stress signals or circadian cues from the SCN activate the paraventricular nucleus in the dorsal hypothalamus, which subsequently secretes corticotrophin-releasing hormone and arginine vasopressin. These act on the pituitary gland, causing it to produce and release adrenocorticotropic hormone, which in turn acts on the adrenal gland to initiate glucocorticoid production and release. Glucocorticoid then acts on an organism's circadian rhythm in two ways: (1) it regulates its own production level by signaling back to the SCN via a negative feedback loop and (2) it acts on peripheral oscillators by synchronizing them and producing rhythmic outputs, such as behavior, physiology, and metabolism [Nader2010] (Figure 6).

When peripheral tissues are removed from the SCN and adrenal gland, the synchronizing stimuli evidently cease to influence these oscillating cells. Bioluminometric studies have impressively shown this for various tissues such as heart, lung, liver, and kidney [Yoo2004]. For these studies, rodents were genetically modified in such a way that a luminescent reporter was linked to the expression of a core clock gene, e.g. *Per1* [Yamazaki2002, Yamazaki2009] or *Per2* [Yoo2004]. Experimental output is a photic signal which oscillates correlated to the expression of the reporter gene. Studies with explant cultures [Yoo2004] have shown that peripheral tissues exhibit a stable circadian rhythm for several days *in vitro*, but this rhythm is gradually dampened in period length due to the missing synchronizing stimuli provided by the SCN and subsequently the adrenal gland. Circadian oscillation of these explant cultures can, however, be reinitiated by providing external stimuli such as a serum shock or a synthetic glucocorticoid agonist such as dexamethasone [Balsalobre1998].

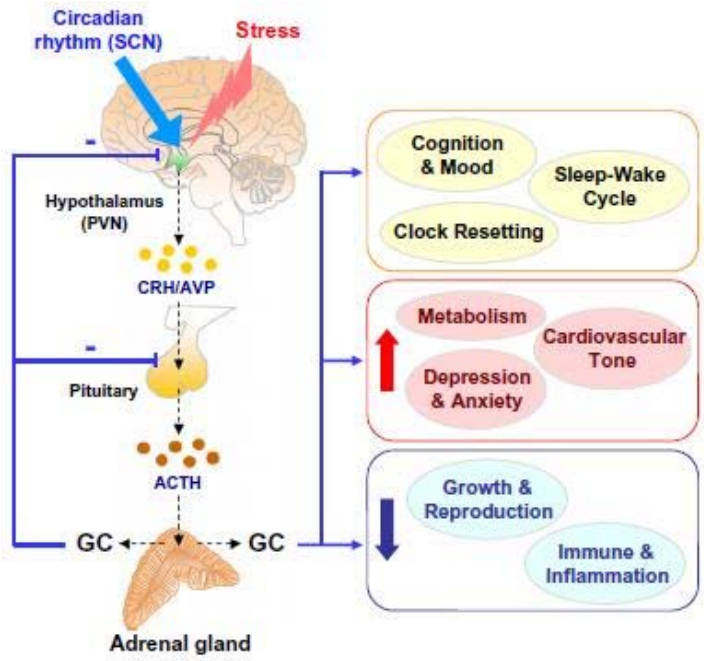

Figure 6 Signalling pathway and influence of the SCN on glucocorticoid production of the adrenal gland Stress signals or circadian cues from the SCN activate the paraventricular nucleus (PVN) in the dorsal hypothalamus, which subsequently secretes corticotrophin-releasing hormone (CRH) and arginine vasopressin (AVP). These act on the pituitary gland, causing it to produce and release adrenocorticotropic hormone (ACTH), which in turn acts on the adrenal gland to initiate glucocorticoid (GC) production and release. GC then acts on the circadian rhythm of an organism in two ways: (1) it regulates its own production level by signaling back to the SCN via a negative feedback loop and (2) it acts on peripheral oscillators by synchronizing them and producing physiologic outputs [Nader2010]. Courtesy of [Son2011]

1.2.2 Circadian rhythm in oncology

As the circadian clock gates cell replication and a dysfunctional cell replication is the essence of cancer, a dysfunctional endogenous clock is likely to play a role in tumorigenesis. Indeed, numerous studies have reported on altered rhythmic expression of core clock genes for a great variety of tumors such as gliomas, leukemia, lymphomas, lung cancer, prostate cancer, and breast cancer [JungHynes2010, Mazzaccoli2010, Oh2010, Pendergast2010, Shukla2011, Taniguchi2009, Xia2010, Yang2011]. Filipski et al. has shown in a mouse model that the destruction of the SCN leads to accelerated tumor growth of osteosarcoma and pancreatic adenocarcinoma [Filipski2003] and that chronic jet lag

accelerates tumor growth in the liver [Filipski2009a], while meal timing dampened the effect of chronic jet lag and slowed down tumor growth [Filipski2009b].

Other studies focusing on single circadian genes or melatonin have identified their specific roles in tumorigenesis or suppression of cancer development. Gery et al. [Gery2006] report on *Per1* to play a role as tumor suppressor, the expression of *Per1* being downregulated in several tumors, Hua et al. [Hua2006] and Zhang et al. [Zhang2008] describe the proliferation inhibiting and apoptosis inducing effects of *Per2*, and Fu et al. [Fu2002] report on *Per2*-deficient mice which are much more sensitive to γ-radiation and develop cancers thereafter much more frequently than irradiated wildtype control mice. Sharma et al. [Sharma2010] credit long-term melatonin administration with radioprotective effects. The role of a malfunctioning circadian clock seems evident in the development in cancer.

On the other hand, not just healthy tissue, but neoplastic tissue as well, has been shown to display a circadian rhythm concerning the proliferation rate, albeit not in phase with the circadian rhythm of the originating tissue [Klevecz1987a, Klevecz1987b, Barbason1998, Smaaland1995]. As cells are most sensitive to DNA damage when proliferating, this fact has given rise to the tempting concept of exploiting the shifted temporal sensitivity to maximize DNA damage in the tumor whilst reducing negative side-effects to the surrounding healthy tissue, regardless of whether by radio- and/or chemotherapy. Circadian rhythms have recently become the focus of clinical interest during chemo- and/or radiotherapy, as they influence the severity of side-effects. Rahn et al. [Rahn2011] and Shukla et al. [Shukla2010] have found that for radiotherapy of brain tumors and cervical cancer, the (therapy limiting) side-effect of mucositis is more severe when radiation is applied in the morning and evening, respectively. This is due to the fact that mucosal cells have a higher proliferation rate during these times of day, making them more radiosensitive. This also indicates that cell proliferation is subject to a circadian rhythm, a condition hypothesized to “shield” the DNA damage sensitive S-phase of the cell cycle from damaging ultraviolet light from the sun [Nikaido2007, Collis2007, Sharma2010]. Not just cell proliferation but also the reaction of cells to exogenous stimuli such as chemo- and/or radiotherapy via apoptosis is reportedly influenced by the time of day [Becciolini1997, Ruifrok1998, Ijiri1988, Ijiri1990].

The effects of radiotherapy on circadian rhythmic output have not just been studied on patient data, but were able to be reproduced in the laboratory with a variety of rodents (mice, rats and hamsters) and even cell lines, which have been reported to sustain an endogenous circadian rhythm in vitro. Oklejewicz et al. [Oklejewicz2008] have shown that ionizing radiation has a phase-shifting effect on rat1-fibroblasts and mice *in vivo*. Liver slice cultures [Yoo2004] as well as adrenal gland organ cultures [Oster2006, Andrews1971,

Andrews1964] have been shown to have a robust rhythm in culture, even after 20 days *in vitro* (div). Pancreas explant cultures show a robust bioluminometric rhythm in culture [Sadacca2011] as well as a circadian expression of major clock genes [Mühlbauer2004]. The pancreatic endocrine system as well as the exocrine system both have been reported to function rhythmically [Völkl1983, Maouyo1993, Peschke1998, Neuschwander-Tetri1996], irrespective of fasting. Irradiation of rhythmic biological test systems at different times of day therefore lead to different responses.

1.3 Organotypic slice cultures

Standard biological test models for drug and radiation research consist of various (immortal) cell lines, which can be kept in culture indefinitely, primary cell cultures which proliferate only a limited number of times, and of course animal *in vivo* models. Cell lines serve as an easy to handle testing system, they are usually made from a primary cell culture derived from an organism or biopsy. Due to mutations during the cell cycle and dedifferentiation, certain cells of these primary cultures outlive other cells, which die after a certain number of cell divisions. Eventually, cell lines consist of a few number of (robust) original cells, which keep dividing due to dedifferentiation, resulting in a (usually monolayered) immortal monoculture.

Cell lines offer several advantages, from their easy handling and maintenance in culture for a long time to their ability to rest in a frozen state indefinitely and come out with no losses concerning their reproductive ability. Yet cell lines have certain disadvantages, especially in light of patient treatment.

Cells in their physiological state are usually in close proximity to different types of cells, be them either parenchymal or stromal cells. The parenchymal cells of an organ are cells which, in a mature and differentiated state, carry out the function typical for that specific organ. The parenchyma is embedded into the stroma, which is composed of connective tissue and serves as a frame for the different parenchymas. In addition to being surrounded by many different cell types, cells in tissue are surrounded by the extracellular matrix and neighboring cells from all sides – as opposed to the monolayer culture representative of cell lines. They are also subject to an immune system, which can potentially intervene, mimicking *in vivo* conditions.

In order to analyse effects on biological material in a more physiological state, so called organotypic slice cultures (OSC), also known as precision-cut slices, can be used. OSC are made from primary tissue, maintaining the three-dimensional architecture of the tissue, thus ensuring that the extracellular matrix is conserved and remains functional. As compared to

cell lines, OSC allow us to study the reaction of tissues and organs in a more physiological state and, as compared to irradiation of whole animals, OSC allow us to elucidate the cellular and molecular mechanisms of the response to various agents, be them radiation or chemotherapeutic agents, in greater detail in a larger number of experimental specimens.

In addition to evaluating the effects of therapeutic measurements on pathological tissue, OSC of healthy tissue allow for the assessment of (long-term) treatment side-effects. The assessment of long-term radiation side-effects, especially the risk of secondary malignancies for example in paediatric cancer patients, is at the present determined by theoretical predictions due to the lack of experimental/ clinical data [Newhauser2011]. As yet, OSC of various organs and young donor animals can be kept in vitro for weeks and even months [Gähwiler1997]. Therefore, short- to mid-term side-effects could be evaluated. For the risk-assessment of secondary malignancies, current culturing conditions need to be optimized to keep OSC viable in vitro for months or years. However, even short- to mid-term OSC of healthy tissue will provide data regarding repair capacity (of individual cell types) and general response (to radiation) to aid in the risk-assessment of treatment side-effects.

The first tissue explants were cultured by Otto Warburg in 1923 [Warburg1923]. In these very first attempts to culture complete tissues, organs were manually cut into very thin slices of more than 0.3 mm thickness. As thickness is a crucial parameter for slices to stay viable in culture due to oxygen and nutrient transport [Parrish1995, Guo2007], noteable improvements in the culturing of tissue slices was not made until the 1980s, when Krumdieck [Krumdieck1980] invented a tissue chopper that would automatically prepare tissue slices of several tens of micrometers thick.

Liver OSC (OLSC) of rodents are mainly used for studies on metabolism [vanMidwoud2010, vanMidwoud2011], drug toxicity [deGraaf2010, Parrish1995, Vickers2009], cryopreservation [deGraaf2002, Martin2000, Martin2002, Rypka2006], and ischemia [‘tHart2005, Olinga1998]. The liver plays a major role in an organism's metabolism, and various studies have concluded the technique of OLSC to yield reliable results. OLSC have been used in drug toxicity tests ranging from everyday drugs such as caffeine [Berthou1989, Bienvenu1993, Warszawski1981] to more substantial drugs such as cocaine [Conners1989, Connors1990] to therapeutic side-effects of various pharmaceuticals [Vickers2009]. Finally, OLSC have been kept in hypoxic and other culturing conditions to optimize the procedure of organ transplants.

Histologically, the liver consists of roughly hexagonal-shaped lobules made of hepatocytes which are organized radially around a central vein in the center of the lobule. Portal triads, consisting of a bile duct, a terminal branch of the hepatic artery and a terminal branch of the

portal vein, are located at the vertices of the lobules. Different cell types found in the liver are hepatocytes, epithelial cells, endothelial cells, Kupffer cells and hepatic stellate cells (Ito cells). Hepatocytes are the parenchymal cells of the liver, epithelial and endothelial cells form the arteries and bile ducts, Kupffer cells are macrophages specific for the liver, and hepatic stellate cells are pericytes which are involved in the generation of fibrosis in the liver.

The viability of hepatocytes in OLSC for various times *in vitro* has been reported by various authors. Verrill et al. [Verril2002] report that hepatocyes of neonatal rat OLSC and human OLSC stay viable up to 3 weeks *in vitro* in a membrane based culture system, with a significant drop in viability after 10 div. In general, it seems the viability of neonatal rat OLSC resembles human OLSC viability *in vitro* more closely than murine OLSC [Verrill2002]. Hepatocytes of adult murine liver were found to die after 2-3 div, neonatal mouse hepatocytes having a similar survival as neonatal rat tissue [Verrill2002]. After 8 div, hepatic stellate cells are activated and form bile duct-like structures. This, however, was not seen in adult murine OLSC [Verrill2002]. Vickers et al. [Vickers2004] report of rat hepatocytes remaining viable up to 96 h *in vitro* (hiv) in a special culturing system, the tissue showing signs of repair via collagen deposition and an increased proliferation of biliary cells and hepatocytes after 48 hiv. After this time, the hepatic stellate cells peak in activity, indicating an active repair process. Olinga et al. [Olinga2001a,b] and de Kanter et al. [deKanter2002] have shown that Kupffer cells and endothelial cells of rat liver remain viable up to 24 hiv.

With the generation of transgenically altered laboratory animals, it has become possible to induce tumors more efficiently *in vivo*. As OLSC are produced from cores which get stamped from the liver, if the neoplasms have not infiltrated all of the liver, then it is possible to prepare OLSC from healthy and neoplastic tissue separately, subsequently co-culture them and expose them to the exact same experimental conditions. OLSC thus provide the possibility to evaluate the response of neoplastic and normal tissue to the same conditions without having to account for interindividual differences while providing information in a tissue environment.

In principle, OSC of pancreas can be prepared in much the same way as those from liver. However, as pancreas is a much less dense tissue than the liver, reports on pancreas OSC describe the necessity of supporting the tissue during the slicing procedure. For this, usually agarose is employed. While Meneghel-Rozzo et al. [MeneghelRozzo2004] and Speier and Rupnik [Speier2003] perfuse the pancreas with low-melting agarose to stabilize the tissue intrinsically, van Geer et al. [vanGeer2009] and Speier et al. [Speier2005] embed the

isolated pancreas in liquid low-melting agarose, let the agarose harden and then cut the agarose block with the unperfused pancreas inside.

Next to this method of preparing thin pancreatic tissue slices, several authors [Chen1954, Jones1967, Resau1983] also report of the pancreas being suited for explant cultures. Explant cultures are prepared manually cutting an isolated organ into smaller pieces without a defined thickness. As was mentioned for the liver, not every tissue is suited for (especially long-term) explant culture as the cells located at the inside of these explant cultures can easily be deprived of oxygen and nutrients. Jones [Jones1967] however, has reported on successfully culturing organotypic pancreas explant cultures (OPEC) for up to 9 div.

The pancreas is an endocrine and exocrine gland at the same time. The endocrine pancreas, the so-called Langerhans islets, is embedded in the exocrine pancreas, the acini. The Langerhans islets are composed of alpha cells, beta cells, delta cells, pp cells, and epsilon cells, which produce the hormones glucagon, insulin and amylin, somatostatin, pancreatic polypeptide, and ghrelin, respectively, which are released directly into the bloodstream [Elayat1995]. The exocrine pancreas is made up of acinar cells which are organized into clusters called acini. The acinar cells produce digestive enzymes, which they release into the lumen of the acini, from where they are transported in an extensive duct system into the duodenum. The duct system is lined with epithelial cells, which reach into the lumen of the acini, where they are called centroacinar cells.

A common concern encountered in OPEC is autolysis. The exocrine pancreas produces various digestive enzymes which it releases through an intricate duct system present throughout the whole pancreas into the duodenum. These enzymes are needed to digest food and other incorporated substances, but can cause substantial damage to the tissue if released, causing the tissue to – simply put – digest itself, a process also known as autolysis. Pancreatitis, the clinical condition of a pancreas which leaks digestive enzymes into the surrounding tissue, is a life-threatening condition.

Due to the mechanic trauma of cutting, digestive enzymes naturally get released into the tissue and culturing medium in OPEC preparation. Jones [Jones1967] has reported on the autolytic response of OPEC from different species. In his experiments, the acinar organisation of rat and hamster pancreas deteriorated, after its deletion, islet tissue became unrecognizable, and overall cultures were a mass of dissociated cells after 10 hiv. Murine OPEC, on the other hand, did not display any signs of autolysis, even after 9 div. Autolysis in autolysis-prone pancreata can be avoided by adding protease inhibitors to the culturing medium [Sadacca2011].

1.4 Aims of this thesis

OSC represent a link between biological test models previously employed in radiation research, the cell culture and whole animal irradiation. From the abundance of organs potentially threatened by developing neoplasms, the organs focused on in this thesis are the two organs with the bleakest prognosis: liver and pancreas. While already an established model system in research areas of drug toxicity or diabetes mellitus, OSC are rather unknown in radiation research. This thesis means to elucidate the significance of OSC for comparing radiation side-effects of carbon ions and X-rays. Additionally, OSC are evaluated for a possible response difference due to irradiation at different times of day and possible phase shift caused by radiation.

In order to evaluate whether liver and pancreas remain rhythmic *in vitro*, OLSC and OPEC were prepared from transgenic *Per2*^{luc} mice. In these mice, a bioluminescent reporter gene gives information on the rhythmic expression of the core clock gene *Per2*. OLSC and OPEC prepared at different times of day are bioluminometrically measured for a certain period of time prior to and post-irradiation. Rhythmic recordings indicate a rhythmic output of the reporter gene, indicating a rhythmically functioning OLSC or OPEC. Subsequently, mice were killed at two different circadian timepoints so that their circadian time will differ when irradiated simultaneously.

First irradiation experiments were performed with X-rays, as X-rays are the standard reference radiation type in clinical radiation research. Melatonin-proficient adult C3H mice were used as donor animals. These mice are healthy, radiation experiments were thus performed to elucidate the side-effects of radiation damage on healthy liver and pancreas tissue. The radiation response was determined via immunohistochemistry. Biological effects analyzed were proliferation, apoptosis, and DNA damage. Especially for the analysis of DNA damage, OSC and OEC were fixed 1 h and 24 h post-irradiation. Changes in the amount of positively labelled cells give information on the repair capacity of the different tissues. As hepatocytes are known to be radioresistant, irradiation doses of 2 Gy, 5 Gy, and 10 Gy were applied, 2 Gy being the standard clinical dose applied in a single fraction.

Finally, ^{12}C irradiation experiments were performed with a spread out Bragg peak (SOBP). After the X-ray experiments had been completed, the chance arose to prepare OLSC and OPEC from double transgenic mice with an inducible liver tumor, offering the chance to not only evaluate the side-effects of ^{12}C on healthy liver, but also the effect of ^{12}C on tumor tissue. The ^{12}C irradiation experiments were therefore carried out with co-cultured OSC of normal and neoplastic liver from these transgenic mice. The comparison of the quantitative results with regard to the different radiation types was subsequently only carried out for the

healthy livers. Similar relative frequencies of positively labelled cells in the controls showing no significant differences in the individual biological markers were prerequisite for the comparison of effects of the different radiation types. In addition to the comparison of tissue responses to different radiation types, OLSC of the double transgenic tumor mouse model offered the chance of a direct *in vitro* comparison of malignant and normal tissue to ^{12}C.

2 Simulations of nuclear beams in matter

Any therapy is usually accompanied by negative side-effects which will affect a patient's well-being up to the point at which therapy may have to be interrupted or terminated. It is therefore necessary to keep side-effects as minimal as possible. One possibility to limit side-effects in radiotherapy is to apply the prescribed dose as conformal to the tumor as possible and thus spare the surrounding healthy tissue. Heavy ions, such as ^{12}C, fulfil this requirement already by their depth-dose profile, characterized by a sharp dose fall-off at the end of their track, the so-called Bragg peak. Depending on the beam delivery system and the inhomogeneous target to be irradiated, treatment planning codes which calculate the energy loss in matter are required to establish tailored individual treatment plans.

The implication of such codes strongly depends on the type of beam delivery system (active/passive), the type of projectile used (proton, heavy ion), and the biological effective dose. Apart from these factors which influence the design of a treatment planning code, two main trends to realize such calculations have emerged: deterministic codes and Monte Carlo codes. Deterministic codes for the stopping power of ions in matter implement equations that result in the stopping power given a certain particle energy. Monte Carlo codes on the other hand use cross sections for the interaction probability of each ion that passes matter. The path an ion will take in matter or the damage it produces may always be a little different, as the interaction processes are generated at random, following only the probability of this interaction to take place.

Both models have advantages and disadvantages. An important argument for deterministic codes is that they calculate depth-dose profiles much faster than Monte Carlo codes, ruling Monte Carlo codes out for clinical use. On the other hand, deterministic codes are based on empirical information and it is thus difficult to extend these models to conditions other than those to which they were originally fitted. Alternatively, Monte Carlo codes, using only cross sections, may calculate interactions of different ions with many different, inhomogeneous target materials rather easily, as long as transport cross sections are known.

In this thesis, several codes (TRiP98, ATIMA, TRIM, MCHIT) were used to calculate the depth-dose profile as well as the mean LET-values of the single Bragg peaks comprising the spread-out Bragg peak (SOBP). This SOBP was applied to irradiate the organotypic healthy and neoplastic liver slice cultures (OHLSC and ONLSC, respectively) at GSI with ^{12}C. Where possible, the fragmentation yield was also calculated. The primary aim for the

simulation of the OHLSC and ONLSC irradiation with these codes was to offer a direct comparison between the results acquired with a deterministic model (TRiP98) and Monte Carlo model (MCHIT). This comparison was extended by the simulation with TRIM, a widely popular Monte Carlo code for simulating the effects of ions penetrating matter. ATIMA served as a deterministic complement to TRIM.
This chapter is organized as follows: in the first section, the different codes are introduced. The second section gives a detailed description of the beam line setup for the irradiation of the OHLSC and ONLSC at GSI. In the third and last part of the chapter, the results from the different codes are presented and discussed.

2.1 Codes to calculate energy loss in matter

2.1.1 TRiP98

TRiP98 (TReatment planning for Particles) is a code designed at GSI specifically for patient irradiation at GSI, i.e. for an active beam shaping system including a ripple filter [Weber1999] and carbon ions (Krämer2000a, Krämer2000b, Krämer2006). It calculates the distribution and energy loss of primary and secondary particles through water as a function of depth.
TRiP98 is a code that uses deterministic equations based on experimental data of energy loss of carbon ions in water. For practical uses, energy loss values for primary energy values between 50-500 MeV/u in 10 MeV/u increments are calculated only once and stored in tables. Energy loss values for energy values in between these precalculated values are calculated via linear interpolation. As the energy loss calculations are based on measurements in water, the patient treatment plans are calculated by converting air, bone, muscle, fat, etc., which the particles pass until reaching the tumor, into water-equivalent targets. The RBE of carbon ions is incorporated into TRiP98 via the Local Effect Model (LEM) [Scholz1996a, Scholz1996b, Scholz1997], which calculates the biologically effective dose based on the response of cells to X-ray irradiation, the structure of a heavy ion track and the size of a cell nucleus.

2.1.2 ATIMA

Atima is a deterministic code developed at GSI. Amongst other physical parameters characterizing the transition of ions through matter, it calculates particle energy loss in an energy range from 1keV/u up to 450 GeV/u. At energies above 30 MeV/u, ATIMA calculates the stopping power from the relativistic theory of Lindhard and Soerensen,

including shell corrections, a Barkas term, and the Fermi-density effect [ATIMA]. At energies below 10 MeV/u, the stopping power is calculated according to an older version of SRIM (see section 2.1.1). For the stopping power of ions with a primary energy between 10-30 MeV/u, ATIMA interpolates between the two theories.

2.1.3 TRIM

TRIM (TRansport of Ions in Matter) is a Monte Carlo computer program which calculates the slowing down and scattering of energetic ions in amorphous targets [Ziegler1985]. It calculates the ion range, damage distributions, angular and energy distributions of backscattered and transmitted ions in an energy range of 0.1 keV up to several MeV. The energy loss is calculated by nuclear and electronic scattering incidences.

For the sake of computer-time, TRIM works with two main approximations: 1) atom-atom collisions are simulated using the analytic so-called "Magic Formula", and 2) between collisions, particles are assumed to move in straight free-flight-paths. The „Magic Formula" allows to calculate the scattering angles of ions and target atoms using only the impact parameter, the charge of the ion and target atom, the distance of closest approach, and a correction factor. The free-flight-paths concept makes use of the fact that TRIM only calculates collisions above a defined minimum energy transfer. Any collisions above this minimum energy transfer are considered to lead to negligible energy loss of the ion and negligible deflection angles [Ziegler2008]. TRIM does not calculate fragmentation, either of primary ions or target atoms.

2.1.4 MCHIT

MCHIT (Monte Carlo model for heavy-ion therapy) is a program developed at the Frankfurt Institute for Advanced Studies (FIAS) by Igor Pshenichnov. It calculates the energy loss of charged particles in matter via Monte Carlo calculations based on the GEANT4 toolkit (Pshenichnov2005).

All calculations are based on the Bethe-Bloch formula, taking into account shell corrections and the density effect. For electromagnetic processes of primary and secondary particles, MCHIT employs a GEANT4 set of equations called „standard electromagnetic physics". For electrons and positrons, this includes Bremsstrahlung as well as annihilation processes. MCHIT does not calculate low-energy electromagnetic processes. It allows photons to interact via photoeffect, Compton effect, and pair production. Charged particles interactions considered are multiple scattering, ionization energy loss and hadronic interactions. Elastic scattering and inelastic scattering comprise hadronic interactions, processes which are energy dependent (Mishustin2010).

As MCHIT is a code employing Monte Carlo methods, its calculations are rather time-consuming. At the present state of technology, this has ruled out the use of Monte Carlo codes in routine clinical application for treatment planning. However, calculations with MCHIT reproduce experimental data of energy loss of primary particles very well [Pshenichnov2008], as well as fragmentation [Pshenichnov2005, Pshenichnov2010] and subsequently, PET monitoring [Pshenichnov2007]. Therefore, it is currently a well-suited program to check results from therapy irradiations.

2.2 Beamline setup at GSI

The OLSC and OPEC were irradiated at the former patient irradiation site, Cave M, at GSI. The beam delivery system at GSI is characterized by its active raster scan technique [Haberer1993]. A three-dimensional structure to be irradiated is divided into several slices in longitudinal direction. Primary particles of predefined energies stop inside these slices. Each slice, however irregularly shaped, is scanned in horizontal and vertical direction by deflecting magnets.

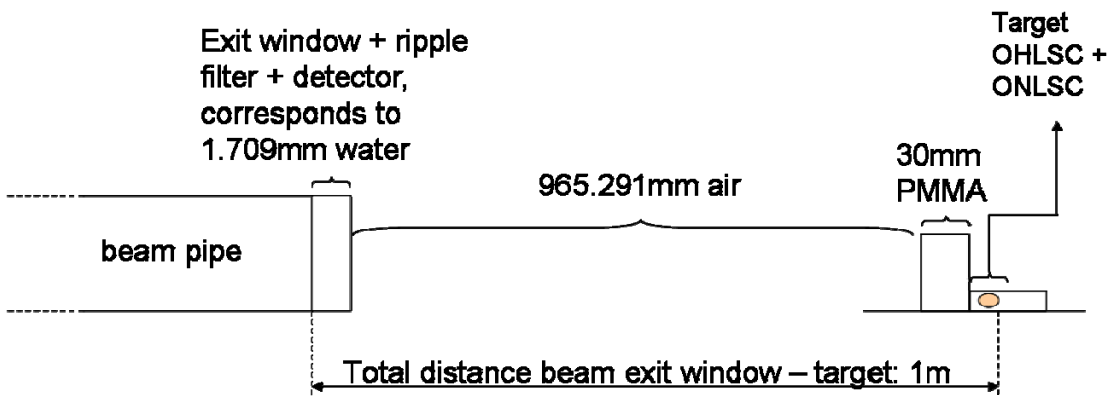

Figure 7 Beamline setup in Cave M at GSI. After having been accelerated, carbon ions pass through the exit window, ripple filter, and detector towards the OHLSC and ONLSC. These are irradiated with a spread-out Bragg peak (SOBP). After the particles pass through air, they still have too much energy to stop inside the OHLSC and ONLSC, and are thus decelerated further by a PMMA bolus.

For therapy, energies for ^{12}C range from 80 MeV/u to 430 MeV/u (Krämer2000). Particles are accelerated to these energies by first being accelerated by the UNILAC, which preaccelerates particles up to 11.4 MeV/u. Following, particles are fed into the SIS, which accelerates particles up to the needed energy for irradiation. Once particles are brought up to the right energy, they exit the beam line through the exit window and hit the target (Figure 7). The matter particles pass through behind the exit window are important parameters for calculations with codes, as they calculate the particle energy loss before the particles have reached the critical target. The material, thickness and density of the individual elements for the irradiation of OHLSC and ONLSC are given in Table 1. All

materials in front of the OHLSC and ONLSC amounted to a water-equivalent thickness of 39.45 mm.

Table 1 Parameters of materials used according to their position in beamline (see Figure 7) for ^{12}C-irradiation of OHLSC and ONLSC.

Position in beamline	Material/element	Density (mg/cm³)	Length (mm)	Water-equivalent length (mg/cm²)
1	Exit window, ripple filter, detector	-	-	170.9
2	Air	1.204	965.291	116.221
3	PMMA	1.16	30	3450
4	Polystyrene	1.04	1	104
5	Air	1.204	1	0.1204
6	Polystyrene	1.04	1	104
7	Tissue (modeled as water)	1000	16	1600

The SOBP for the ^{12}C-irradiation of OHLSC and ONLSC consisted of 26 single Bragg peaks. The energies ranged from (95.67-180.89) MeV/u. In a water target, this corresponds to particle ranges from approximately (20-70) mm (Figure 8A). The OHLSC and ONLSC were located at approximately (40-56) mm, and were thus completely within the range of the SOBP.

2.3 Results and discussion

Dose-depth distributions and mean LET-values for the 26 individual Bragg peaks comprising the SOBP were calculated with the four different algorithms mentioned above (section 2.1). The depth-dose distribution calculated with TRiP98 was used for the irradiation of OHLSC and ONLSC (Figure 8A). The mean LET ranges between approximately 50-120 keV/µm with a sharp maximum of approximately 275 keV/µm at the distal end of the SOBP. The dose is homogeneously 2 Gy for almost the complete SOBP. Only at the very end of the SOBP (correlating with the highest LET) the dose has a small peak (approximately 2.2 Gy), and then falls off steeply to approximately 0.2 Gy. This low dose behind the SOBP is due to fragments. Fragmentation of the projectile is calculated with the GSI in-house program YIELD (Krämer2000). Nuclear fragments created in

fragmentation of target nuclei have much lower kinetic energies in the laboratory system compared to projectile fragments and stop in target material very close to their production point. Therefore, TRiP98 does not simulate such target fragments.

The mean LET-values from the ATIMA calculations increase seemingly linearly in a range between 80-90 keV/µm. The Bragg peak from primary energy 131 MeV/u is a little higher. This does not influence the dose-depth distribution, however. The dose distribution generated from ATIMA calculations ranges between 2.1-2.5 Gy, gradually increasing with increasing primary particle energy. This is due to the fact that ATIMA does not calculate either projectile or target fragmentation. As will be shown further on, projectile fragmentation especially at the distal part of the SOBP is extensive (Figure 9).

Of the four codes, TRIM results in the most irregular dose-depth distribution. The dose of the SOBP ranges between 2.0-2.5 Gy with large and unsystematic ripples in the distribution. These come from the superposition of the LET-values from the individual Bragg peaks and the ripple filter approximation. The ripple filter was incorporated into these calculations as an additional 1 mm, 2 mm and 3 mm of water before the actual material list. Due to this discrete ripple filter and the internal binning of the program TRIM, the individual Bragg peaks show two ripples before the highest LET-value. The superposition of these rippled peaks leads to the irregularly shaped dose-depth distribution. Despite the irregularly shaped dose-profile, the dose generally increases with increasing depth. As in the case of ATIMA, TRIM does not take fragmentation into account causing a linear increase of dose.

The MCHIT dose-distribution resembles the TRiP98 dose distribution most. The dose in the SOBP is calculated homogeneously at approximately 2.1 Gy, a little higher than TRiP98 results. There is also a slightly higher dose at the distal end of the SOBP, corresponding to the Bragg peak of the highest primary particle energy, before a sharp fall off of dose to about 0.2 Gy. This residual dose again stems from fragments, which have a longer range and deposit energy in the target behind the SOBP.

The LET-depth profiles of TRiP98 and ATIMA show increasing peak values at longer penetration depths, corresponding to particles with a higher primary energy. Bragg peaks calculated with TRIM are unsystematic, again due to the distinct implementation of the ripple filter. The Bragg peaks calculated with MCHIT, characterized by decreasing peak values, are directly opposed to the increasing LET values calculated with TRiP98 and ATIMA. While TRiP98 and ATIMA calculate the linear energy transfer, i.e. the energy transfer from the primary ions to the target material, MCHIT calculates the linear energy deposition, i.e. the energy deposited in the material. As MCHIT also calculates the

fragmentation of primary ions as well as delta electrons, the energy deposition values decrease at longer ranges due to the fact that less ions reach these depths.

MCHIT calculates the fragments of projectile ions and target atoms depending on penetration depth of the primary particles. The fragmentation for an exemplary fluence of $5.2 \cdot 10^7$ particles/cm² at an energy of MeV/u is given in Figure 9. The yield of most fragments reaches a peak at a depth of 50-60mm. Only He-ion fragments reach their production maximum a little farther on at approximately 70mm. The maximum yields (in % of original primary particles) are given in Table 2.

To analyze whether the increasing dose of the ATIMA calculation depends mainly on the neglected fragmentation process, a correction to this calculation was performed using the fragmentation yield obtained from the MCHIT calculation. The energy distribution of any fragment type is rather broad at any depth *x*, as the fragments there a) may just have been produced, b) are traversing this depth *x,* or c) may have been produced at a proximal depth and come to a stop at depth *x*. An accurate correction would therefore need to determine the energy distribution of each fragment as a function of depth and then calculate the average LET as a function of depth in order to finally obtain depth-dose profiles from each fragment. These single depth-dose profiles for all fragments added to the depth-dose profile of the ^{12}C-projectiles would result in an accurate correction considering fragmentation.

However, due to matters of time and complexity, a simpler correction was chosen for the ATIMA depth-dose profile. First, the reduction in the number of primary carbon ions as calculated by MCHIT (Figure 9A) was multiplied to the ATIMA depth-dose profile. Second, MCHIT was used to calculate an average depth-dose profile for all fragments. Subsequently, a correction factor C as a function of depth x was estimated in order to determine the contribution of fragments to the total dose:

$$C = \frac{D_{fragments}(x)}{D_{^{12}C}(x)}. \tag{2.1}$$

Here, $D_{fragments}(x)$ is the estimated dose from fragments at depth *x* as calculated by MCHIT, $D_{12C}(x)$ is the dose from primary carbon ions at depth *x* as calculated by ATIMA and corrected by the reduced number of primary ions from MCHIT. Finally, the dose from carbon ions and fragments was added at each depth *x* in order to give the total dose (Figure 10). As can be seen, including fragmentation does not lead to a more accurate depth-dose profile of the SOBP, but rather underestimates the absorbed dose. Only fundamental differences in the programs' algorithms can account for these deviations from the ideal SOBP depth-dose profile. Such differences are the basic design as deterministic (ATIMA) or Monte Carlo (MCHIT) codes as well as the physical models employed at different

energies, such as an interpolation between two theories/codes at energies between (10-30) MeV/u for ATIMA and a detailed consideration of various physical effects at this energy as in MCHIT (subsections 2.1.2 & 2.1.4)

In conclusion, the comparison of this SOBP model calculation of a water target shows that the best results are given by programs which are specially designed for this purpose with regard to a medical application (TRiP98 and MCHIT). More general programs, such as ATIMA and TRIM, which are mainly used in atomic physics, give an approximation of the depth-dose profile. Yet even accounting for the most prominent difference of these programs – the fragmentation – does not improve the result. While TRiP98 may still be superior to MCHIT for now, if not in the final result but in computer calculation-time, MCHIT may prove valuable for checking dose-application after therapy sessions and even therapy planning itself, depending on the advancements in technology, i.e. improvements on computational costs and time.

Table 2 Yield of primary projectiles (^{12}C) in water target

Depth in water (mm)	% of primary particles
5	98,9
10	96,6
15	94,4
20	92,1
25	87,3
30	82,1
35	76,6
40	71,1
45	64,5
50	58,3
55	51,2
60	42,4
65	32,3
70	16,9

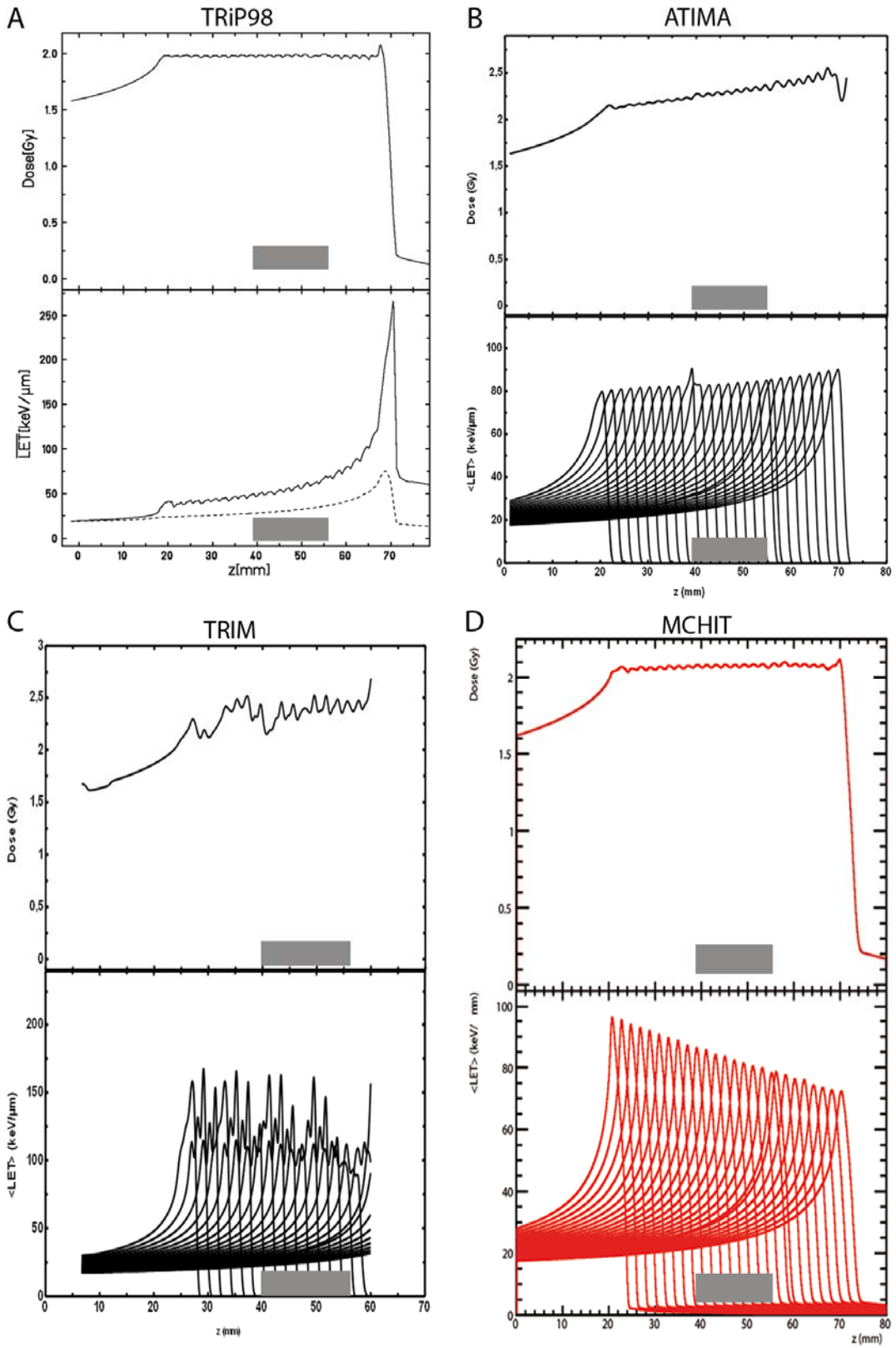

Figure 8 Depth-dose distributions and individual Bragg peaks of SOBP. Shown are mean LET values of 26 Bragg peaks comprising the SOBP and corresponding depth-dose distributions. Grey bar denotes OHLSC and ONLSC, located at approximately 40-56mm. (A) TRiP98 calculations. OHLSC and ONLSC were irradiated according to this result, which served as a reference for the other code calculations. (B) ATIMA calculations. (C) TRIM calculations. (D) MCHIT calculations.

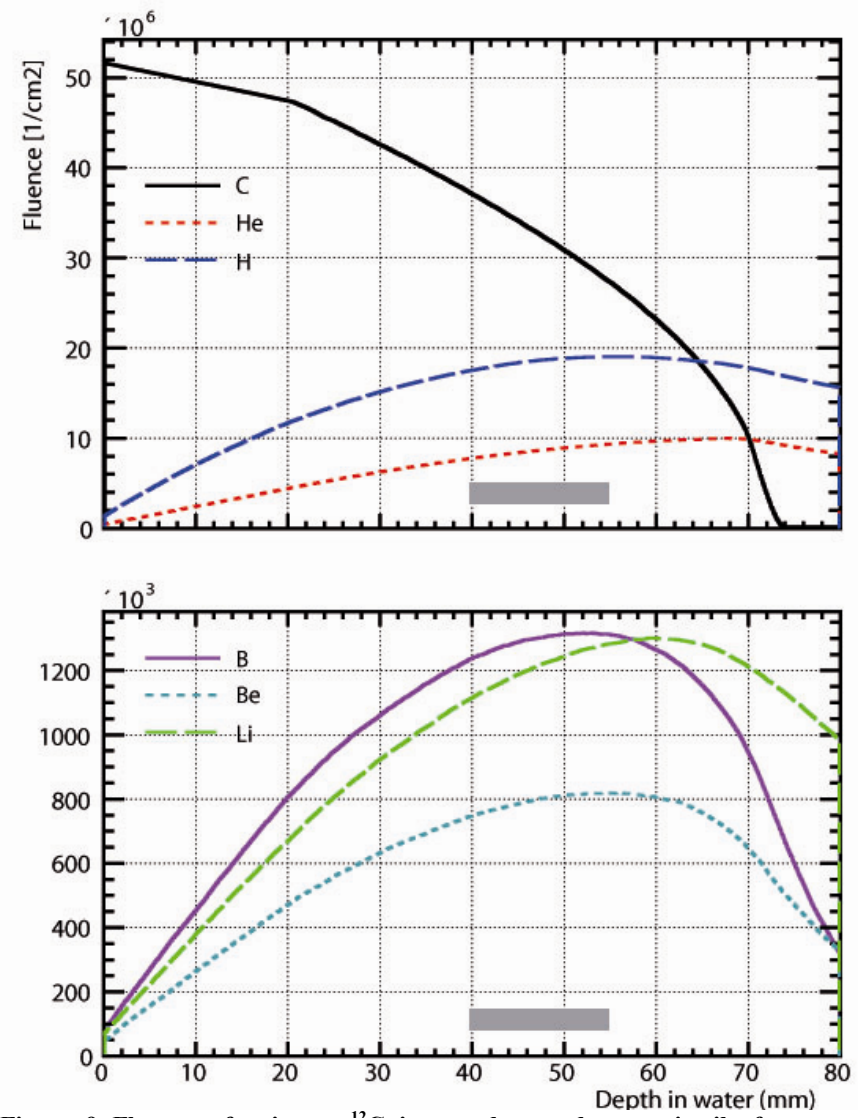

Figure 9 Fluence of primary ^{12}C ions and secondary projectile fragments depending on depth in water. OHLSC and ONLSC are denoted by grey bar. In the OHLSC and ONLSC, the percentage of fragments from incident primary ions and secondary fragments are as follows: C: ~56-74%, B: ~2.4-2.5%, Be: ~1.4-1.5%, Li: ~2.1-2.4%, He: ~15-30%, p: ~32-34%

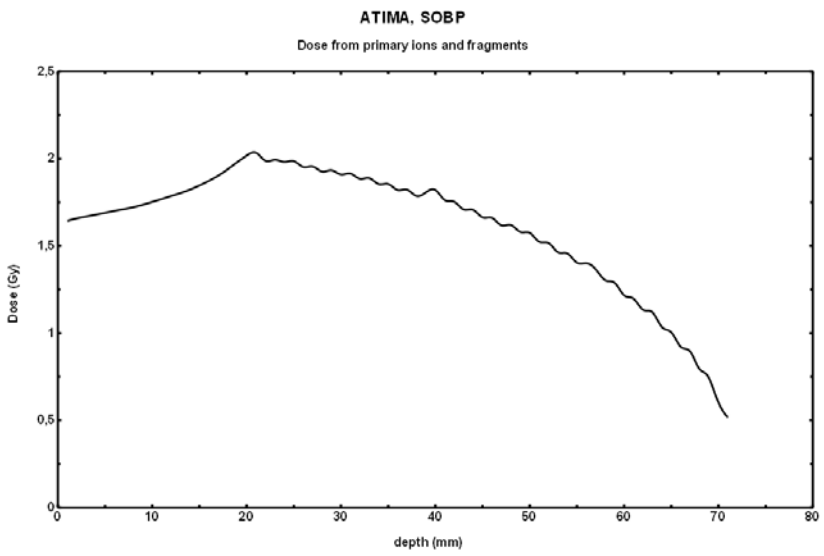

Figure 10 Depth-dose profile of ATIMA-SOBP with correction for fragments. The original ATIMA calculation of the SOBP with linearly increasing dose was corrected using the fragmentation from MCHIT calculations. The dose decreases with increasing depth and only reaches a value of 2 Gy at the very beginning of the SOBP.

3 Materials and Methods

3.1 Animals

3.1.1 C3H wildtype mice

X-ray experiments were performed using liver and pancreas from adult male C3H/HeNHsd wildtype (wt) mice, aged 8-14 weeks. All C3H wt mice were purchased from Harlan (Horst, Netherlands).

3.1.2 Transgenic mice

Double transgenic c-myc/TGF-α mice with an inducible liver tumor were generously supplied by Dr. Piiper (Innere Medizin, Universitätsklinikum Goethe Universität Frankfurt am Main). The manufacturing of these transgenic mice is described in [Murakami1993]. The manufacturing of the *Per2*^{luc} mice used for bioluminescence studies is described in [Yoo2004]. *Per2*^{luc} mice were kindly provided by Charlotte von Gall (Institut für Anatomie II, Universitätsklinikum Goethe Universität Frankfurt am Main).

The proliferation and apoptosis rate in liver and pancreas *in vivo* was assessed as a by-product of an experiment with wildtype (wt) Bmal1-knockout mice. Transgenic animal strains were bred in the Zentrale Forschungseinheit of the Universitätsklinikum Goethe Universität Frankfurt am Main.

3.1.3 Housing of animals prior to organotypic slice/explant culture preparation

All experiments with animals performed in this thesis were conducted in accordance with the policy on the use of Animals in Neuroscience Research and the Policy on Ethics as approved by the Society for Neuroscience and by the Directive of the European Union (2010/63/EU).

Prior to tissue culture preparation, all mice were kept in a 12h light/12h dark cycle (LD12:12) for at least two weeks. The time of lights on is defined as *zeitgeber* time (ZT) 00. Prior to tissue preparation, the animals were released into constant darkness (DD) for at least one complete circadian phase. Circadian time (CT) 00 is defined as lights on in the previous LD cycle. During the whole time period, all animals had access to food and water *ad libitum*. The C3H wildtype and *Per2*^{luc} mice were grouped up to three animals per cage, the c-myc/TGF-α mice were kept in individual cages.

3.2 Preparation of organotypic slice/ explant cultures

3.2.1 Preparation of organotypic liver slice cultures for irradiation experiments

For the preparation of organotypic liver slice cultures (OLSC), normal livers of adult C3H wt (10-14 weeks old at tissue explantation) and neoplastic livers of adult c-myc/TGF-α mice (about 6 months old at tissue explantation) were sliced with a Krumdieck tissue chopper (TSE Systems, Bad Homburg, Germany). Neoplastic and healthy liver parts of the c-myc/TGF-α mice were sliced separately to distinguish the radiation effects of normal and neoplastic liver. In the following, organotypic slice cultures from healthy transgenic liver will be abbreviated OHLSC, organotypic slice cultures from neoplastic transgenic liver will be abbreviated ONLSC.

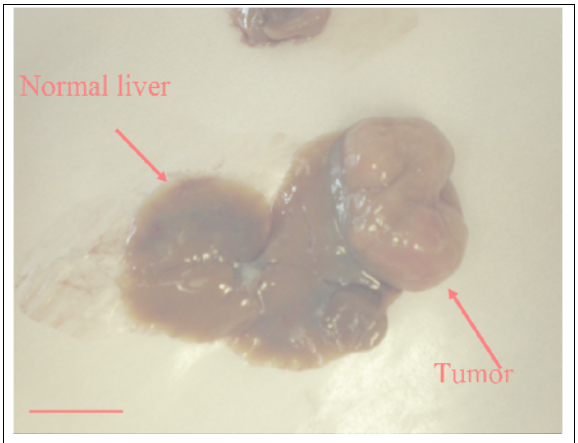

Figure 11 Freshly excised liver from a c-myc/TGF-α mouse Representative image of a freshly excised liver bearing a tumor on the right side. Thus, healthy and neoplastic liver can easily be distinguished macroscopically and healthy organotypic liver slice cultures (OHLSC) and neoplastic organotypic liver slice cultures (ONLSC) can be prepared separately. Bar denotes 1 cm. Courtesy of C. Schmithals.

Mice were sacrificed according to their circadian timepoint by decapitation and the inner organs were exposed via an abdominal incision. With sterile tweezers and scissors, the liver (including the tumor where applicable) was removed and placed in ice-cold Custodiol (a generous gift from F. Koehler Chemie AG, Bensheim, Germany). Cores of 8 mm in diameter were punched out from both liver regions. Identification of tumorous tissue was based on visual judgment depending on whether a macroscopic tumor could be seen (Figure 11). The cores were then placed in the fixture of the Krumdieck tissue chopper, and 250 µm-thick slices were prepared. The reservoir of the chopper was filled with ice-cold Hanks Balanced Salt Solution (Sigma-Aldrich, Steinheim, Germany). At the end of each run, slices were collected in a sterile Petri dish, placed on cell culture inserts (Falcon, Becton Dickinson, Franklin Lakes, NJ, USA), and then transferred to 6-well-plates (Falcon, Becton Dickinson, Franklin Lakes, NJ, USA) containing 1 ml prewarmed culture medium, modified according to [Verrill2002]. The medium consisted of DMEM (Gibco/invitrogen, Paisley, UK) supplemented with 10% fetal calf serum (invitrogen Corporation, Grand Island, NY, USA), 100 U/ml penicillin (Gibco/invitrogen, Paisley, UK), 0.1 mg/ml streptomycin (Gibco/invitrogen, Paisley, UK), 10 mmol/l HEPES (Sigma-Aldrich, Steinheim, Germany), 1 µg/ml insulin (Sigma-Aldrich, Steinheim, Germany),

8 µg/ml ascorbic acid (Sigma-Aldrich, Steinheim, Germany), and 20 mmol/l sodium pyruvate (Gibco/invitrogen, Paisley, UK).
Slices were incubated at 37°C and 5% CO_2. The medium was changed the following day, at least 2 h before irradiation.

3.2.2 Preparation of OLSC for bioluminescence experiments

OLSC of *Per2*^{luc} mice were prepared using a vibratome, model VT1000 S (Leica, Nussloch, Germany). The liver was explanted as described in section 3.2.1, placed in ice-cold Custodiol for transport to the vibratome and then glued to a mounting table with tissue adhesive Histoacryl® (B. Braun/Aesculap, Tuttlingen, Germany). The mounting table was inserted in and fastened to a dish filled with ice-cold Hanks' Balanced Salt Solution (HBSS) and 250 µm thick liver slices were cut. The slices were then placed on tissue culture inserts (Millipore, Tullagreen, Ireland), which were put in 35 mm Petri dishes filled with 1 ml prewarmed culture medium. The culture medium consisted of the same ingredients as described in section 3.2.1, only the DMEM (Invitrogen/Gibco, Paisley, UK) used in the bioluminometric experiments did not include phenol red. Additionally, the medium was supplemented with 1 µmol/ml luciferin (Promega, Madison, WI, USA).

3.2.3 Preparation of organotypic pancreas explant cultures

For the preparation of organotypic pancreas explant cultures (OPEC), the same mice as for the precision-cut liver tissue slices were used. After the trunk had been opened and before the liver was removed, the pancreas was removed and placed in ice-cold Custodiol (F. Koehler Chemie, Bensheim, Germany) in a Petri dish. Under sterile conditions, the pancreas was manually cut into pieces ~1 mm³ using a scalpel. Pairs of pancreas pieces of C3H wildtype mice or c-myc/TGF-α mice were placed in cell culture inserts (Falcon, Becton Dickinson), which were put in 6-well-plates (Falcon, Becton Dickinson, Franklin Lages, NJ, USA) containing 1 ml of prewarmed culture medium. The medium used for pancreas was the same as was used for normal and neoplastic liver slice cultures (see section 3.2.1). Pairs of pancreas pieces prepared from *Per2*^{luc} mice were placed on tissue culture inserts (Millipore, Tullagreen, Ireland), which were put in 35 mm Petri dishes filled with 1 ml prewarmed culture medium. The medium was the same as described in section 3.2.2.
All OPEC were incubated at 37°C and 5% CO_2. The medium was changed the following day, at least two hours before irradiation.

3.2.4 Preparation of organotypic adrenal gland explant cultures

Organotypic adrenal gland explant cultures (OAEC) were prepared from *Per2*^{luc} mice to serve as controls in the bioluminescence study. Procedure for OAEC preparation was the same as for the OPEC (see section 3.2.3), adrenals were excised after the pancreas, before the livers.

3.2.5 Perfusion of Bmal1-wt mice

The proliferation and apoptosis rate in liver and pancreas *in vivo* was able to be assessed as a by-product of an experiment with Bmal1-wt mice. These mice were intraperitoneally injected with 100 mg BrdU per 1 kg body weight on three consecutive days. At *zeitgeber* time (ZT) 02, animals were transcardially perfused with phosphate buffered saline (PBS) and subsequently with 4% paraformaldehyde (PFA). Livers and pancreata were excised and post-fixed with 4% PFA for 24 h before being placed in 15%, subsequently 30% saccharose prior to being cryosectioned.

3.3 Irradiation of tissue cultures

3.3.1 X-ray irradiation

Slices were irradiated at the patient irradiation site of the Frankfurt Universitätsklinikum. The electron accelerator (Model SL75, Elekta, Crawley, UK) was set to 6 MV and a dose rate of 4 Gy/min for all irradiations. The anode of the accelerator is made of tungsten, any filters used for patient irradiation were removed from the exit window. The electrons are accelerated and focused by a traveling wave, ensuring that any electrons not of the desired energy are prevented from hitting the anode.

The 6-well-plates containing the organotypic slice cultures (OSC) and organotypic explant cultures (OEC) (section 3.2) were irradiated by placing them on the patient bed at a distance of 100 cm directly below the exit window. Standard doses were 2 Gy, 5 Gy, and 10 Gy. The irradiation procedure lasted between 1-5 min, depending on the dose. For a one-time irradiation with a dose of 50 Gy, the irradiation procedure lasted ~13 min. Generally, the samples were out of normal culturing conditions for one hour at the most.

3.3.2 Heavy ion (^{12}C) irradiation

Heavy ion irradiation experiments were performed at Cave M at the GSI Helmholtzzentrum für Schwerionenforschung (GSI). Cave M is the former medical cave in which patient irradiation took place [Eickhoff1999]. Samples were irradiated with a spread out Bragg peak (SOBP), imitating a tumorpatient irradiation. An SOBP is achieved by superimposing Bragg peaks of different energies, covering the length of the tumor region (Figure 12). For the irradiation of OSC and OEC, particles are accelerated to energies between 95.67MeV/u -180.89MeV/u. To acquire this amount of energy, particles are pre-accelerated by a linear accelerator (UNILAC – UNIversal Linear ACcelerator) to 11.4MeV/u and are then injected into the GSI heavy ion synchrotron, the SIS 18. Without any additional materials in the beamline except for the exit window, the particles would pass through the OSC and OEC, located a few tens of cm behind the exit window, at a low linear energy transfer (LET) and could not be formed into an SOBP. To this end, an additional 30mm-bolus made of Poly(methyl methacrylate) (PMMA) was placed in the beamline so as to guarantee for the right LET inside the OSC and OEC.

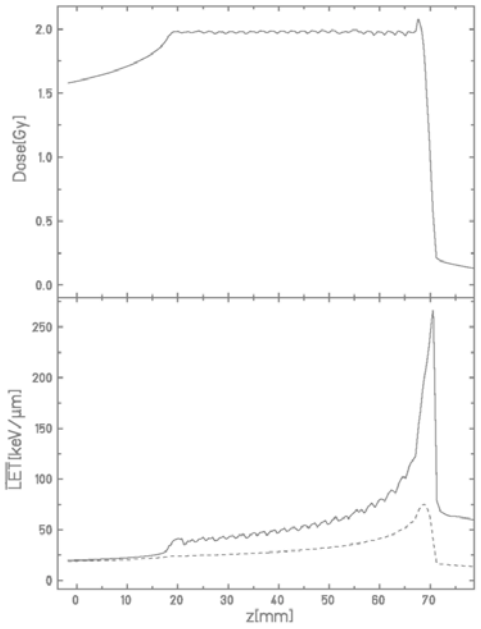

Figure 12 Calculation for SOBP of OSC and OEC. The lower graph depicts the calculation of the linear energy transfer (LET) of 26 particle shots with energies ranging from 95.67MeV/u-180.89MeV/u. The superimposed dose of each shot is given in the upper graph. Over a range of 50mm (20mm-70mm), the dose is homogeneously deposited in the OSC and OEC. Courtesy of M. Scholz.

The samples were irradiated in 6-well-plates in stacks of two. Only three wells of one side of the plate were filled with inserts. This ensured a homogeneous irradiation of all samples, as the side of the plate containing the insert was placed perpendicular to the beam direction. Three stacks of two plates each were irradiated in one round (~20-25min), two plates were mock-irradiated. Each round of samples was outside of the incubator for about 1h.

3.4 Histological and immunofluorescent staining

3.4.1 Cryosectioning

Before slices could be stained immunohistochemically, they were cryosectioned. Therefore, slices were cryoprotected in 15% and 30% sucrose (Applichem, Darmstadt, Germany) for at

least 24h each. For cryosectioning, the slices were embedded in Tissue Tek (Sakura Finetek Europe, Alphen aan den Rijn, Netherlands) and cut at -20°C into 10µm thick sections using a Leica cryostat (Leica, Nussloch, Germany). Sections were collected on Superfrost glass slides (Thermo Scientific, Braunschweig, Germany).

Each slice was sectioned in series, meaning that consecutive slices are found on consecutive glass slides. This ensures that part of the complete slice is always present on all glass slides and spatial patterns can efficiently be detected (see Figure 13).

Sections were stored at 4°C until staining.

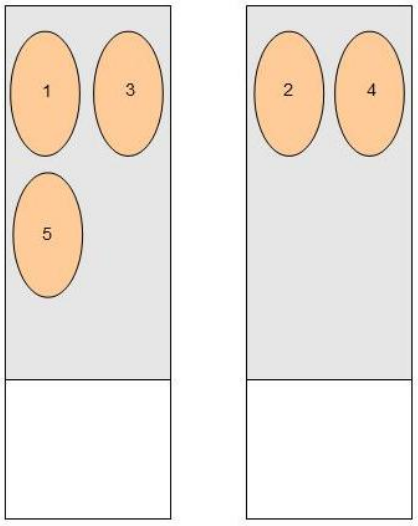

Figure 13 Schematic of a cryoseries. The OSC in this scheme is cut into five cryosections. The cryosections are arranged on two glass slides according to the given order: the first section is collected on slide 1, the second section on slice 2, the third section again on slide 1, the fourth section on slide 2. This pattern is repeated until the slice had been completely sectioned. Usually, slices were cut into 10 – 30 sections.

3.4.2 Histological staining – Hematoxylin-Eosin

For morphological analysis of the tissue cultures after several days *in vitro*, the standard histological hematoxylin and eosin (HE) staining was employed. Hematoxylin stains so-called basophilic structures, such as nuclei, blue. Eosin is an acidic dye which binds to the cytoplasm and dyes it pink.

For the HE staining, sections were immersed in Mayer's Hemalum (AppliChem, Darmstadt, Germany) for 14 min and subsequently washed with tap water for 10 min to turn the dye blue. Before staining the sections with eosin (Roth, Karlsruhe, Germany) for 30 s, they were shortly dipped in distilled water. After the eosin staining, sections were immediately placed in 70% ethanol to remove excess dye, then dehydrated in an ascending alcohol series (70%, 80%, 96%, 99% ethanol) for 2 min each and placed in xylene (Sigma-Aldrich, Steinheim, Germany). Lastly, the sections were mounted with Entellan (Merck, Darmstadt, Germany) and left to air dry before recording.

3.4.3 Immunofluorescent staining

For the immunofluorescent characterization of certain antigens in the tissues, an indirect staining method was chosen. For this method, an antigen-specific unconjugated (primary) antibody binds to the antigen to be analyzed. In order to visualize the binding sites of the antibody, a second antibody, which is labeled with a fluorophore and binds specifically to the primary antibody, was used. All primary and secondary antibodies used in this thesis are listed in Table 3.

In order for the primary antibody to bind, sections were prepared by rinsing them with 0.02 M phosphate buffered saline (PBS) to remove any left-over Tissue Tek. To reduce surface tension and to permeabilize the tissue, the sections were rinsed with PBS supplemented with 0.3% Triton X-100 (Sigma-Aldrich, Steinheim, Germany) (PBST) for 5 min. Thereafter, sections were incubated with 10% normal goat serum diluted in PBST for 30 min in order to block any unspecific binding sites. Sections were then washed with PBS and incubated with the primary antibody diluted in 0.5% albumin from bovine serum (BSA – Sigma, Steinheim, Germany)/PBST over night at room temperature. Subsequently, sections were rinsed with PBS three times for 5 min each to remove any excess primary antibody. They were then incubated for 1 h with the secondary antibody diluted in PBS. Thereafter, sections were rinsed twice for 5 min each with PBS, then stained with Hoechst (Sigma Aldrich, St. Louis, MO, USA) at a dilution of 1:10000 for 5 min and subsequently washed five times for 5 min each with PBS. Sections were mounted with Dako flourescent mounting medium (Dako, Glostrup, Denmark) and stored lightproof at 4 °C.

Table 3 Primary and secondary antibodies used for immunofluorescent staining

Primary antibody	Dilution	Secondary antibody	Dilution
Anti-BrdU Roche, Indianapolis, IN, USA mouse	1:50	Goat anti mouse Alexa Fluor 488 IgG Invitrogen, Eugene, OR, USA	1:200
Cleaved Caspase3 Cell Signaling Technology, Danvers, MA, USA rabbit	1:100	Goat anti rabbit Alexa Fluor 488 IgG Invitrogen, Eugene, OR, USA	1:500
Anti-Insulin Abcam Cambridge, UK guinea pig	1:100	Goat anti guinea pig Alexa Fluor 568 IgG, Invitrogen, Eugene, OR, USA	1:500
Ki67 DCS, Hamburg, Germany rabbit	1:200	Goat anti rabbit Alexa Fluor 488 IgG Invitrogen, Eugene, OR, USA	1:500
Phospho-H2Ax (γH2Ax) Cell Signaling Technology, Danvers, MA, USA rabbit	1:100	Goat anti rabbit Alexa Fluor 488 IgG Invitrogen, Eugene, OR, USA	1:500

3.5 Recording tissue-specific circadian rhythms via luminometry

For luminometric studies of circadian rhythms in OSC and OEC, transgenic *Per2*^{luc} mice were used. In *Per2*^{luc} mice, luciferase is expressed under the control of the *Per2* promoter. Thus, high expression of *Per2* subsequently leads to a high expression of luciferase. If the OSC and OEC medium is supplemented with luciferin, the luciferase will react with the luciferin, emitting photons. Therefore, high expression of luciferase, indicating a high expression of *Per2*, can be determined by the detection of a higher photon signal.

Per2^{luc} mice entrained to an LD12:12 cycle were sacrificed at CT06 and CT18. OLSC and OPEC were prepared as described in section 3.2.2 and 3.2.3. As positive controls, the adrenal glands were also harvested and taken – as a whole – into culture. Immediately after slice preparation, bioluminescence from a part of the prepared OLSC, OPEC, and OAEC from four animals was measured for 5d. During this time, the OLSC and OEC did not receive fresh medium. After 5d, these OLSC and OEC were discarded. Additional OLSC and OEC from these four mice were kept in normal culturing conditions for 7d, were then irradiated and subsequently measured for bioluminescence. The medium of the OLSC and OAEC irradiated at 7div was changed every other day prior to irradiation. OPEC which were not recorded

immediately after culturing begin but kept in standard culturing conditions to be irradiated at 7 div received a medium change every day to prevent autolysis (Figure 14A).

OLSC and OAEC from four additional mice were measured for bioluminometric activity for 24 h immediately after OLSC and OEC preparation. After this, the recording was interrupted, the medium was changed, the OLSC and OEC were irradiated, luciferin was replenished and the recording was recommenced (Figure 14B).

Photon emission was detected using a LumiCycle (Actimetrics, Wilmette, IL, USA). The LumiCycle is a light-tight box which is equipped with four photomultiplier tubes (PMTs), which record the photons emitted by the luciferin reacting with the luciferase expressed by the tissue. The PMTs are located about ¼ in. above the specimens. Photon counts were integrated over 10 min intervals. Background noise consisted of 30-40 counts/s at 35 °C. The LumiCycle was kept in an incubator at 37 °C and 5 % CO_2, enabling an experiment to run for several days. Air humidity was increased by placing Petri dishes filled with water inside the LumiCycle.

The data was collected in Microsoft Excel files and analyzed using the LumiCycle Analysis program, version 2.3 (Actimetrics, Wilmette, IL, USA). The analysis program was used to subtract background noise from the recorded data and to ascertain the periodicity of the recorded data. In order to remove the baseline drift from the raw data, the data were smoothed with an applied running average of 24 h.

A tissue-specific characteristic to describe the circadian rhythmicity is the period of the oscillatory bioluminescence. For the periodicity calculations, the data were fit to a damped sine wave. The spurious decay present at the start of each recording, due to the tissue slices adjusting to the culturing condition, was omitted from the part of the reading used for these calculations. For the OSC and OEC recorded before irradiation, the data were pooled according to the time of death of the donor animals. Due to synchronization of the circadian rhythms via medium exchange prior to irradiation, the data were pooled depending on whether OSC and OEC had been irradiated or not.

Phase maps were used to analyze whether radiation has a phase-shifting effect on liver OSC. Mapped are the time of day of the peaks in bioluminescence between 12 h and 36 h *in vitro* before and after irradiation, respectively, as described in [Yoo, 2004].

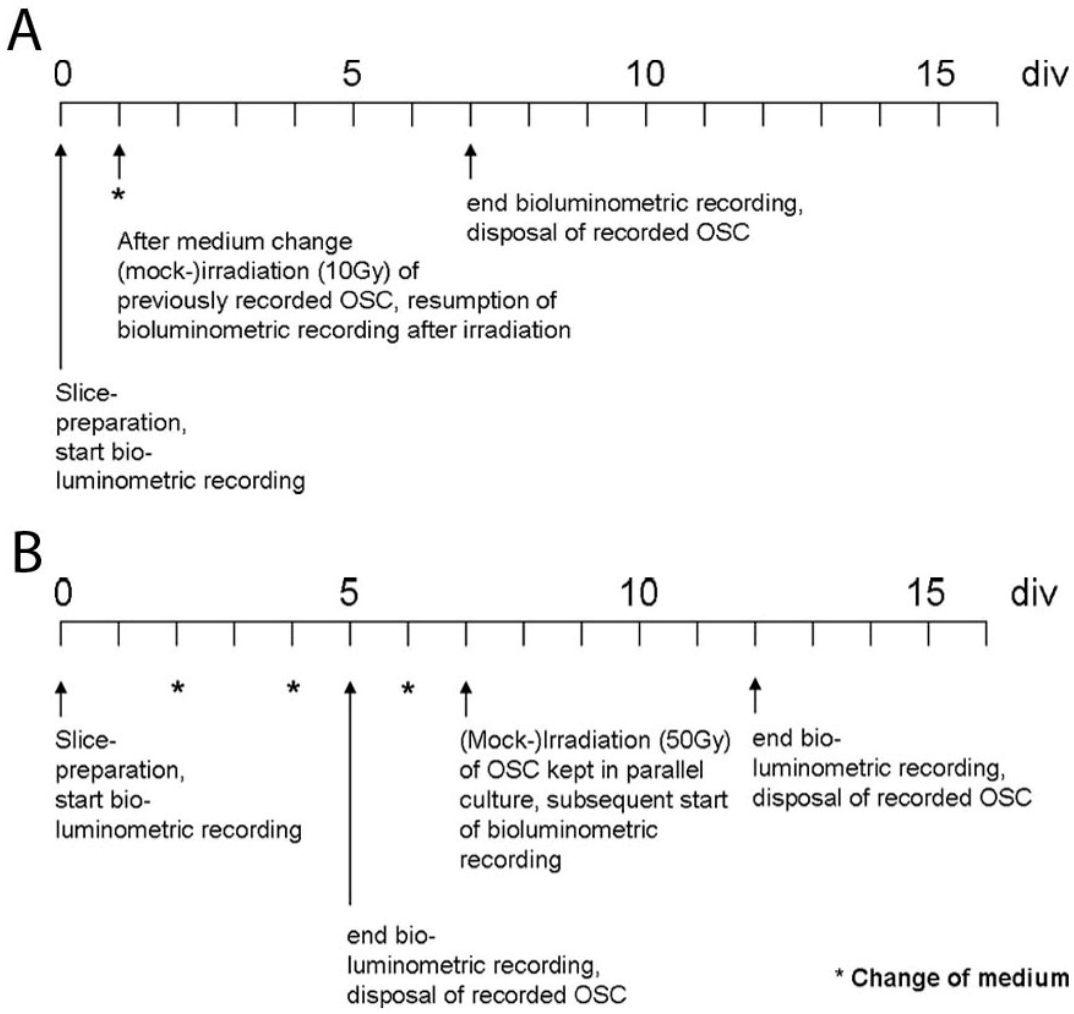

Figure 14 Experimental procedure according to the standard protocol for irradiation experiments. At 0 div, livers, pancreata, and adrenal glands from two mice were excised at timepoint CT06 and CT18, respectively. Livers were sectioned into 250µm-thick OLSC using a vibratome. Adrenal glands were cultured as complete organs. Pancreata were manually cut into smaller pieces of ~1 mm³. After all livers had been sectioned, all slices were placed in 1 ml prewarmed medium substituted with 1 µmol/ml luciferin. (A) Bioluminescence was subsequently measured for 24 h. The recording was then interrupted, the medium was changed, the OLSC and OEC were irradiated (dose D = 10 Gy), after the irradiation, luciferin was added to the medium and recording recommenced for 5 d. (B) After OLSC and OEC preparation, bioluminescence was recorded for 5d. Additional OLSC and OEC were kept under standard culturing conditions for 7 d. Their medium was changed every other day. Bioluminescent recording was stopped after 5 d and the recorded OLSC and OEC were discarded. After 7div, the remaining OLSC and OEC, which had been kept in standard culturing conditions, were irradiated (dose D = 50 Gy), and after luciferin had been added to their medium, they were recorded for bioluminescent activity for 5 d.

3.6 Microscopes and data acquisition software

3.6.1 Zeiss light microscope

Images of HE stained tissue sections were recorded with a Zeiss microscope, model Axioplan (Zeiss, Göttingen, Germany). The images were magnified 100x, using a 10x magnifying ocular lens and a 10x magnifying objective. Digital images were taken with an AxioCam MRc, Version 5.06.09 (Zeiss, Göttingen, Germany) using the acquisition software AxioVision, Version 3.1 (Zeiss, Göttingen, Germany).

3.6.2 Confocal microscope

Fluorescence refers to the phenomenon of a substance absorbing light of a specific wavelength and emitting light of another, usually longer, wavelength. An orbital electron of a fluorophor absorbs energy from an outside source and is lifted into an excited state. By relaxing into the ground state, the excess energy is emitted in form of a photon and other types of energies, usually vibrational energy (as opposed to translational or rotational energy). Since the electron cannot emit more energy than it has absorbed, the wavelength of the emitted photon is usually longer than the wavelength of the absorbed photon (an exception to this rule is the two-photon absorption). The observed shift in wavelength is also known as the Stokes' shift.
Fluorescence microscopes use the phenomenon of fluorescence in order to acquire image data of the specimen. Most flourescence microscopes are epifluorescence microscopes, in which the specimen is illuminated from above (epi-).

3.6.2.1 Setup and operation

The confocal microscope was first invented in 1957 by Marvin Minsky. It was invented to overcome resolution issues innate in wide-field fluorescent microscopy. In wide-field fluorescent microscopy, the specimen is illuminated in a wide area, only limited by the focusing parameter of the objective lens. Thus, all of the fluorophors in this area are excited and will emit light and can thus be detected by a camera. However, the detected image by the camera will consist of images inside and outside of the focal plane, leading to sharp images of the focal plane, but also to a high background caused by light emitted outside the focal plane.
To overcome this issue and acquire improved resolution images, the illuminated area of the specimen was reduced by placing a pinhole between the light source and the specimen [Minsky1961]. As only fluorophors in the focal plane get excited, only these will in turn emit light. The emitted light passes through the pinhole and can then be detected. Any light emitted outside the focal plane is blocked by the pinhole, further improving the signal-to-noise ratio.
As only a point-like area of the specimen is illuminated with this setup, it is necessary to scan the image in the XY-plane. Current state-of-the-art technology employs lasers to scan a

specimen. Lasers have the advantage of further limiting the emitted light spectrum as they excite only specific fluorophors due to their monochromatic light. A mirror is used to scan the light across the specimen. The light emitted by the fluorophors is reflected towards this dichroic mirror. After the light has passed this mirror and various filters, it is collected by photo multiplier tubes. These convert the optical signals into electronic signals which can then be displayed on a monitor for a real time image and for further post-processing.

3.6.2.2 Olympus FV-1000

The Olympus FV-1000 confocal microscope consists of an epifluorescent microscope with several laser scanners. It houses a He-Ne-laser (λ = 543 nm), an argon laser (λ = 458 nm, 488 nm, and 515 nm) and two laser diodes (λ_1 = 405 nm and λ_2 = 635 nm). It is equipped with a mercury burner and fluorescent filters for three channels (blue: excitation filter 360 nm-370 nm, emission filter: 420 nm+; green: excitation filter: 460 nm-490 nm, emission filter: 520 nm+; red: excitation filter: 510 nm-550 nm, emission filter: 570 nm+).

3.6.2.3 Acquisition software

The image acquisition software used was FV10-ASW, Version 01.07. The lasers used (Hoechst-staining: laser diode 405 nm, excitation maximum: 346 nm, emission maximum: 460 nm; Alexa Fluor 488: argon laser 488 nm, excitation maximum: 495 nm, emission maximum: 519 nm) were set to an intensity of 20%, the photomultiplier tubes were run at a voltage of approximately 450 V, gain was set to 2 and the offset was 10% for each channel. For the sake of comparability, the parameters were kept constant for sections which were stained as one batch. Changes in parameters – if necessary – were made either between different batches of stained sections or the different tissues liver and pancreas. All images were acquired using a 20x-magnification objective. The ocular lens provides 10x magnification.

For statistical analysis, six images were taken from each slice, three from one section. The images were taken arbitrarily for the pancreas. For the OLSC, OHLSC, and ONLSC, images only at the edges of each section were considered to be suitable because these did not show central necrosis. Images at the edge of the sections were chosen randomly.

3.7 Image processing and evaluation

The number of total and positively immunostained cells was automatically determined using the commercial image processing software Volocity, version 5.5.1 (Improvision, PerkinElmer, Waltham, MA, USA). For each antibody and tissue type, a different evaluation protocol was established. These protocols were used to batch process generated images, facilitating and speeding up the quantified data acquisition.

Figure 15 shows the image of a cryosection from an OLSC which had been irradiated with X-rays at a dose of 50 Gy after 7 div and was stained for the DNA double-strand break marker γH2Ax and Hoechst. The Hoechst-staining is rather pale, but most prominently, the γH2Ax-staining is constricted to the outer edge of the section. As there is no physical argument that only the outer edges of the slices were irradiated, there is no reason why the central part of the

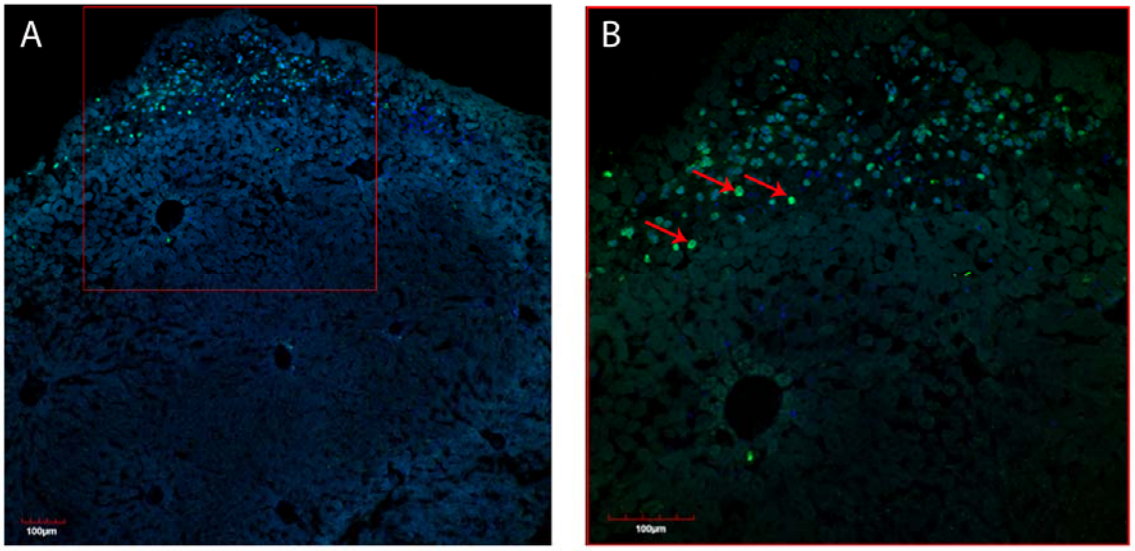

Figure 15 Image of a γH2Ax-Hoechst-stained OLSC after an X-ray irradiation at dose 50 Gy. (A) The central part of the slice is faintly stained with Hoechst (blue), but positively stained γH2Ax-cells (green) can only be found at the outer edge of the slice. Magnification 10x. (B) Close-up of (A). The γH2Ax-staining is clearly a nuclear staining which colocalizes with Hoechst. There is a distinct border to the central part of the OLSC, separating the positively immunostained part from the non-stained part of the OLSC. Magnification 20x.

section should not be stained as well, especially after an extremely high dose of 50 Gy. A close-up (Figure 15B) shows the specific nuclear γH2Ax-staining (red arrows). Figure 15 is exemplary for all images recorded, regardless of the antibody. The quantitative analysis therefore is based on counting positively stained cells at the outer edges of the sections. As the square optical field of the microscope always recorded parts of the central unstained part of the sections, these were later manually removed for counting, i.e. the images were cropped in post-processing. There is a well-defined transition from the stained to the unstained part of the slice (Figure 15). Images were cropped along this transition line.

General procedure for the establishment of protocols consisted of first optimizing a specific protocol to one image (Figure 16A, Figure 17A). The results of this image were validated with a batch of 24 additional images, generated with the identical settings of the microscope and showing the same antibody and tissue. The automatically generated number of identified objects (for example, Hoechst-stained cells – Figure 16B and positively γH2Ax-labeled cells –

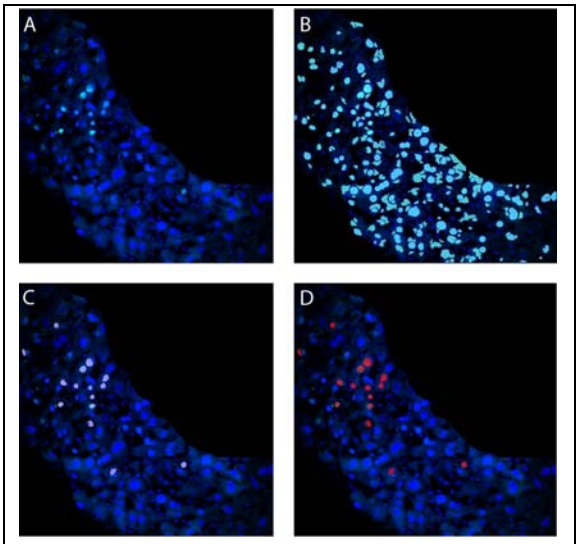

Figure 16 Single images of an OLSC for evaluating the relative frequency of positively stained γH2Ax-cells (A) Original 2-channel image. Hoechst and γH2Ax both stain the nuclei. (B) Positively identified Hoechst-stained cell nuclei are marked in light blue. (C) Positively identified γH2Ax-nuclei are marked in purple. (D) Cross section of positively-labeled Hoechst nuclei from image (B) and positively labeled γH2Ax-nuclei from image (C) are marked in red.

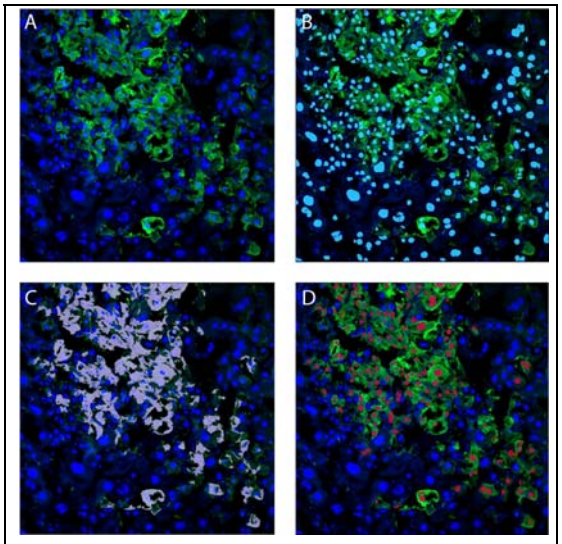

Figure 17 Single images of an OLSC for evaluating the relative frequency of positively stained Cas3-cells (A) Original 2-channel image. Hoechst-stained cells are blue, Cas3-stained cells are green. Hoechst stains the nuclei, Cas3 is a cytoplasmic staining. (B) Positively identified Hoechst-stained cell nuclei are marked in light blue. (C) Positively identified Cas3-cells are marked in purple. (D) Cross section of positively-labeled Hoechst nuclei from image (B) and positively labeled Cas3-cells from image (C) are marked in red.

Figure 16C) was then compared to the number of manually determined falsely identified and non-identified objects, respectively. Objects labeled as „falsely identified“ included multiple nuclei which were identified as one object, a single nucleus in which multiple objects were identified, and objects which were identified due to high background but where there were no cell nuclei. Protocols were optimized to a maximum error of 5%.

Immunohistochemistry was done as single labeling with addition to Hoechst. To acquire the relative frequency of positively-stained cells, protocols for Hoechst and the respective antibody-labeling were optimized according to tissue-type and staining-batch, i.e. all images acquired from sections stained in one session were subjected to the same protocol. This assured

the comparability of the results. Results from Hoechst-stained cells were counted in a first step (Figure 16B, Figure 17B). In a second step, the number of positively labeled cells with either a cytoplasmic (Cas3 – Figure 17C) or nuclear (Ki67, γH2Ax – Figure 16C) staining were identified. In a third step, the number of positively-labeled cells that either surrounded (Cas3 – Figure 17D) or were colocalized (Ki67, γH2Ax – Figure 16D) with an identified Hoechst-positive cell nucleus was determined. Finally, the relative frequency of positively labeled cells was calculated from these data for each image. In a further post-processing step, this data was taken to evaluate the relative frequency of positively labeled cells per organ.

3.8 Statistical analysis

3.8.1 Irradiation data

3.8.1.1 Errors

Uncertainties in the counted number of positively stained cells follow a Poisson distribution:

$$\Delta x = \sqrt{\frac{x}{n}} . \tag{2.1}$$

The error bars are denoted as standard errors of the mean. For a Poisson distribution, the standard error of the mean is calculated as

$$\sigma = \sqrt{\frac{\bar{x}}{n}} . \tag{2.2}$$

3.8.1.2 Friedman test

In a reduced form, the experimental design consists of multiple OSC and OEC from one experimental animal to be irradiated with different doses and fixed at different timepoints (Figure 18). As these slices are to be considered originating from the same experimental animal, these data are said to be dependent and can usually be analyzed using ANOVA with repeated measures, a common parametric test in biostatistics. When comparing the effect of time of day (circadian effect) on the radiation response, the data are independent (the OSC and OEC compared are prepared from different animals) and can usually be analyzed using the Student t-test.

The ANOVA and Student t-test are parametric tests. The application of these tests requires normally distributed data, however, and the Shapiro-Wilks test did not verify this prerequisite for the acquired data. The Shapiro-Wilks test analyzes data for normal distribution and is

designed for a small sample size. Possible dose effects and fixation timepoint effects were thus analyzed using the non-parametric Friedman test.

The data for the Friedman test is arranged in a table of *n* rows and *k* columns. The data is ranked across rows, and the sum of the ranks is calculated for each column. These sums of ranks are compared according to the following formula:

$$M = \frac{12}{n \cdot k(k+1)} \sum R_j^2 - 3n(k+1), \tag{2.3}$$

where *M* is the Friedman test statistic, *k* the number of columns, *n* the number of rows, and R_j the sum of ranks in column *j*. The significance of *M* can be looked up in χ^2 distribution tables with k-1 degrees of freedom. The Friedman test in this thesis was performed using GraphPad Prism, version 5.01 (GraphPad Software, La Jolla, CA, USA). The significance level was $p = 0.05$ for all tests.

3.8.1.3 Linear regression

Where appropriate, a possible dose-dependence was analyzed using linear regression. In linear regression, the data is fit to a line $y = a + bx$ that, according to the method of least squared, best predicts y-values. If the slope of the line was significantly ($p < 0.05$) different from zero, the linear dose-dependency was considered significant. Linear regression was performed using GraphPad Prism, version 5.01.

3.8.1.4 Kruskal-Wallis test

The Kruskal-Wallis test is a non-parametric test that is performed on more than two groups. Like the Friedman test, it does not require normally distributed data. Contrary to the Friedman test, which tests dependent variables, the Kruskal-Wallis test is designed for independent measurement variables. The test is performed on ranked data, ranks are assigned across the whole data set, i.e. the lowest data point is assigned a value of 1, the second lowest data point a value of 2, and so on. The Kruskal-Wallis test statistic *H* is calculated according to the following formula:

$$H = \frac{12}{n(n+1)} \sum \frac{R_j^2}{n_j} - 3(n+1), \tag{2.4}$$

where n is the total number of observations and R_j is the sum of the ranks to observations in the *j*th sample. The significance of *H* can be looked up in χ^2 distribution tables with k-1 degrees of freedom. The Kruskal-Wallis test in this thesis was performed using GraphPad Prism, version 5.01 (GraphPad Software, La Jolla, CA, USA). The significance level was $p = 0.05$ for all tests.

3.8.2 Circadian data

Statistical analysis for dose effects was performed using repeated measured one-way ANOVA. The significance level was set to 0.05. Analysis for circadian effects was performed via the standard one-way ANOVA, significance level set to 0.05.

Data for all OAEC were pooled irrespective of the time of death of the donor animal, as it is most likely that the culturing process reset their endogenous clock. Post-irradiation OLSC data from animals killed at different timepoints were pooled, to distinguish only between irradiated and mock-irradiated OLSC.

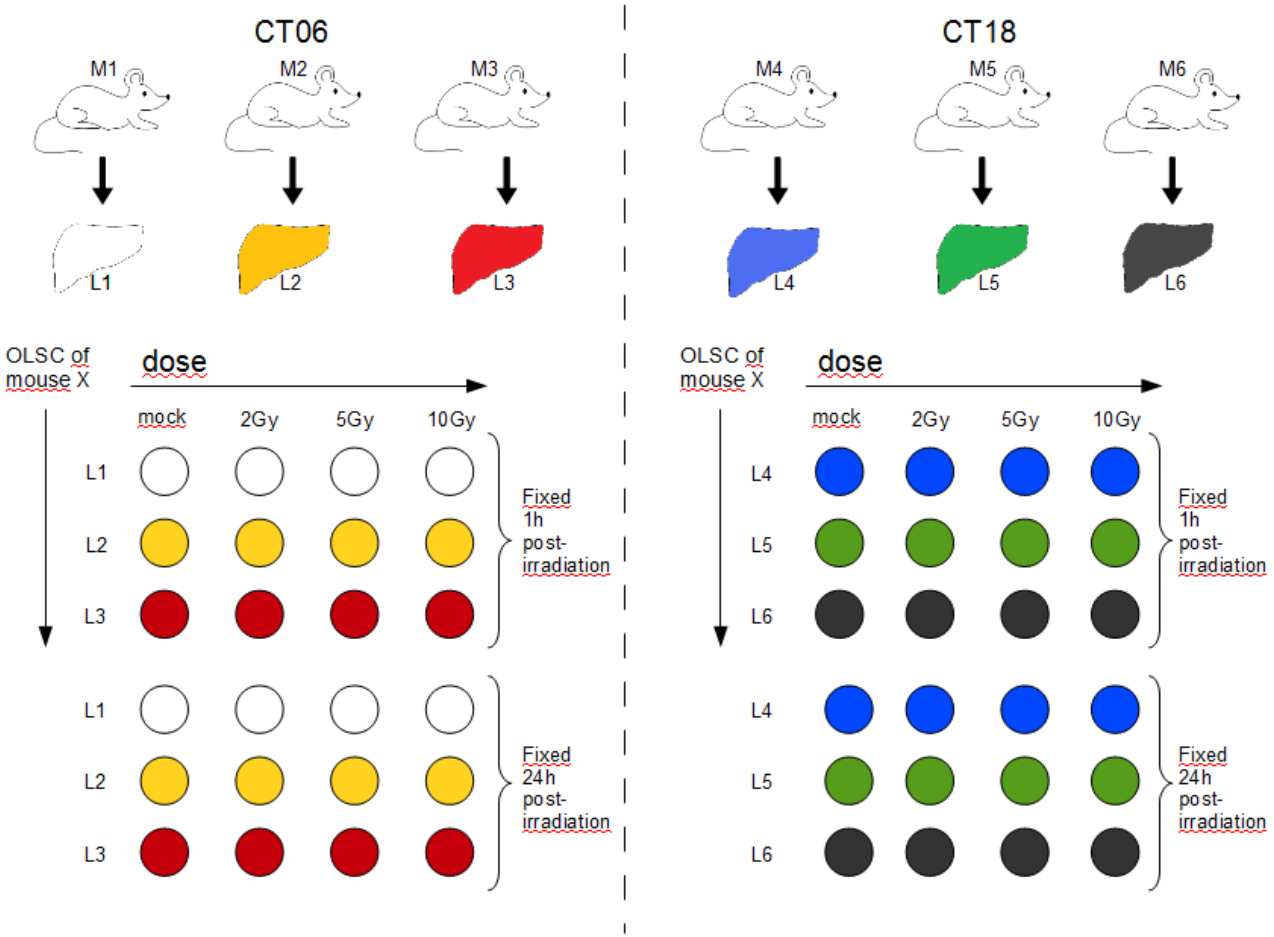

Figure 18 Scheme of experimental design for OLSC irradiation experiments. In each irradiation experiment, three mice were killed at the middle of the subjective day (CT06) and middle of the subjective night (CT18). The liver from each mouse was isolated and eight OLSC or eight OHLSC and eight ONLSC were prepared from each liver. The eight OSC were randomly distributed so that three OSC from three different mice comprised each dose value and each fixation timepoint. Each dose value and corresponding fixation timepoint consisted of three OSC, each one from a different donor animal. Analysis for dose effect and fixation timepoint effect are considered dependent variables, as the OSC considered in this analysis originate from the same donor animals. The circadian effect is considered to be an independent variable, as the experimental results comprising this analysis are generated from different animals.

4 Results

This chapter summarizes the results from the irradiation experiments as well as from preliminary experiments and analyses for the detailed description of the irradiation data. The chapter is devided into three main sections: the data from X-ray and ^{12}C irradiation experiments, the morphological assessment of the organotypic slice and explant cultures, and the summary of bioluminometric studies to analyze the circadian rhythm of organotypic slice and explant cultures *in vitro*. For reasons of readability, following abbreviations will be used for the organotypic slice and explant cultures from different tissues:

- OLSC for organotypic liver slice cultures from healthy C3H mice,
- OHLSC for organotypic healthy transgenic liver slice cultures from double transgenic c-myc/TGF-α mice,
- ONLSC for organotypic neoplastic transgenic liver slice cultures from double transgenic c-myc/TGF-α,
- OPEC for organotypic pancreas explant cultures from healthy C3H mice, and
- OTPEC for organotypic transgenic pancreas explant cultures from double transgenic c-myc/TGF-α mice.

4.1 X-ray irradiation

In the following sections, the irradiation data with X-rays and ^{12}C will be presented. Biological endpoints analyzed were proliferation, apoptosis, and DNA double-strand breaks (DSBs) 1h and 24h post-irradiation.

The Shapiro-Wilks test did not result in normally distributed data for proliferation or apoptosis. The data was thus analyzed for significant differences in dose and fixation timepoint using the non-parametric Friedman test. Where reasonable, a linear regression analysis was performed to test for linear dose-dependency. A possible circadian effect was analyzed using the Kruskal-Wallis H-test. The level for significance was $p = 0.05$ for all tests.

4.1.1 Proliferative data in OLSC

Proliferation takes place only when the environment of a cell proves suitable for division. The cell cycle has several so-called checkpoints, at which the process of cell division can be aborted. This may be due to various reasons – either certain environmental parameters are not optimal (i.e. temperature, pH-value, food supply) or the genetic constitution was erroneously replicated, leading to considerable damage and possible death of the daughter cells. In tumor

cells, these checkpoints are no longer effective, leading to an uncontrolled proliferation, which is the essence of cancer. A marker for proliferation is thus an indispensable experimental method to analyze the effects of culturing conditions and cell damage, in this thesis particularly via ionizing radiation.

Healthy C3H liver showed very few proliferative cells in vitro

In Figure 21A-C, the confocal flourescent images of a Ki67-stained C3H cryosection are shown, (A) depicts the Ki67-signal, (B) is the Hoechst-signal, (C) is the merged image of (A) and (B). This is an exemplary excerpt for the proliferation rate in healthy liver. Of several hundred Hoechst-stained cell nuclei, only one cell showed a positive immunereaction to Ki67. The quantitative result of mock-irradiated OLSC (Figure 19) proved of a proliferation rate that was extremely low, below 0.2%. No significant circadian effect, i.e. the difference between time of death of the donor animal, ($p=0.70$; Kruskal-Wallis H-test) nor between the two fixing timepoints ($p=0.30$; Friedman test) could be established. Therefore, for studies on the proliferation rate of OLSC it did not make a difference whether C3H mice were killed in the middle of the day (CT06) or in the middle of the night (CT18).

4.1.1.1 Irradiation with X-rays had no effect on proliferation rate

The data for the proliferation rate of X-ray irradiated OLSC is shown in Figure 20A. Proliferation rates were inhomogeneous with no apparent systematic radiation response. No dose-effect (p-values range: 0.21-0.71; Friedman test) or fixation time effect (p-values range: 0.44-0.65; Friedman test) could be determined. In order to analyze for a possible circadian effect, the data were therefore pooled according to dose and circadian timepoint, regardless of the fixation timepoint. In general, the proliferation rates at the middle of the day (CT06) were higher than at the middle of the night (CT18). A significant circadian effect ($p=0.003$; Kruskal-Wallis H-test) was established. In summary, X-ray radiation did not affect the proliferation rate in C3H OLSC, regardless of the dose or fixation timepoint. The

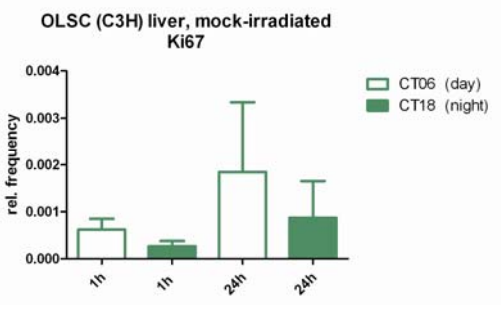

Figure 19 Mock-irradiated OLSC showed a low proliferation rate. Cryosections of mock-irradiated OLSC were stained for Ki67 and counterstained with Hoechst. The number of proliferative cells in sections of 12 mice is shown. At below 0.2% the rate was very low. Error bars are the standard error of the mean (SEM) representing the sampling error of scored OLSC from three independent X-ray radiation experiments.

time of day at which irradiation occurred did, however, have a significant effect on the proliferation rate.

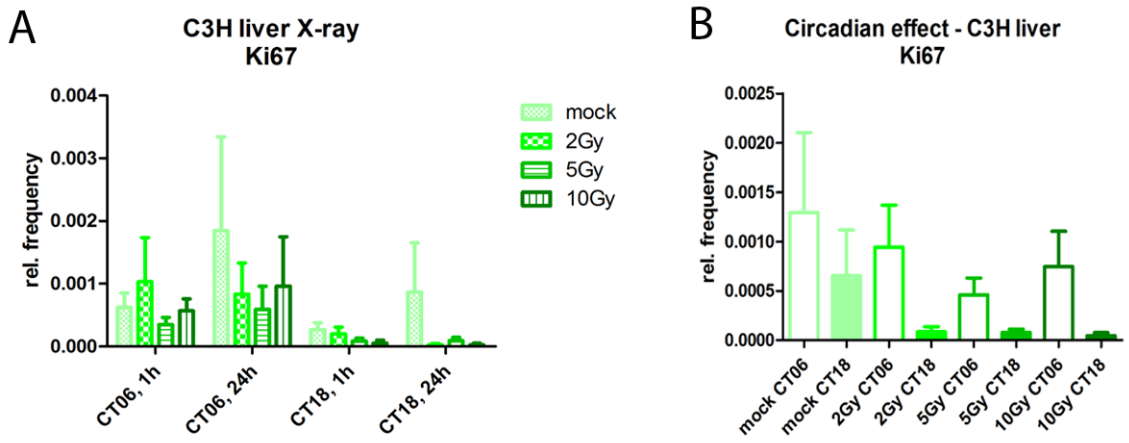

Figure 20 Proliferation rates for healthy OLSC are unaffected by dose and circadian timepoint. (A) OLSC prepared from C3H liver were irradiated with X-rays at different doses at 24h *in vitro*. Mice were killed at circadian timepoints CT06 and CT18. 1h and 24h post-irradiation, OLSC were fixed, cryosectioned and immunohistochemically stained for the proliferation marker Ki67 as well as counterstained with Hoechst. Shown are mean ± SEM (standard error of the mean) of 6 mice per circadian timepoint. Error bars are the SEM representing the sampling error of scored OLSC from three independent X-ray radiation experiments. No statistically significant differences could be established for dose or fixation timepoint ($p>0.05$; Friedman test). B) As fixation time did not have an effect on proliferation rate, data from different fixation times were pooled according to dose and circadian timepoint in order to check for a circadian effect on proliferation rate. As can be seen, proliferation rates for OLSC irradiated during the subjective night (CT18) were significantly lower than for the subjective day (CT06) ($p=0.003$; Kruskal-Wallis H-test).

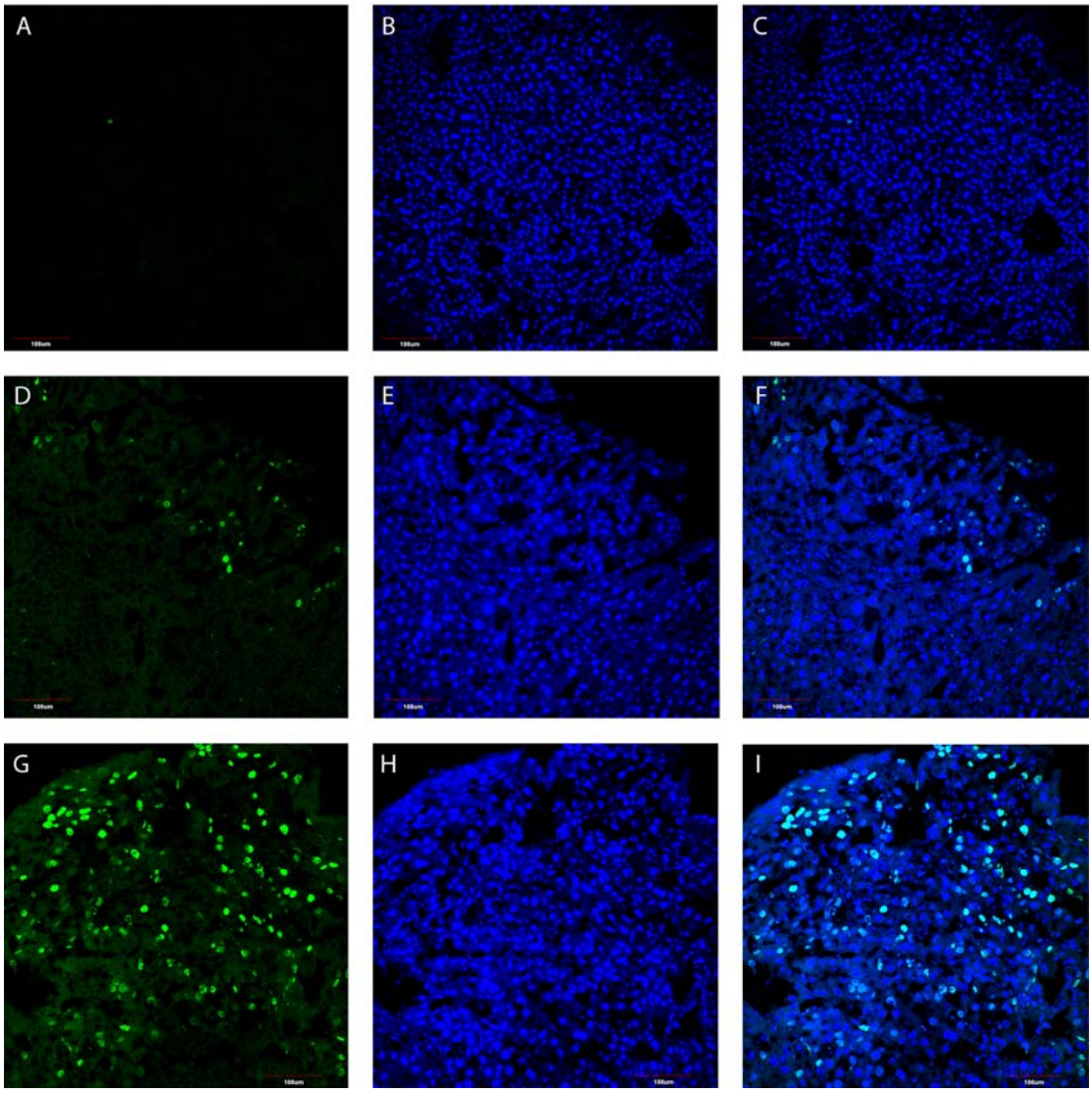

Figure 21 Exemplary confocal images of Ki67-stained and Hoechst counterstained cryosections of different liver OSC. Green signals are Ki67-positively stained cells, blue signals are Hoechst-stained cell nuclei, the third column shows the merged images of the two channels. (A-C) Confocal images of a C3H OLSC cryosection. Only one positively Ki67-labeled cell was visible in the green channel. (D-F) Confocal images of an OHLSC cryosection. The number of positively Ki67-labeled cells was increased in comparison to OLSC. (G-I) Confocal images of an ONLSC. This section showed the highest number of positively Ki67-labeled cells.

4.1.2 Apoptotic data in OLSC

Apoptosis describes the process of programmed cell death. Various reasons may lead to apoptosis, but it is always a sign a cell has recognized that it has been damaged too severely to uphold its function properly and thus induces its own death. During this process, caspase3 can be activated, which can be visualized with the according antibody in an immunohistochemical staining. Caspase3 is activated in the cytoplasm, positive signals are therefore cytoplasmic. Exemplary caspase3-stainings for the different liver tissues are given in Figure 24.

4.1.2.1 OLSC showed apoptotic cells in vitro

Apoptosis *ex vivo* was virtually non-existent in the livers of C3H and Bmal1-wt mice at ZT02 (see section 4). *In vitro*, apoptosis did occur, quantitative results for mock-irradiated samples are given in Figure 22. As can be seen, apoptosis rated roughly around 2-3%. Non-parametric tests did not indicate a fixing time effect or circadian effect (p=0.65; Friedman test and p=0.50; Kruskal-Wallis H-test, respectively). This means that the number of apoptotic cells was independent of the culturing time as well as the circadian time.

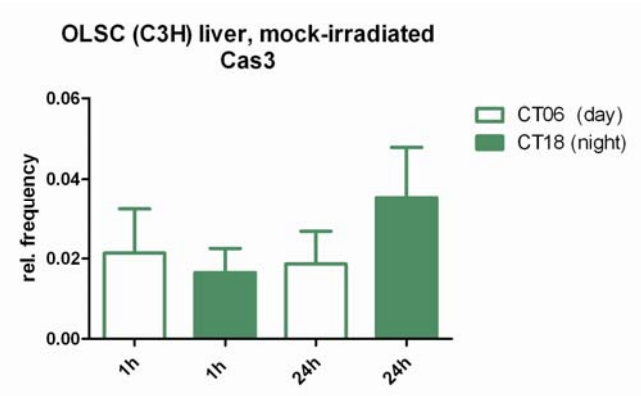

Figure 22 Mock-irradiated OLSC show positively labeled apoptotic cells. Cryosections of mock-irradiated OLSC were stained for cleaved caspase3 and counterstained with Hoechst. The number of apoptotic cells in sections of 12 mice is shown. The apoptosis rate was approximately 2-3% in all mock-irradiated OLSC, irrespective of circadian or culturing time. Error bars are the standard error of the mean (SEM) representing the sampling error of scored OLSC from three independent X-ray radiation experiments.

4.1.2.2 Irradiation with X-rays had no effect on apoptotic rate

The data for the apoptotic rate of X-ray irradiated OLSC is shown in Figure 23. OLSC fixed 1h post-irradiation did not show an effect of radiation on apoptosis. OLSC fixed 24h post-irradiation seemingly allowed the hypothesis of a linear dose dependence. This was not validated by linear regression analysis. However, linear regression for samples *CT06,24h* resulted in a trend towards a significantly non-zero slope (p=0.06). Overall, no dose-effect could be established (p-values range: 0.09-0.67; Friedman test). Evaluation of the fixation time was significant at CT06 (p=0.02; Friedman test), meaning that the culturing time the cells have

to repair damage caused by ionizing radiation before they are fixed did affect the number of apoptotic cells. Therefore, the Kruskal-Wallis H-test to analyze a circadian effect was carried out for both fixation timepoints separately. No circadian effect (p-values range: 0.22-0.59; Kruskal-Wallis H-test) could be determined. It should be noted, however, that the relative frequency of apoptotic cells 24h post-irradiation was generally slightly higher at the middle of the night (CT18) than at the middle of the day (CT06).

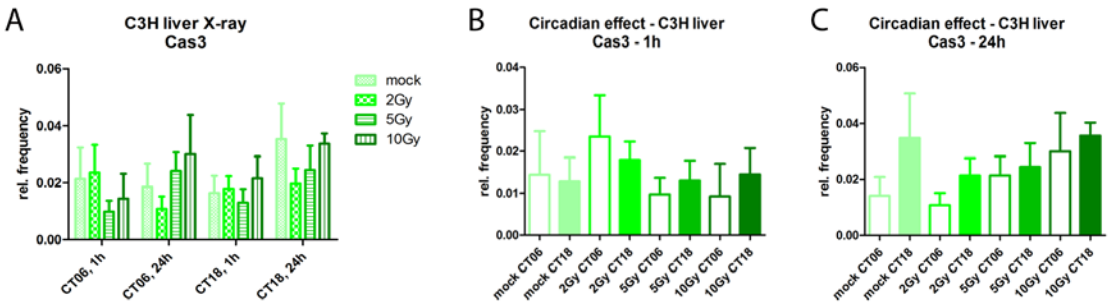

Figure 23 Apoptosis in healthy OLSC is unaffected by dose and circadian timepoint. (A) OLSC were irradiated with X-rays at different doses at 24h *in vitro*. Mice were killed at circadian timepoints CT06 and CT18. 1h and 24h post-irradiation, OLSC were fixed, cryosectioned and immunohistochemically stained for the apoptosis marker cleaved Cas3 as well as counterstained with Hoechst. Shown are mean ± SEM of 6 mice per circadian timepoint. Error bars are the SEM representing the sampling error of scored OLSC from three independent X-ray radiation experiments. No statistically significant differences could be established for dose (p–values range: 0.09-0.67; Friedman test), but for fixation timepoint at CT06 (p=0.02; Friedman test). Values fixed after 24h suggested a linear dose-dependency. (B) As a significant fixation time effect was established, apoptotic data according to the fixation timepoint were evaluated separately in order to check for a circadian effect on apoptosis. Rates 24h post-irradiation were generally, but not significantly higher at the middle of the night (CT18) than at the middle of the day (CT06) (p=0.25; Kruskal-Wallis H-test).

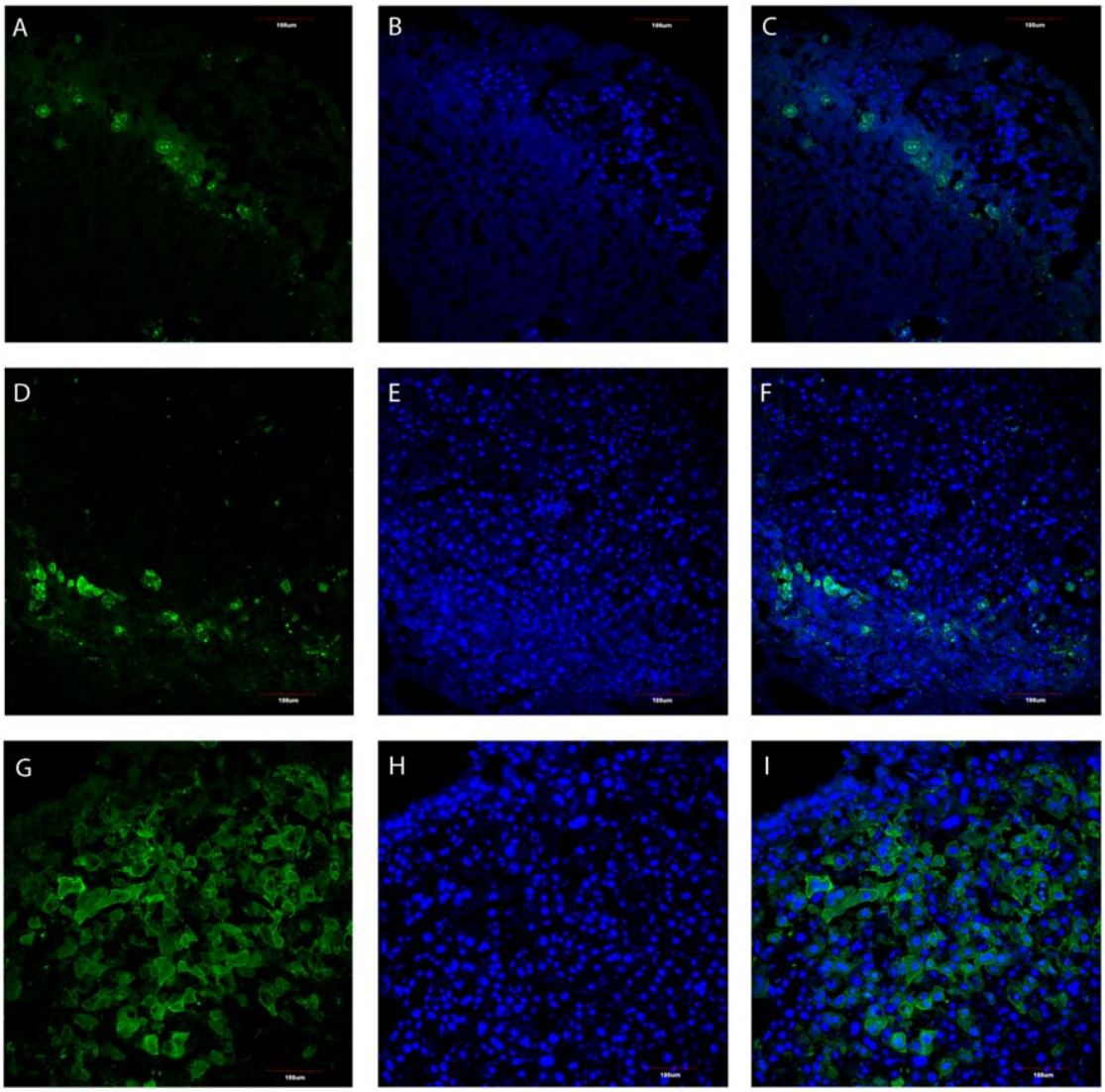

Figure 24 Exemplary confocal images of Cas3-stained and Hoechst counterstained cryosections of different liver OSC. Green signals are Cas3-positively stained cells, blue signals are Hoechst-stained cell nuclei, the third column shows the merged images of the two channels. (A-C) Confocal images of an OLSC cryosection. Few apoptotic cells marked the transition line from clearly Hoechst-stained cells at the outer edge of the cryosection to the faintly Hoechst-stained cell in the center of the cryosection. (D-F) Confocal images of an OHLSC cryosection. Compared to the OLSC, the number of apoptotic cells was increased. Apoptotic cells were limited to the outer edge of the cryosection. (G-I) Confocal images of ONLSC. The number of apoptotic cells was clearly increased, apoptotic cells were homogeneously distributed throughout the cryosection.

4.1.3 DNA DSB data in OLSC

There are two forms of DNA breaks, the single-strand break (SSB) and the double-strand break (DSB). An SSB occurs when one strand of the DNA is broken. This type of damage is relatively easy for the cell to repair. DNA DSBs are more difficult for the cell to repair, as they may lead to repaired, but mismatched nucleotides. Any break of both DNA strands within the range of eight base pairs is considered a double-strand-break. DNA DSBs at the histone 2A can be visualized with the help of the antibody γH2Ax, which recognizes the phosphorylated damage site following a DNA DSB.

4.1.3.1 OLSC did not show DNA DSBs *in vitro* nor after X-ray irradiation

DSBs were virtually not present in the C3H liver *ex vivo* (see section 4). Mock-irradiated samples as well as X-ray irradiated OLSC, irradiated at doses of up to 10Gy, also showed very little DSBs. In Figure 25A-C, confocal images of an OLSC cryosection stained for γH2Ax and counterstained with Hoechst are shown. Clearly, the number of positively stained γH2Ax foci was limited. This holds true even for samples which had been irradiated with doses of 10Gy. The number of detected DSBs was not noteworthy for any dose, either circadian time, or either fixation time and was thus set to zero.

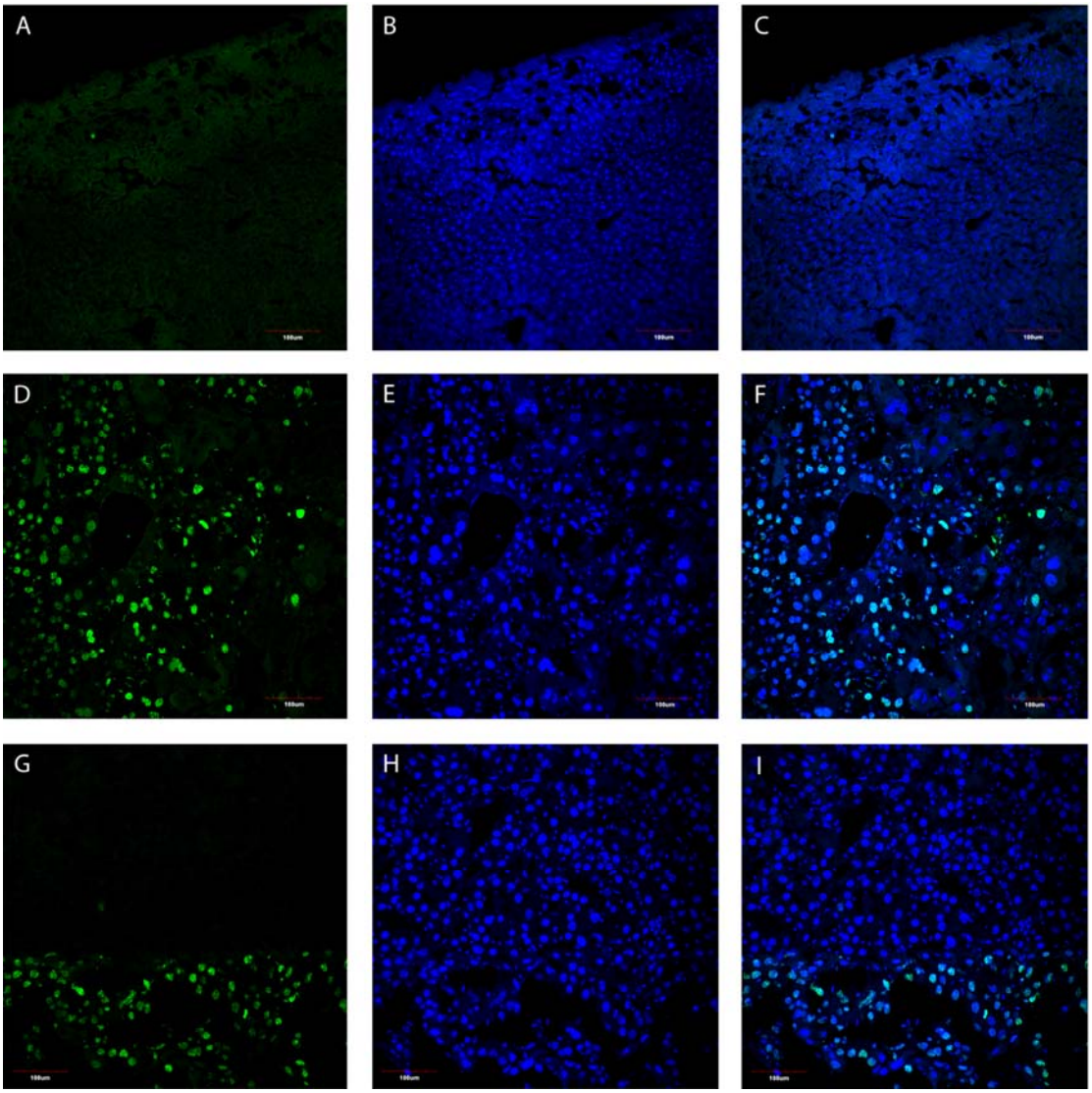

Figure 25 Exemplary confocal images of γH2Ax-stained and Hoechst counterstained cryosections of different liver OSC irradiated at 5Gy and fixed 1h post-irradiation. Green signals are γH2Ax-positively stained cells, blue signals are Hoechst-stained cell nuclei, the third column shows the merged images of the two channels. (A-C) Confocal images of OLSC. Only one cell showed a positively γH2Ax-stained cell. (D-F) Confocal images of an OHLSC. Positively γH2Ax-stained cells were distributed homogeneously throughout the cryosection. (G-I) Confocal images of an ONLSC. Positively γH2Ax-stained cells were limited to the outer edge of the cryosection.

4.2 ^{12}C irradiation

4.2.1 OHLSC from c-myc/TGF-α mice showed very few proliferative cells *in vitro*

The essence of a neoplastic cell growth, commonly called cancer, is uncontrolled cell proliferation. Ionizing radiation has been known to induce DNA damage, which, depending amongst other things on the dose, is severe enough to kill cells - the desired outcome when treating cancer. As ionizing radiation damages also healthy surrounding tissue, organotypic liver slice cultures from healthy double transgenic liver (OHLSC) were irradiated to analyze radiation side-effects. To this end, these were irradiated at different doses and fixed after two timepoints, 1h and 24h post-irradiation. To elucidate whether the circadian timepoint, at which irradiation occurred, played a role in the efficacy of the radiation dose, OHLSC were prepared at two different circadian timepoints, CT06 and CT18.

Figure 21D-F shows the confocal flourescent images of a Ki67-stained cryosection of a c-myc/TGF-α OHLSC (green – Ki67, blue – Hoechst). Compared to the images of Ki67-

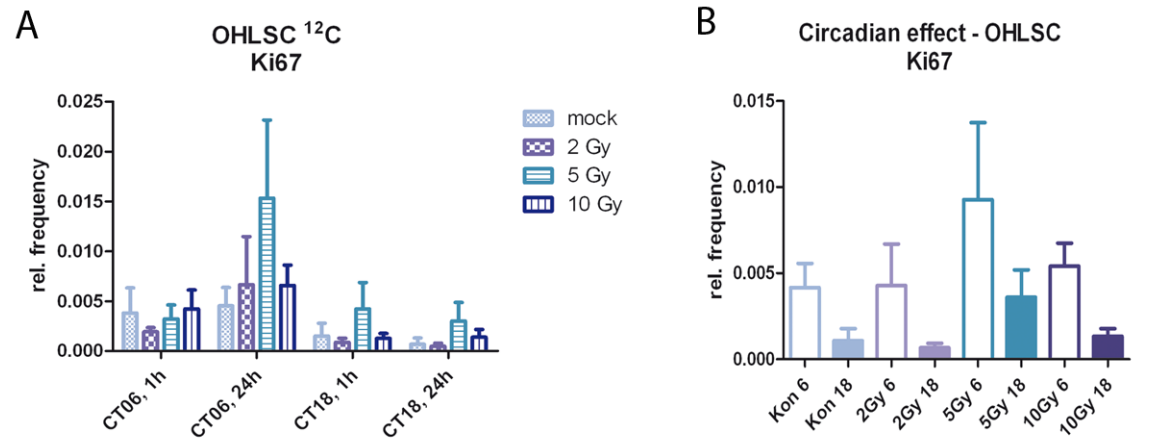

Figure 26 Proliferation rates in OHLS. (A) OHLSC were irradiated with ^{12}C at different doses at 24h *in vitro*. Mice were killed at circadian timepoints CT06 and CT18. 1h and 24h post-irradiation, OHLSC were fixed, cryosectioned and immunohistochemically stained for the proliferation marker Ki67 as well as counterstained with Hoechst. Shown are mean ± SEM of 12 mice. Error bars are the SEM representing the sampling error of scored OHLSC from two independent ^{12}C radiation experiments. No statistically significant differences could be established for dose (p-values range: 0.12-0.96; Friedman test) or fixation timepoint (p-values range: 0.35-0.61; Friedman test). Compared to proliferation rates of OLSC, proliferation rates were clearly higher. (B) As there was no effect for fixation time detected, the data of the different fixation times were pooled according to dose and circadian timepoint to evaluate a possible circadian effect. Proliferation rates were significantly higher during the subjective day (CT06) than during the subjective night (CT18) (p=0.0002; Kruskal-Wallis H-test). Note that proliferation rates in OHLSC are higher than in OLSC (see Figure 20)

stained OLSC, the OHLSC showed increased proliferation. Quantitatively, this apparent difference was not statistically significant.

The proliferation rate was determined for OHLSC and ONLSC separately. The results for proliferation in OHLSC are shown in Figure 26. The proliferation rate was very low, generally below 1%. No significant dose effect could be established for any of the data sets (p-values range: 0.12-0.96; Friedman test). Fixation 1h or 24h post-irradiation also did not lead to significant differences in proliferation rate (p-values: 0.35-0.61; Friedman test). An apparent circadian effect – proliferation at the middle of the day (CT06) was generally higher than at the middle of the night (CT18), Figure 26B – was established as highly significant ($p = 0.0002$; Kruskal-Wallis H-test).

In summary, the irradiation of healthy transgenic liver with ^{12}C did not have an effect on the proliferation rate, nor did the fixation time. The time of day at which OHLSC were irradiated did make a significant difference in proliferation rate.

4.2.2 ONLSC showed an increased proliferation rate *in vitro*

Comparing the results of the proliferation rate of ONLSC with that of OHLSC, ONLSC showed an increased proliferation rate, it ranged roughly around 3-5 %. Concerning a possible radiation effect on the proliferation rate, as in the case of OHLSC, no dose-dependency could be established (p-values range: 0.054 - 0.94; Friedman test) (see Figure 22A). However, linear regression revealed a trend towards a significantly non-zero slope for samples CT06, 24h ($p = 0.051$).

Likewise, fixing samples either 1h or 24h post-irradiation, respectively, did not make a significant difference (p-values range: 0.29 - 0.73; Friedman test). To elucidate the effect of the circadian timepoint of irradiation, samples from the same circadian timepoint and same dose were pooled irrespective of their fixing timepoint. The resulting diagram can be seen in Figure 27B. The circadian timepoint of irradiation did not have an effect on the proliferation rate ($p=0.10$; Kruskal-Wallis H-test). The p-value, however, revealed a trend towards a significant circadian effect. Strictly, however, neither dose, nor time of day, nor fixation time had an effect on the proliferation rate of ONLSC.

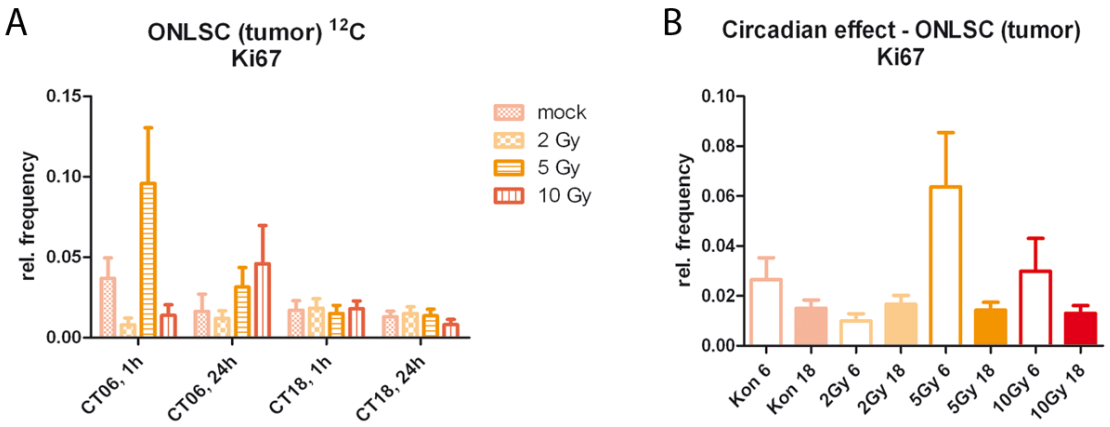

Figure 27 Proliferation rates in ONLSC. (A) ONLSC were irradiated with ^{12}C at different doses at 24h *in vitro*. Mice were killed at circadian timepoints CT06 and CT18. 1h and 24h post-irradiation, ONLSC were fixed, cryosectioned and immunohistochemically stained for the proliferation marker Ki67 as well as counterstained with Hoechst. Shown are mean ± SEM. Error bars are the SEM representing the sampling error of scored ONLSC from two independent ^{12}C radiation experiments. No statistically significant differences could be established for dose (p-values range: 0.54 - 0.94; Friedman test) or fixation timepoint (p-values range: 0.29 - 0.73; Friedman test). Compared to proliferation rates of OHLSC, proliferation rates were clearly higher. (B) As there was no effect for fixation time detected, the data of the different fixation times were pooled according to dose and circadian timepoint to be able to evaluate a possible circadian effect. No circadian effect was detected (p=0.10; Kruskal-Wallis H-test). Note that proliferation rates in ONLSC are significantly higher than in OHLSC (see Figure 26)

4.2.3 OHLSC showed very few apoptotic cells *in vitro*

As opposed to the perfused Bmal1-wt liver stained for apoptosis, which gave insight into the apoptotic rate in liver *ex vivo* (see section 4), the amount of apoptotic cells in OHLSC *in vitro* was clearly increased (see Figure 24D-F). The apoptotic rate in mock-irradiated OHLSC was also very low, but detectable up to approximately 5% (see Figure 28A).

Apoptotic rates of OHLSC fixed 1h post-irradiation seemed to increase with increasing dose, whereas the apoptotic rates of OHLSC fixed 24h post-irradiation were more heterogeneous with a defined peak at 5 Gy. Analysis of a dose effect resulted in a significant effect for samples irradiated at CT18 fixed 24h post-irradiation (p=0.03; Friedman test). The other sample batches did not show a significant dose effect (p-values range: 0.30 - 0.61; Friedman test). Linear regression resulted in a significantly non-zero slope for samples CT18, 1h ($p = 0.04$) and revealed a trend towards a significantly non-zero slope for samples CT06, 1h ($p = 0.057$). This indicated a linear dose-dependency for apoptotic radiation response. Analysis of the fixing timepoint did not result in a significant difference (p-values range: 0.0503 - 0.61; Friedman test). A p-value of 0.0503 for samples irradiated at CT18 was strictly not significant,

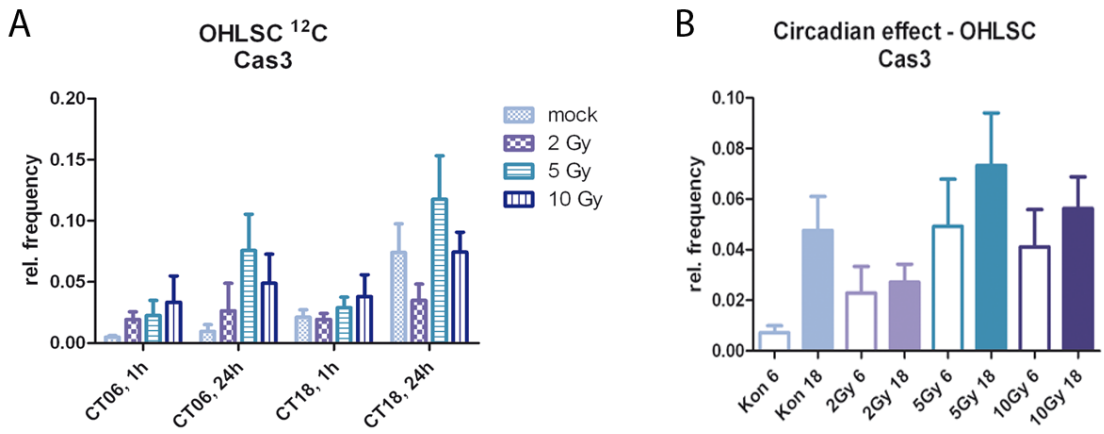

Figure 28 Apoptotic rates in OHLSC. (A) OHLSC were irradiated with ^{12}C at different doses at 24h *in vitro*. Mice were killed at circadian timepoints CT06 and CT18. 1h and 24h post-irradiation, OHLSC were fixed, cryosectioned and immunohistochemically stained for the apoptosis marker cleaved Caspase3 as well as counterstained with Hoechst. Shown are mean ± SEM. Error bars are the SEM representing the sampling error of scored OHLSC from two independent ^{12}C radiation experiments. A significant dose effect could only be established for samples irradiated at CT18 and fixed 24h post-irradiation. No fixation time effect could be established. (B) Data were pooled according to dose and circadian timepoint, as there was no indication of a fixation time effect. Apoptosis rates were significantly higher at the middle of the subjective night (CT18) than at the middle of the subjective day (CT06) ($p = 0.02$; Kruskal-Wallis H-test). Apoptotic rates in OHLSC were comparable to apoptotic rates in OLSC (see Figure 23).

yet it did point towards a trend. The data from different fixing timepoints were pooled according to dose and circadian timepoint to elucidate an effect of the circadian timepoint. Results can be seen in Figure 28B. Analysis of the circadian effect resulted in a significant difference of the two timepoints ($p=0.02$; Kruskal-Wallis H-test), the apoptotic rate at the middle of night (CT18) generally being higher than at the middle of day (CT06).

In summary, a dose effect on the apoptotic rate in healthy transgenic liver could only be established for samples irradiated at CT18, fixed 24h post-irradiation. For the rest of the samples, irradiation with ^{12}C did not have an effect on apoptotic rate, nor did the fixation timepoint. However, the time of day at which OHLSC were irradiated did influence the apoptotic rate significantly.

4.2.4 ONLSC showed an increased apoptosis rate *in vitro*

Compared to the apoptotic rates detected for OHLSC (see Figure 28A+B), the amount of apoptotic cells in ONLSC was clearly higher. Generally, the apoptotic rates were rather inhomogeneous (Figure 29A). At *CT06,1h*, for example, apoptotic rate in controls was higher than in irradiated ONLSC, whereas 24h later, the apoptotic rate was higher in irradiated ONLSC. Subsequently, no dose effect could be established for any circadian and fixation timepoint (p-values range: 0.38-0.47; Friedman test). However, linear regression resulted in a significantly non-zero slope for samples *CT18,1h* ($p = 0.006$). The fixing timepoint did not result in significant differences (p-values range: 0.38-0.44; Friedman test). This allowed for the pooling of these data according to dose and circadian timepoint in order to check for a circadian effect with regard to apoptosis. The results are shown in Figure 29B. No significant difference for the two circadian timepoints could be established (p=0.54; Kruskal-Wallis-H test).

In summary, the number of apoptotic cells depended on the tissue which was subject to radiation. It did not depend of the time of day at which ONLSC were irradiated, nor on the applied dose, nor on the fixing timepoint.

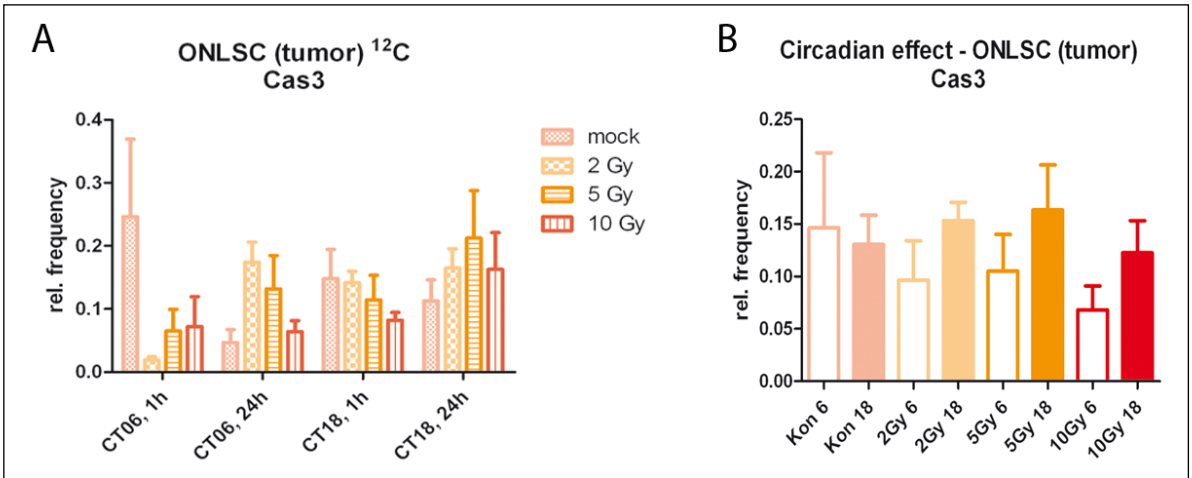

Figure 29 Apoptotic rates in ONLSC. (A) ONLSC were irradiated with ^{12}C at different doses at 24h *in vitro*. Mice were killed at circadian timepoints CT06 and CT18. 1h and 24h post-irradiation, ONLSC were fixed, cryosectioned and immunohistochemically stained for the apoptosis marker cleaved Caspase3 as well as counterstained with Hoechst. Shown are mean ± SEM. Error bars are the SEM representing the sampling error of scored ONLSC from two independent ^{12}C radiation experiments. No statistically significant differences could be established for dose (p-values range: 0.38-0.47; Friedman test) or fixation timepoint (p-values range: 0.38-0.44; Friedman test). Compared to apoptotic rates of OHLSC, apoptotic rates were seemingly, yet not significantly higher. (B) As there was no significant effect of fixation time, the data were pooled according to dose and circadian timepoint. No effect of circadian time could be detected (p=0.54; Kruskal-Wallis H-test). Apoptosis rates for ONLSC were higher than apoptosis rates in OHLSC (see Figure 28).

4.2.5 OHLSC showed very few DNA DSB sites *in vitro* and post-irradiation

Compared to the amount of DNA DSBs *ex vivo* or after X-ray irradiation, the number of DNA DSBs caused by ^{12}C-irradiation was clearly increased (Figure 25D-F). The number of DNA DSBs in OHLSC ranged between 2-8 %. The rates of DNA DSBs were inhomogeneous with regard to dose (Figure 30A) with no hint at a trend (p-values range: 0.18-0.47; Friedman test). The fixation time did not have a significant effect on the DNA DSB rate as well (p-values range: 0.21-0.39; Friedman test). Therefore, the data were pooled according to dose and circadian timepoint in order to check for a circadian effect. The DNA DSB rate was significantly higher at the middle of night (CT18) than at the middle of day (CT06), regardless of the dose (p = 0.006; Kruskal-Wallis H-test). The amount of DNA DSBs in OHLSC was therefore independent of dose and fixation time, but dependent on the time of day which OHLSC were irradiated.

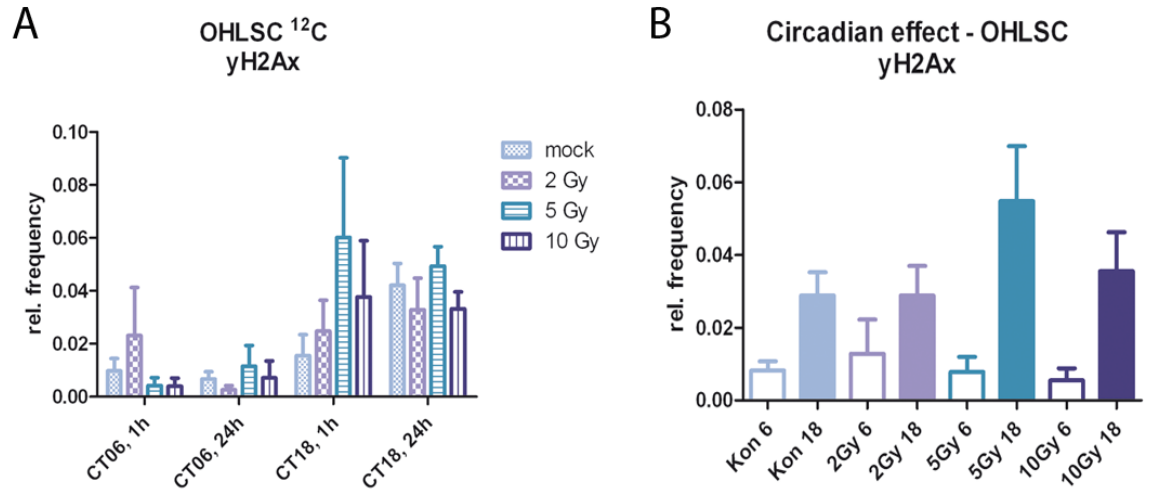

Figure 30 DNA damage in OHLSC was not significantly increased after irradiation with ^{12}C. (A) OHLSC were irradiated with ^{12}C at different doses at 24h *in vitro*. Mice were killed at circadian timepoints CT06 and CT18. 1h and 24h post-irradiation, OHLSC were fixed, cryosectioned and immunohistochemically stained for the DNA double-strand-break (DSB) marker γH2Ax as well as counterstained with Hoechst. Shown are mean ± SEM of 12 mice. Error bars are the SEM representing the sampling error of scored OHLSC from two independent ^{12}C radiation experiments. No statistically significant differences could be established for dose (p-values range: 0.18-0.47; Friedman test) or fixation timepoint (p-values range: 0.21-0.39; Friedman test). (B) No effect for fixation time was detected. The data from different fixation times was therefore pooled according to dose and circadian time in order to check for a circadian effect. A significant circadian effect was detected, the DNA DSB rates at the middle of the subjective night were significantly higher than at the middle of the subjective day (p = 0.006; Kruskal-Wallis H-test).

4.2.6 ONLSC showed an increased DNA DSB rate *in vitro*

The results for the DNA DSB rate in ONLSC are given in Figure 31A. Values at *CT06,1h* were inhomogeneous, whereas values at *CT06,24h* and *CT18,1h* showed an almost linear dose-dependency. Linear regression analysis resulted in a significantly non-zero slope for samples *CT18,1h* and revealed a linear dose-dependency ($p = 0.0075$). Linear regression analysis of *CT06,24h* samples resulted in a trend towards a significant linear dose dependency ($p = 0.059$). Values of irradiated ONLSC at *CT18,24h* did not differ much from the values of the mock-irradiated samples. Non-parametric analysis of variance did not result in a significant dose effect for either circadian or fixation timepoint (p-values range: 0.0503-0.63; Friedman test). It should be noted, however, that the p-values for *CT06,1h*; *CT06,24h* and *CT18,1h* all ranged around 0.05, revealing a trend to a significant dose effect (p-values: 0.0538; 0.0538; 0.0503, respectively). Differences in fixation time were established significant (p-values range: 0.01-0.03: Friedman test). Therefore, a possible circadian effect was analyzed separately for the two fixation timepoints. For the fixation timepoint 1h post-irradiation, a significant circadian effect was established ($p = 0.03$: Kruskal-Wallis H-test). The circadian effect for the fixation timepoint 24h post-irradiation was not significant, but revealed a trend ($p = 0.052$; Kruskal-Wallis H-test). However, the circadian effect was not homogeneous. At 1h post-irradiation, DNA DSBs were more frequent at the middle of the day in mock-irradiated and 5 Gy samples. At 24h post-irradiation, DNA DSBs were more frequent at the middle of the day in 5 Gy and 10 Gy samples.

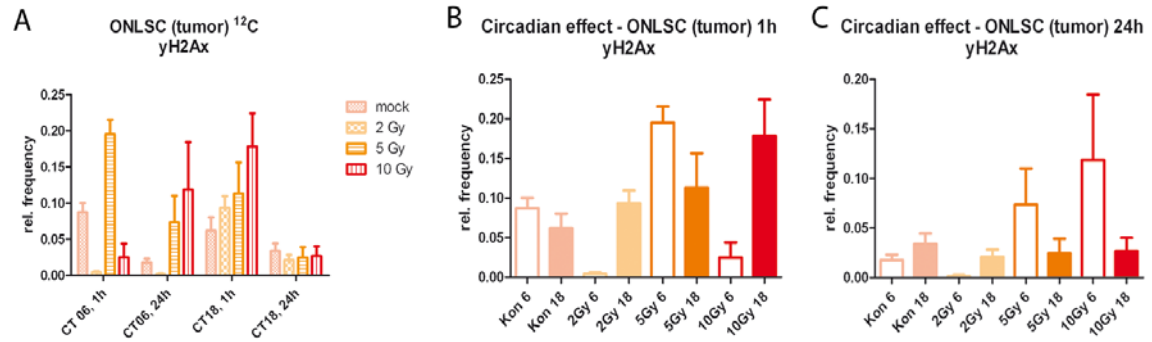

Figure 31 DNA DSBs in ONLSC are not significantly increased after irradiation with ^{12}C. (A) ONLSC were irradiated with ^{12}C at different doses at 24h *in vitro*. Mice were killed at circadian timepoints CT06 and CT18. 1h and 24h post-irradiation, ONLSC were fixed, cryosectioned and immunohistochemically stained for the DNA double-strand-break (DSB) marker γH2Ax and counterstained with Hoechst. Shown are mean ± SEM of 12 mice. Error bars are the SEM representing the sampling error of scored ONLSC from two independent ^{12}C radiation experiments. No statistically significant differences could be established for dose. For *CT06,24h* and *CT18,1h*, a linear dose-dependency could be assumed. The fixation timepoint was determined significant (p-values range: 0.01-0.03: Friedman test). (B, C) Comparison of the DSB rate according to dose and circadian timepoint 1h and 24h post-irradiation, respectively. A significant circadian effect 1h post-irradiation was established ($p = 0.03$: Kruskal-Wallis H-test).

4.3 Comparison of X-ray- and ^{12}C-data

As experiments with different ionizing radiation types were done with liver OSC prepared from different mouse types, only results which were generated for OLSC and OHLSC were used for the comparison of X-ray and ^{12}C-irradiation data. To assess whether a statistical comparison for irradiated samples was valid, the comparison between mock-irradiated samples was used as reference. Mock-irradiated OLSC and OHLSC differed significantly in proliferation and apoptotic rate. Therefore, a further statistical evaluation of different radiation types in liver slice cultures derived from different mouse types (C3H and c-myc/TGF-α) was not performed. However, to rudimentarily unmask a possible radiation effect, proliferation and apoptotic rates were given as relative frequency in percent (%). The mean relative frequency of OLSC and OHLSC at CT06 was defined as 100%. As the OLSC showed no signs of DNA DSBs post-irradiation, this comparison was rendered mute.

4.3.1 Proliferation rate

Results for the proliferation rate in OLSC after X-ray irradiation were compared to the results for the proliferation rate in OHLSC after ^{12}C irradiation in order to check for a possible higher efficacy of heavy ion radiation (Figure 32A+B). The proliferation rate, as shown with the proliferation marker Ki67, was generally higher in OHLSC than in OLSC. Mock-irradiated values differed significantly ($p=0.0012$; Kruskal-Wallis H-test). To unmask the radiation effect, proliferation rates of OLSC and OHLSC prepared at the middle of the subjective day (CT06) were defined as 100%. The circadian effect remains dominant, the number of proliferative cells was usually higher at CT06, regardless of tissue type and fixation timepoint. With respect to the subjective time of day, large differences in proliferation rate 1h post-irradiation can be seen at 2 Gy and 5 Gy (Figure 32A). Proliferation rates in OLSC at *CT06, 2 Gy* are approximately 3 times higher and at *CT18,5 Gy* about 8 times lower than in OHLSC, respectively. At 24h post-irradiation, proliferation rates between matching (meaning OLSC and OHLSC of the same circadian and fixation timepoint) OLSC and OHLSC vary even more (Figure 32B). Here, OHLSC show a higher proliferation rate of factors between 3 and 30.

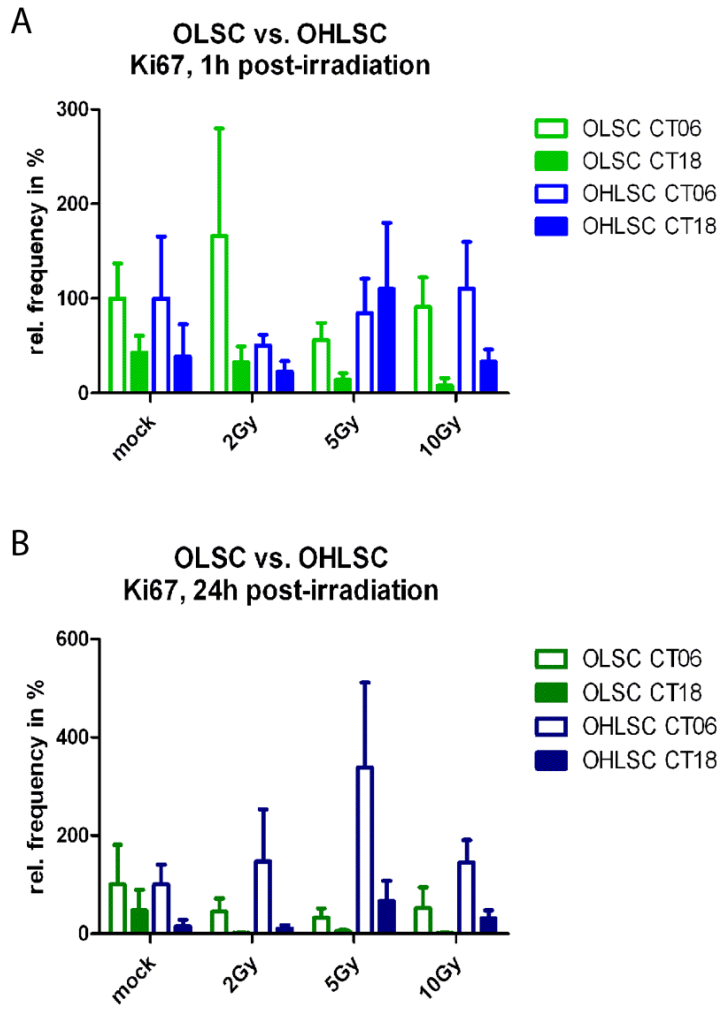

Figure 32 Comparison of proliferation rate after X-ray and ^{12}C irradiation of healthy liver. The results for the proliferation rate in OLSC after X-ray irradiation (green) are compared to the proliferation rates observed in OHLSC (blue) with respect to the circadian and fixation timepoint. At both fixation timepoints, the circadian effect is apparent, with a higher proliferation rate at CT06. (A) 1h post-irradiation, proliferation rates vary up to a factor of approximately 8 (at CT18, 5Gy) between matching OLSC and OHLSC. (B) 24h post-irradiation, proliferation between matching OLSC and OHLSC was between 3-30 times higher in OHLSC.

4.3.2 Apoptosis rate

Apoptosis rates detected in OLSC irradiated with X-rays were compared to apoptosis rates in OHLSC, which had been irradiated with ^{12}C (Figure 28). Apoptotic rates for mock-irradiated samples differed significantly ($p=0.03$: Kruskal-Wallis H-test). Therefore, statistical analysis of a possible dose and thus radiation type effect in liver slice cultures derived from different mouse types (C3H and c-myc/TGF-α) was not performed. Again, as for proliferation data, to unmask a possible radiation effect, apoptotic rates of OLSC and OHLSC at CT06 were defined

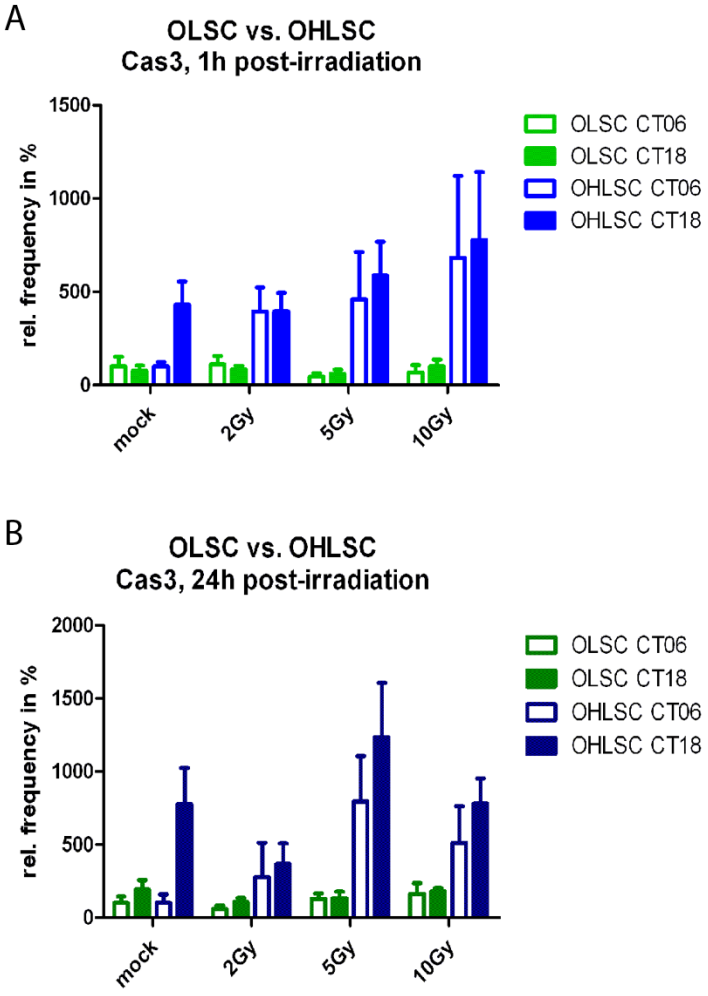

Figure 33 Comparison of apoptotic rate after X-ray and ^{12}C irradiation of healthy liver. The results for the apoptotic rate in OLSC after X-ray irradiation (green) are compared to the apoptotic rates observed in OHLSC (blue) 1h post-irradiation (A) and 24h post-irradiation (B). Values at CT06 were set to 100% for both OLSC and OHLSC. Apoptotic rates in OHLSC are always higher than in OLSC, regardless of the dose or fixation timepoint.

as 100 % (Figure 33A+B). Apoptotic rates in OLSC range between 45 – 180 % for all doses, rates for OHLSC range between 100 – 1200 %. Note that the apoptotic rate in mock-irradiated OHLSC prepared at the middle of the subjective night (CT18) is already much higher than in mock-irradiated OHLSC prepared at CT06, regardless of the fixation timepoint. In general, apoptotic rates in OHLSC are about 7 – 10-fold higher compared to apoptotic rates in matching OLSC.

4.4 C3H pancreas did not show immunohistochemical reaction

In addition to OLSC, organotypic pancreas explant cultures (OPEC) approximately 1mm³ in size, were prepared from C3H mice. These OPEC were subject to the same conditions as the OLSC.

The immunohistochemical staining for proliferating and apoptotic cells as well as for DNA DSBs did not result in any positive signals in any of the samples, regardless of the circadian timepoint of preparation, the fixing timepoint let alone dose. To determine any tissue degeneration due to the release of pancreatic enzymes, α-amylase and lipase were assessed in the supernatants of the OPEC (Figure 34). Plotted were arbitrary units per liter per hour (U/(l·h)), assuming a constant release of enzyme into the supernatant. These data were collected for OPEC which had been kept in standard culturing conditions for 7d before being subjected to 50Gy X-ray radiation. The amount of α-amylase was 6000 times and about 4000 times higher for OPEC prepared at CT06 and CT18 after 1div, respectively, than after 7div. After irradiation with X-rays, especially lipase increases clearly. This indicated an extensive leakage of digestive enzymes into the pancreas tissue.

In addition to the assessment of pancreatic enzymes in the OPEC supernatants, OPEC cryosections were immunohistochemically stained against insulin (Figure 35). Compared to perfused pancreas, in which the insulin staining was limited to the Langerhans islets (Figure 39), the insulin staining in OPEC was homogeneously distributed throughout the tissue (Figure 35), indicating unspecific background staining. Langerhans islets could be identified via Hoechst staining and the specific structure of Langerhans islets within the pancreas tissue, but insulin no longer proved a useful marker for the identification of the endocrine pancreas in OPEC.

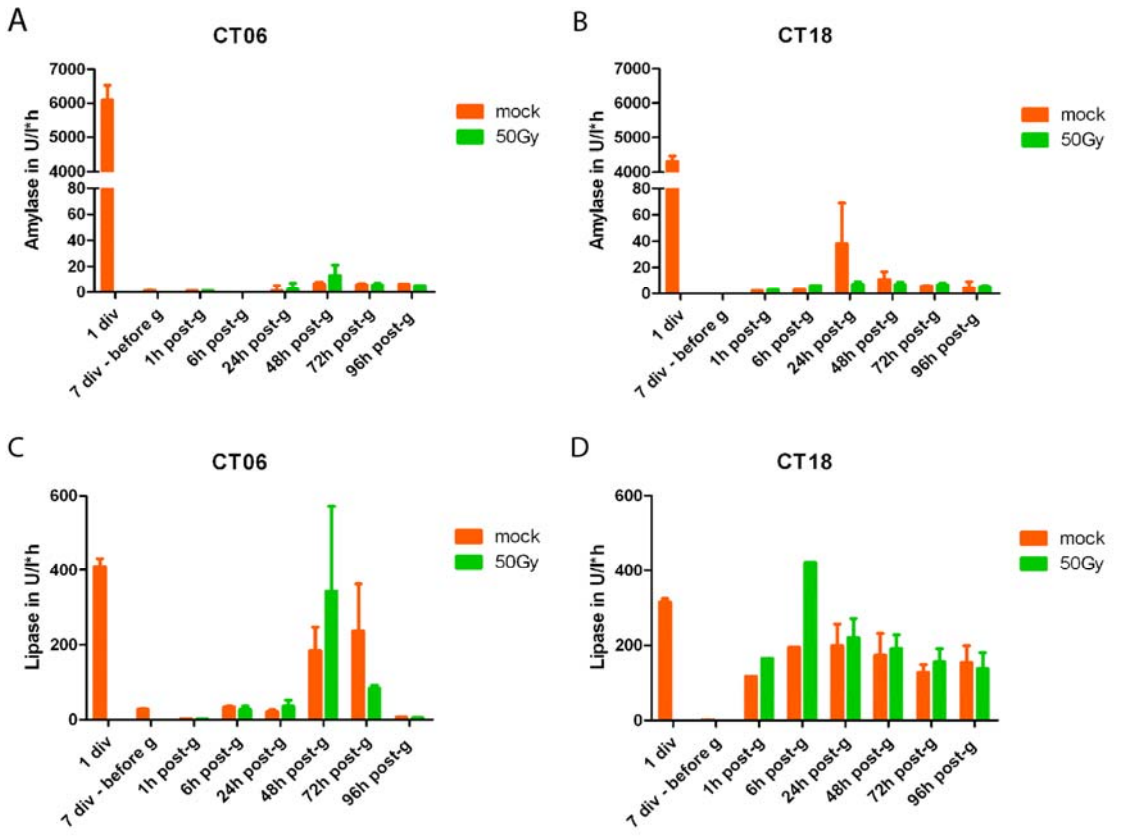

Figure 34 Amylase and lipase data of OPEC irradiated after 7div. (A) Amylase data for OPEC prepared at CT06. The amount of amylase was about 6 000-fold at 1div compared to 7div. Directly after irradiation, there was no distinct increase in the amount of amylase in the supernatant. (B) Amylase data for OPEC prepared at CT18. The amount of amylase was about 4 000-fold at 1div compared to 7div. As for the OPEC prepared at CT06, there was no distinct increase in the amount of amylase in the supernatant after irradiation. (C) Lipase data for OPEC prepared at CT06. The amount of lipase at 1div was about 400-fold higher than at 7div. There was no distinct increase of lipase directly after irradiation. After 48h, lipase secretion increased for both mock-irradiated as well as for irradiated OPEC, and decreased to the 7div-level after 96h post-irradiation. (D) Lipase data for OPEC prepared at CT18. The amount of lipase at 1div was about 300-fold higher than at 7div. Directly after irradiation, there was a distinct increase in lipase for both the mock-irradiated and the irradiated OPEC. Enzyme levels did not reach 7div-level even after 96h *in vitro*. All error bars represent the sampling error from up to three individual samples per timepoint.

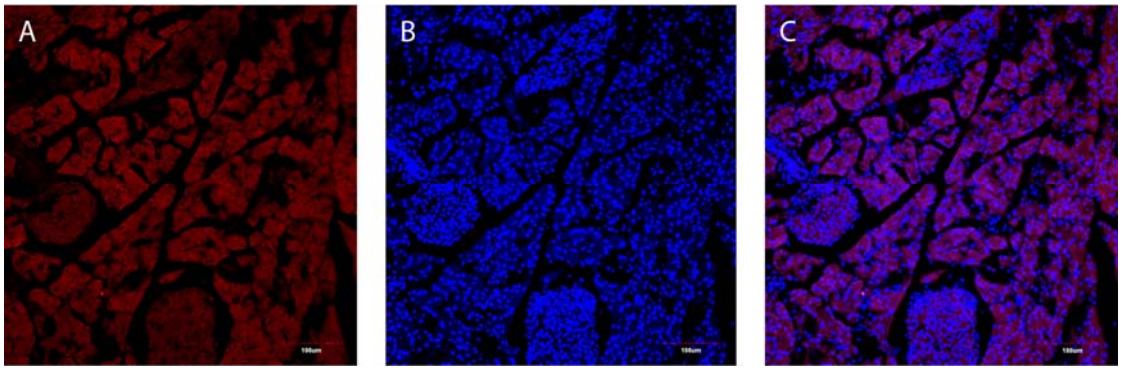

Figure 35 Confocal image of a pancreas cryosection stained for insulin. The OPEC had been kept in standard culturing conditions for 48h, fixed in 4% paraformaldehyde, subsequently cryosectioned and stained for insulin and Hoechst. (A) Insulin-staining (B) Hoechst-staining (C) Merge of (A) and (B). The insulin-staining, which was limited to the Langerhans-islet in perfused pancreas, was homogeneously distributed throughout the whole OPEC, indicating unspecific background staining.

4.5 c-myc /TGF-α pancreas explant cultures showed immunohistochemical reaction in vitro in non-fibrotic areas

Organotypic transgenic pancreas explant cultures (OTPEC) of c-myc/TGF-α mice were prepared at ~1 mm³ using a scalpel. These were treated in the same way as the OHLSC and ONLSC, and subsequently stained for proliferation, apoptosis, and DNA damage markers and counterstained with Hoechst. The fibrotic parts and tubular structures of the differentiated acini of these OTPEC were well visible in the Hoechst staining (Figure 36B). In contrast to the OPEC from C3H mice, the OTPEC stained positive for proliferation (Figure 36). However, due to the general state of the double transgenic pancreas tissue (see section 4.8.2), which did

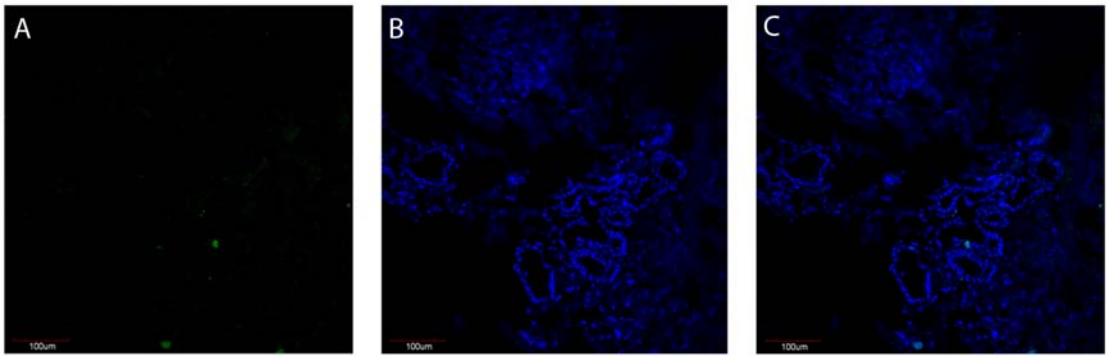

Figure 36 Confocal images of a TGF-α/c-myc pancreas cryosection stained for Ki67 and Hoechst. (A) Ki67-staining (B) Hoechst-staining (C) Merge of (A) and (B). A Ki67-positively labeled cell can be seen in the differentiated exocrine part of an OTPEC cryosection. The Hoechst-staining revealed the tubular structures characteristic for the pancreas tissue of this mouse strain. Adjacent to these differentiated acini were lighter Hoechst-stained fibrotic parts of the pancreas.

not model a human pathologic condition and would thus not be subjected to heavy ion irradiation, these OTPEC were not immunohistochemically evaluated.

4.6 Immunohistochemistry in liver ex vivo

4.6.1 Proliferation rates ex vivo in C3H-liver

The substance 5-bromo-2'-deoxyuridine (BrdU) is a proliferation marker, which replaces thymidine during cell division. The amount of BrdU incorporated into the DNA can immunohistochemically be detected with a specific antibody against BrdU.

The proliferation rate of livers *ex vivo* was assessed as a by-product of an experiment with Bmal1-wt-mice. The mean proliferation rate of liver *ex vivo* was determined to 0.0055 ± 0.0008 (mean ± sem). As this value marks all proliferating cells within a temporal range of three days, it was to be considered higher as the typical temporal snapshot of the proliferation rate as was detected via a standard Ki67-staining (Figure 11). As this accumulated proliferation rate over a period of three days was to be considered very low, it was a first indication of the generally known radioresistance of hepatocytes.

4.6.2 Apoptosis rate and DNA DSB rate *ex vivo* in wt-liver

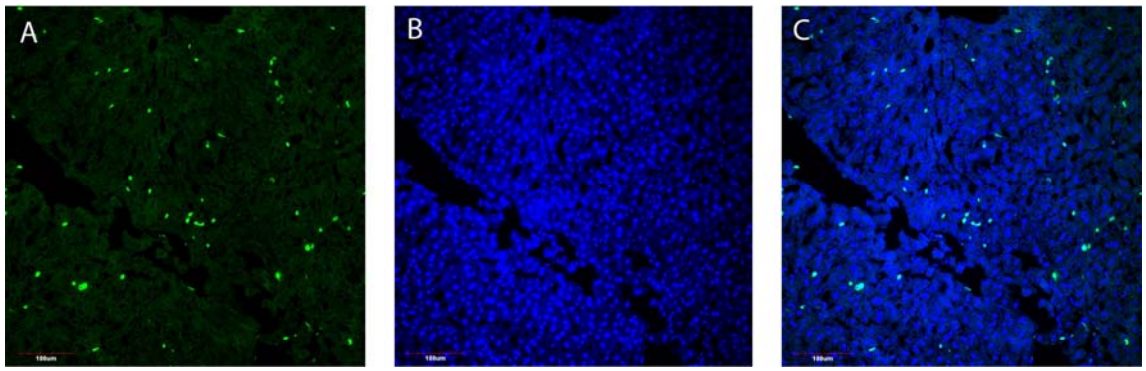

Figure 37 Exemplary confocal images of a Bmal1-wt-liver cryosection stained for BrdU and Hoechst. (A) BrdU-staining (B) Hoechst counterstaining. (C) shows the merged channels. Bmal1-wt-mice were injected intraperitoneally with BrdU for three consecutive days and perfused on the fourth day at ZT02. Livers were excised and processed into 10µm-thick cryosections.

Cryosections of perfused Bmal1-wt and post-fixed C3H liver were immunohistochemically stained for apoptosis with a cleaved Caspase3-antibody and for DNA double-strand-breaks (DSBs) with a γH2Ax-antibody. Both stainings were negative in all liver cryosections of both mouse strains.

4.7 Immunohistochemistry in pancreas "ex vivo"

4.7.1 Proliferation rate

The pancreata of the perfused Bmal1-wt mice (see section 4.6.1) as well as post-fixed pancreata from C3H mice were also immunohistochemically stained with an antibody against BrdU as well as Ki67 in order to assess the proliferation rate of pancreas cells *ex vivo*. As BrdU is incorporated by the DNA, it is passed on to the daughter cells and can be detected there as well. As the mice were injected with BrdU on three consecutive days, the amount of BrdU was higher than for Ki67, which only gave information on the actively proliferating number of cells at the moment of death.

The analysis of proliferating cells in pancreas was done separately for the endocrine and exocrine pancreas. To correctly identify the Langerhans islets from the acini, the cryosections were additionally counterstained with an insulin-antibody. Insulin is produced by the β-cells which are located in the Langerhans islets, the staining is thus spatially limited to these. An exemplary confocal image of a pancreas cryosection stained for Ki67, insulin, and Hoechst is given in Figure 39.

As is shown in Figure 38, the number of BrdU-positive cells was higher than for Ki67-positive cells (shown are the mean ± sem). The proliferation rate was slightly higher in Bmal1-wt than in C3H mice, however, the proliferation rate overall was extremely low. Even the BrdU staining, which revealed the number of proliferative cells over a course of three days, did not reach 1%.

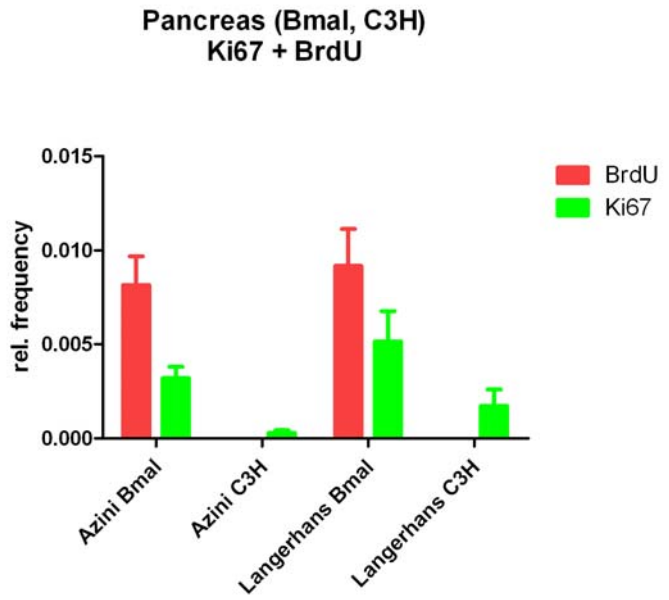

Figure 38 Proliferation rates *ex vivo* in pancreas of Bmal1-wt and C3H mice. Cryosections of Bmal1-wt pancreata of mice that had been intraperitoneally injected with BrdU for three consecutive days were immunohistochemically stained for BrdU and counterstained for Ki67. Cryosections of C3H pancreata which had been placed into 4% paraformaldehyde directly after excision were immunohistochemically stained for Ki67. Analysis of the proliferation rate was determined for acini and Langerhans islets separately via colocalization of an insulin-staining. BrdU rates were higher than Ki67 rates, proliferation rates in Bmal1-wt mice were higher than C3H proliferation rates in pancreas *ex vivo*. Error bars denote the sampling error calculated as SEM.

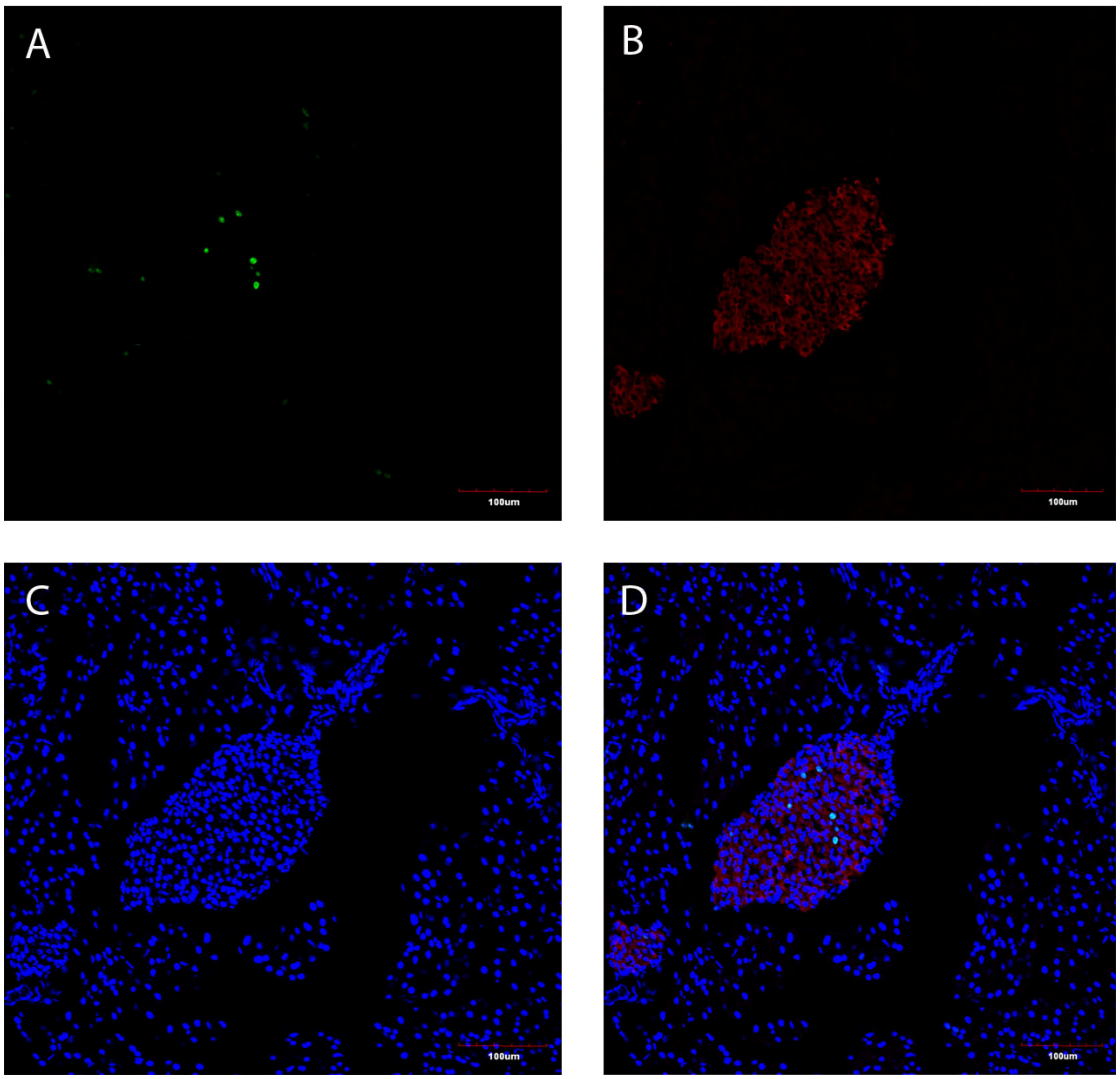

Figure 39 Exemplary confocal images of a pancreas cryosection stained for Ki67 (A), insulin (B), and Hoechst (C). The pancreas of a Bmal1-wt mouse that had been injected intraperitoneally with BrdU for three consecutive days and perfused on the fourth day at ZT02 was cryosectioned at 10µm and immunohistochemically stained for Ki67, insulin and counterstained with Hoechst. The images show a clearly distinguishable Langerhans islet containing insulin-immunoreactive cells (B). (D) shows the merged channels.

4.7.2 Apoptosis rate and DNA DSB rates *ex vivo* in wt-pancreas

Cryosections of perfused Bmal1-wt- and post-fixed C3H pancreata were immunohistochemically stained for apoptosis with a Caspase3-antibody and for DNA DSBs with a γH2Ax-antibody. Both stainings were negative in all cryosections for both acini and Langerhans islets. The exocrine and endocrine pancreas were distinguished via an anti-insulin immunohistochemical staining. In summary, the pancreata of C3H and Bmal1-wt mice showed no signs of apoptosis or DNA-DBSs *ex vivo* at ZT02.

4.8 Morphological assessment of organotypic slice and explant cultures

4.8.1 Liver

In mammals, the liver can be macroscopically subdivided into four lobes: two large lobes (median and left lobe) and two small lobes (right and caudal lobe) (Figure 40C). Histologically, the structure of liver tissue is dominated by roughly hexagonal lobules, at the center of which lies the central vein from which the hepatocytes, the parenchymal cells of the liver, radiate outward. The lobules in murine liver are rather difficult to distinguish as they are not clearly separated by connective septae. At the vertices of these hexagonal lobules, the so-called portal triads are located. A bile duct, a terminal branch of the hepatic artery and a terminal branch of the portal vein comprise the portal triad.

The morphological assessment of a normally developed tissue structure and also from pathological transformed tissues either in the organism or after culturing gives the first information about the state of the tissue, *in vitro* and *ex vivo*. For the morphological assessment of organotypic liver slice cultures (OLSC) kept *in vitro*, livers of healthy C3H murine liver and healthy parts and neoplastic parts of double transgenic c-myc/TGF-α murine liver were analyzed.

Figure 40A+B shows an exemplary HE-stained cryosection of an OLSC after 48 h *in vitro*. The OLSC showed an intact architecture, with preserved characteristic features of the central veins (red arrows) and outwards radiating hepatocytes. Portal triads could not be detected in the OLSC. A distinct staining feature of OLSC was a generally darker staining at the outer edge of the section than in the center (see Figure 40B for a close-up). This may be an indication of better preserved tissue at the outer edge of the slice compared to a – most likely – nourishment and oxygen deprived central part of the slice. However, the hepatocytes and their nuclei were clearly stained in the central part, indicating viable tissue. Thus, OLSC preserved morphological characteristics after 48 h *in vitro*.

Also in OHLSC, the characteristic features such as central veins and outwards radiating hepatocytes could clearly be identified (Figure 42). In contrast to the rather homogeneous cell size of the cell nuclei of the hepatocytes of OLSC (Figure 40B), an increased number of nuclei of different size could be found in OHLSC (Figure 42). This is a common morphological phenomenon for neoplastic tissue, also known as nuclear polymorphy. The cell nuclei were clearly stained throughout the whole OHLSC (Figure 42B), indicating the viability of this tissue.

In ONLSC, the characteristic tissue architecture consisting of central veins and outwards radiating hepatocytes could no longer be identified (Figure 41A+B). Moreover, the section exhibited an unsystematic array of disordered, uncontrolled cell proliferation. Figure 41A again shows the stronger stained outer edge of the ONLSC. Figure 41B shows cell nuclei of various sizes, a common feature of neoplastic tissue.

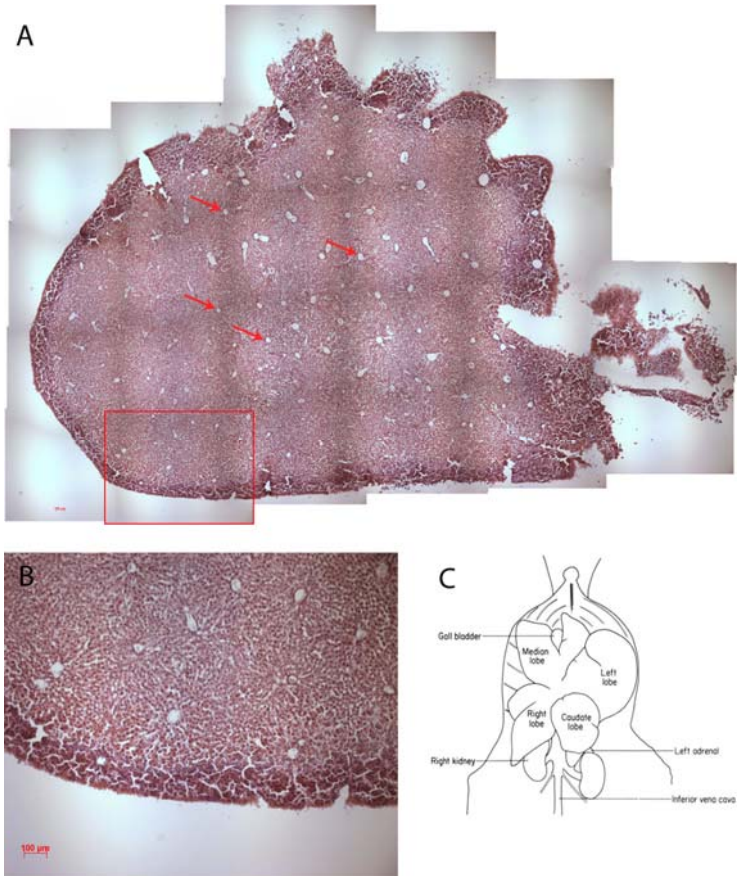

Figure 40 Histological staining of OLSC shows intact tissue architecture (A) Overview of an exemplary HE-stained cryosection of an OLSC. The cryosection was morphologically intact, the central veins of single lobules could clearly be identified (arrows). Portal triads could not be identified. Notable was an outer ring in which the tissue showed a stronger eosin staining. (B) Single image of the cryosection shown in (A). The close-up shows intact cell nuclei in the stronger eosin-stained outer region and in the fainter stained central part of the section. (C) Schematic of the position of the four different lobes comprising the liver with regard to surrounding organs in the mouse. Source: The Anatomy of the Laboratory Mouse by Margaret J. Cook (http://www.informatics.jax.org/cookbook/)

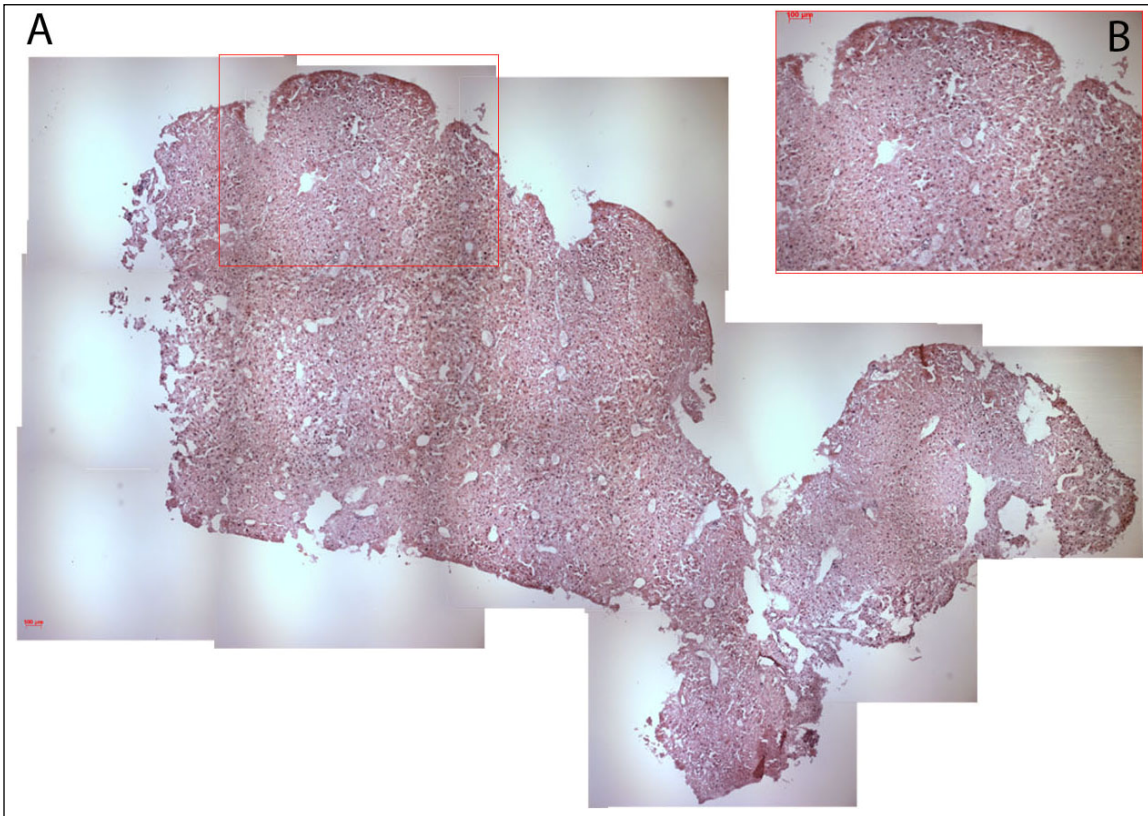

Figure 42 Histological staining of OHLSC shows characteristics of normal liver. (A) Overview of an exemplary HE-stained cryosection of an OHLSC. The tissue could clearly be identified as liver tissue as indicated by the central veins and liver cell plates. At the outer edge of the section, a thin ring of stronger eosin-stained tissue can be seen. (B) Single image of cryosection shown in (A). Besides the stronger eosin-stained edge of the section, the close-up shows the numerous cell nuclei of various sizes.

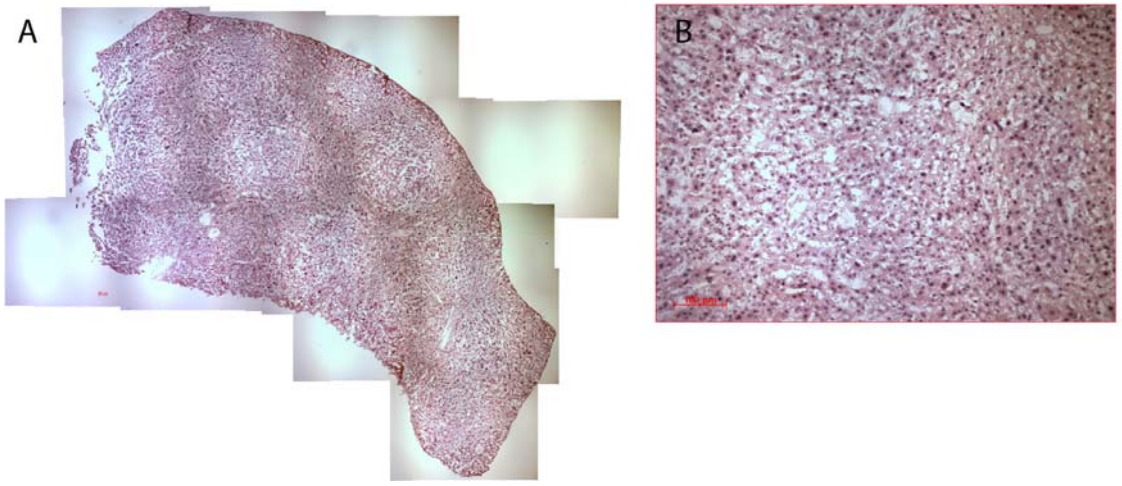

Figure 41 Histological staining of ONLSC shows characteristic disorder of cell proliferation. (A) Overview of an exemplary HE-stained cryosection of an ONLSC. The tissue showed no usual liver structure (central vein, outwards radiating hepatocytes), but is an image of unordered cell proliferation. (B) Single image of cryosection shown in (A). The close-up shows the numerous cell nuclei of various size.

4.8.2 Pancreas

Pancreata were not prepared into OSC due to the soft texture of the organ. Rather, they were manually cut into organotypic explant cultures (OEC) of about 1 mm³ in size. In the following, pancreas OEC from C3H mice will be abbreviated OPEC, pancreas OEC from double transgenic c-myc/TGF-α mice will be labeled OTPEC. Cryosections from OPEC and OTPEC were HE-stained for the morphological assessment of both OEC.

The pancreas is made up of an exocrine (acini) and endocrine (Langerhans islets) part as well as interlobular connective tissue and interlobular deferent ducts. The tissue architecture of C3H pancreas was well preserved in OPEC, even after 8 days *in vitro* (div) (Figure 43A+B). In the close-up of the overview of an OPEC cryosection (Figure 43B), the Langerhans islets (blue arrows), the acini (red arrows), and connective septae (green arrows) were distinctly distinguishable. Note the homogeneously distributed intense nuclear staining with heamatoxylin throughout the OPEC even after 8 div, which allowed for the conclusion of an intact state of the tissue. In comparison, the nuclear staining of liver OSC showed a distinctly fainter staining in the central part of the cryosections than at the outer edges.

The c-myc/TGF-α pancreas was, even from a macroscopic point of view, very different to that of a healthy C3H mouse. Whereas the C3H pancreas was very soft *ex vivo* and unfolded easily in solution, the genetically altered pancreas was hard and compact, also in solution. In contrast to the morphologically intact OPEC, which displayed the characteristic histological features of the pancreas (acini and Langerhans islets distributed in regular lobules with interlobular connective septae), the OTPEC looked completely different (Figure 44). Almost the complete section showed signs of an extensive fibrosis, indicated by an almost complete lack of cell

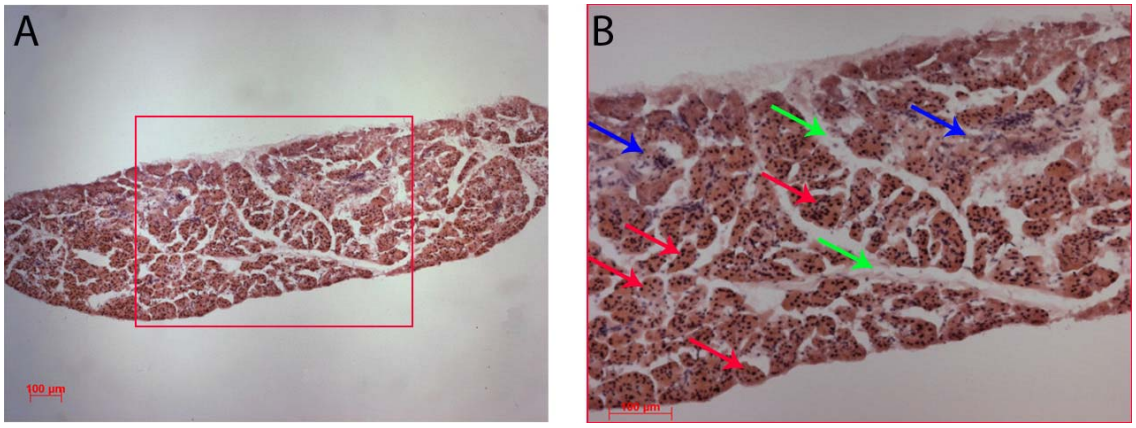

Figure 43 OPEC maintain morphological characteristics in histological staining. (A) Exemplary HE-stained cryosection of OPEC. This slice was kept 8 div. Morphologically, the specific structures of pancreas tissue were well intact even after a week *in vitro*. (B) Close-up of (A). The exocrine (acini, red arrows) and endocrine (Langerhans' islets, blue arrows) pancreas could easily be identified. They were interspersed with strands of connective tissue (green arrows).

nuclei. Only a small part located in the upper part of the section showed a distinct nuclear staining, indicating viable cells. This part was made up of tubular complexes, so-called redifferentiated acini. Langerhans islets could not be identified in this section, which was exemplary for all OTPEC. The pancreas of the c-myc/TGF-α mice could thus not be considered to be morphologically intact tissue and subsequently, suggested functional loss of the pancreatic tissue as well.

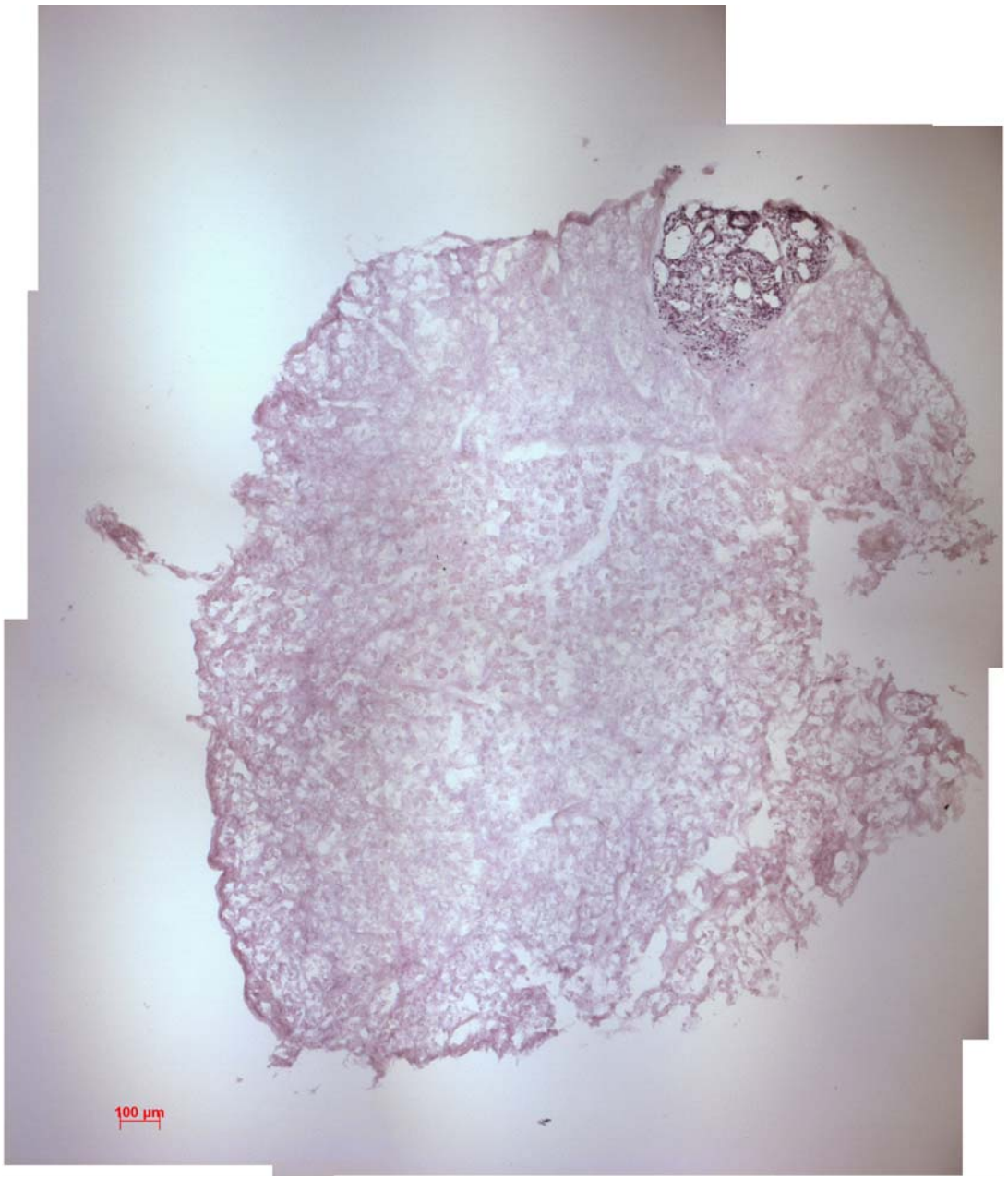

Figure 44 OTPEC showed extensive deterioration in tissue architecture. Overview of an exemplary HE-stained cryosection of an OTPEC kept 2div. The cryosection showed an excessive deterioration/fibrosis of the pancreas tissue, with barely any structures recognizable. Cell nuclei could only be identified at the top of the section, yet morphologically the tissue could no longer be considered intact. Whereas the vast majority of the area was marked by fibrotic tissue, the part with intact cell nuclei was made up of tubular complexes, so-called redifferentiated acini.

4.9 Bioluminometric studies

4.9.1 OLSC showed a distinct circadian rhythm even after irradiation *in vitro*

The liver does not have any photosensory receptors, it therefore does not react to light as an exogenous *zeitgeber*. Nevertheless, the liver is subject to a circadian rhythm superimposed on it via the suprachiasmatic nuclei (SCN). The SCN is the "masterclock" which controls the circadian clock of the complete organism and thus the peripheral tissues. As ingestion is an integral element of daily routine and occurs at given times of day (which in turn are regulated by the SCN), the liver's functions are subject to circadian oscillations.

Yoo et al. [Yoo2004] have shown that if the SCN is destroyed *in vivo* or peripheral organs are separated from the SCN and kept viable in culture, certain organs such as lung, kidney, heart, retina, and liver display self-sustained, stable circadian oscillations in culture. The analysis of these rhythms is possible in an online manner via a bioluminescent reporter system. In $Per2^{luc}$ mice, the expression of one of the central clock genes, *Per2*, is linked to the expression of luciferase, which reacts with luciferin added to the culture medium to produce bioluminescence. This bioluminescent activity can be recorded in real time in a light-tight box using photomultiplier tubes. A higher bioluminescent activity in the recording indicates an increased amount of luciferase, from which an increased expression of *Per2* can be inferred.

A steady oscillation of the bioluminescent activity was recorded in all OLSC, as can be seen in the real time recordings (Figure 45A). All OLSC showed at least one distinctive peak before irradiation and at least two to three peaks post-irradiation. After that, the amplitude damped too much to ascertain further rhythmic luciferase-expression. This, however, was most likely due to the depletion of luciferin as well as nourishment, as these OLSC did not receive a medium change during recording. In Figure 45A+B, the mean real time recordings of mock-irradiated and irradiated OLSC were plotted against the laboratory time, i.e. Central European Time (CET). In Figure 45A, before the experiment (experiment in this case refers to taking samples to the irradiation place and includes all samples, regardless of whether they were irradiated or mock-irradiated), the OLSC from the different circadian timepoints oscillated out-of-phase with a phase shift of approximately 12h. As animals of both circadian timepoints were killed at the same laboratory time, this phase-shift corresponded exactly to the 12h phase-shift the animals had to each other (CT06 vs. CT18). This also showed that the fact of taking liver into culture with medium containing serum initially did not reset its circadian clock.

Figure 45B shows the mean real time recordings of irradiated and mock-irradiated OLSC from mice killed at CT06 and CT18, respectively. Minima and maxima of luciferin expression as well as the time of their occurrence are given as % of maximum in Table 4. The abscissa is

calibrated to laboratory time, i.e. Central European Time (CET). After the experiment, a steady rhythmic expression of luciferase could be detected in the mock-irradiated samples as well as the irradiated OLSC. Both mock-irradiated and irradiated OLSC from different circadian timepoints seemingly oscillated in phase post-experiment. Irradiated OLSC were phase-shifted by approximately 1h, indicating a phase-shift due to the irradiation. OLSC prepared at CT06 or CT18 were no longer phase-inverted (phase-shifted by 12h) as the medium was changed prior the experiment, reinitiating the circadian rhythm.

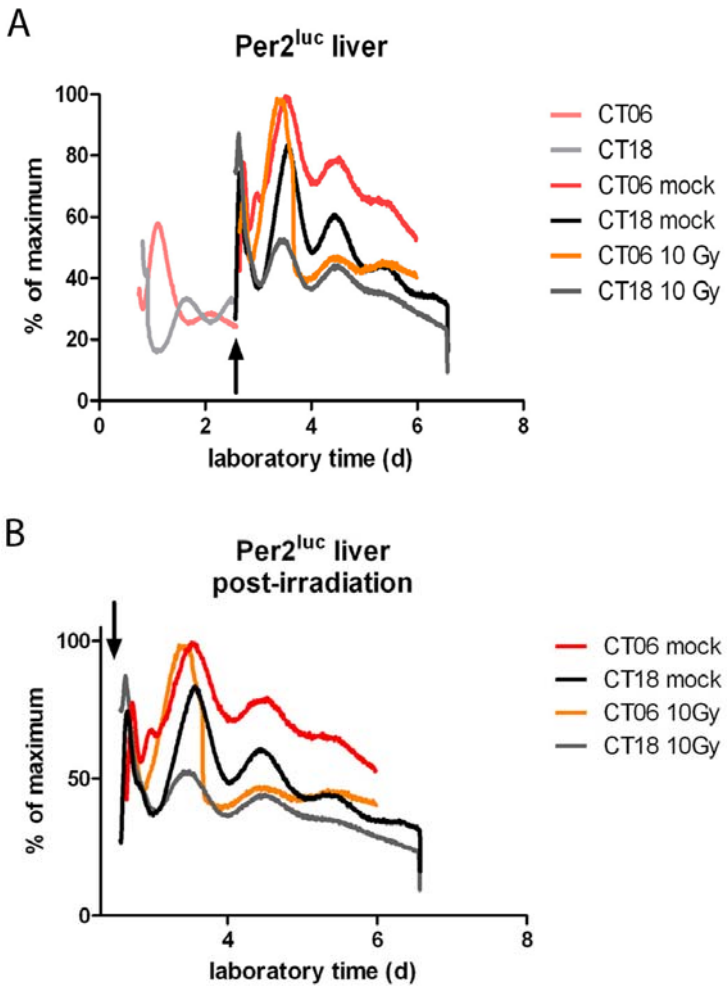

Figure 45 Real time recordings of OLSC recorded before and after the experiment. Mean real time recordings of OLSC prepared at CT06 and CT18. (A) Pre-irradiation recordings are phase-inverted. After the experiment, samples oscillate in phase, regardless of the time of death of the donor animal. (B) Mean real time recordings post-irradiation. Irradiated OLSC are phase-advanced by approximately 1h compared to mock-irradiated OLSC, regardless of the time of death of the donor animal.

Table 4 Minima and maxima of luciferin expression from OLSC. Minima and maxima are given as % of maximum ± the standard error of the mean (SEM). The SEM represents the sampling error of all scored OSC and OEC from two independent experiments. The time of minima and maxima occurrence is given in hours of laboratory time. For example, 40 h would mean the peak occurred at 4 pm at the second day of recording.

	CT06				**CT18**			
Before experiment	**h**		**% of max. ± SEM**		**h**		**% of max. ± SEM**	
1. minimum	40,3		25,2 ± 2		26,2		15,8 ± 10	
2. minimum	-		-		49,8		25,5 ± 3	
1. maximum	26,3		57,8 ± 10		39,5		33,5 ± 2	
2. maximum	50,8		28,9 ± 3		-		-	
After experiment	**mock h**	**mock % of max. ± SEM**	**10 Gy h**	**10 Gy % of max. ± SEM**	**mock h**	**mock % of max. ± SEM**	**10 Gy h**	**10 Gy % of max. ± SEM**
1. minimum	68,0	55,9 ± 8	68,8	45,2 ± 9	72,0	36,7 ± 2	73,2	37,7 ± 11
2. minimum	98,3	70,6 ± 12	93,8	38,7 ± 28	96,3	48,1 ± 2	96,3	36,4 ± 8
1. maximum	85,5	99,0 ± 0,2	82,0	98,2 ± 1	85,0	83,2 ± 16	81,7	52,6 ± 9
2. maximum	108,7	79,4 ± 13	107,7	47,1 ± 35	106,0	60,6 ± 6	105,8	43,8 ± 13

4.9.2 Pancreas showed a distinct circadian rhythm *in vitro*

In all, 26 OPEC were bioluminometrically analyzed. Of these, only two showed a discernible circadian rhythm prior to irradiation. The rest of the OPEC recorded only one peak prior to irradiation (Figure 46). Minima and maxima of luciferin expression as well as the time of their occurrence are given as % of maximum in Table 5. The abscissa is calibrated to laboratory time, i.e. Central European Time (CET). After the experiment, mean real time recordings showed one distinct peak in *Per2*-expression in all samples, followed by a strong dampening of the signal. This indicated that pancreas did oscillate *in vitro* post-irradiation.

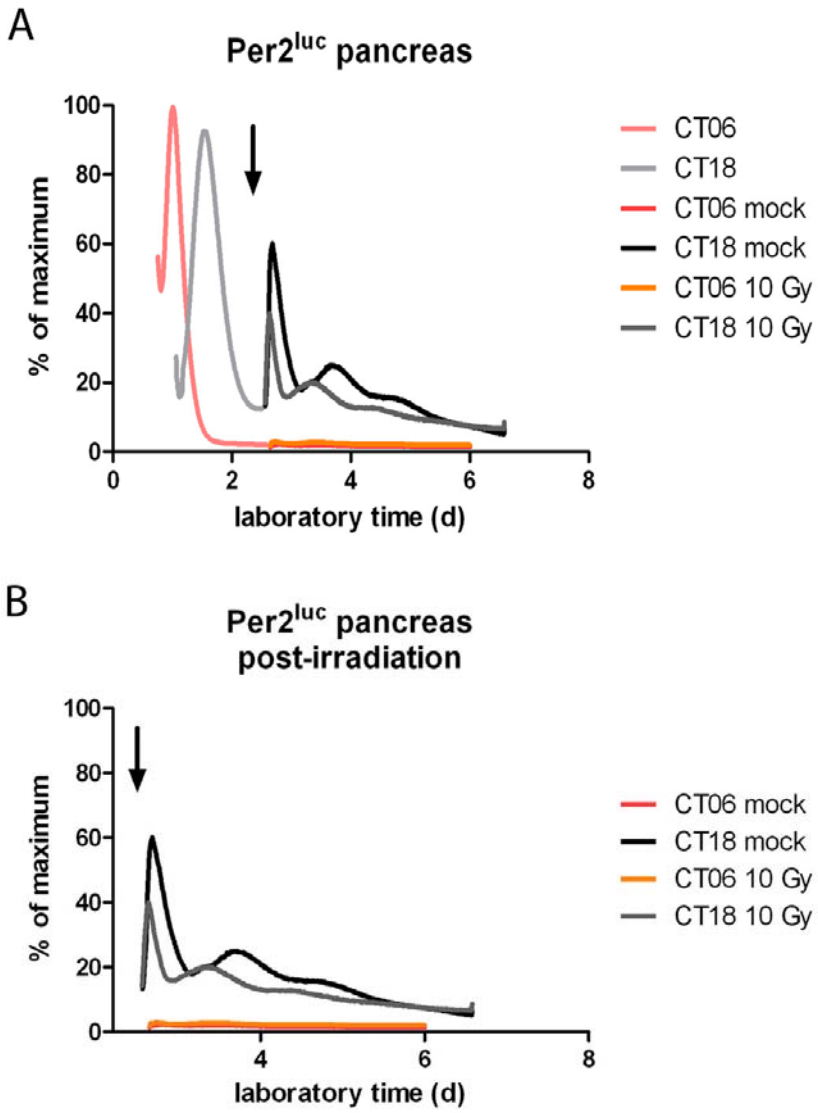

Figure 46 Real time recordings of OPEC irradiated before and after the experiment. Mean real time recordings of OPEC prepared at CT06 and CT18. The abscissa is calibrated to Central European Time (CET). Pre-irradiation, there is only one discernible peak for all OPEC. After the experiment, OPEC prepared at CT18 showed one peak in bioluminescence. OPEC prepared at CT06 show no bioluminescent activity.

Table 5 Minima and maxima of luciferin expression from OPEC. Minima and maxima are given as % of maximum ± the standard error of the mean (SEM). The SEM represents the sampling error of all scored OSC and OEC from two independent experiments. The time of occurrence of minima and maxima is given in hours of laboratory time.

	CT06				**CT18**			
Before experiment	**h**		**% of max. ± SEM**		**h**		**% of max. ± SEM**	
1. minimum	-		-		-		-	
2. minimum	-		-		-		-	
1. maximum	24,2		99,5 ± 0,3		37,0		92,7 ± 4	
2. maximum	-		-		-		-	
After experiment	**mock h**	**mock % of max. ± SEM**	**10 Gy h**	**10 Gy % of max. ± SEM**	**mock h**	**mock % of max. ± SEM**	**10 Gy h**	**10 Gy % of max. ± SEM**
1. minimum	-	-	-	-	76,0	17,8 ± 7	70,3	15,8 ± 7
2. minimum	-	-	-	-	-	-	-	-
1. maximum	-	-	-	-	89,7	24,8 ± 5	80,8	20,1 ± 10
2. maximum	-	-	-	-	-	-	-	-

4.9.3 Adrenal glands showed a distinct circadian rhythm in vitro

OAEC were used as control samples with a known stable circadian oscillation under standard culturing conditions [Oster2006, Andrews1964, Andrews1971]. Mean real time recordings of OAEC recorded for bioluminescent activity prior to and post-irradiation showed distinct peaks for the whole recording time (Figure 47). Minima and maxima of luciferin expression as well as the time of their occurrence are given as % of maximum in Table 6. The abscissa is calibrated to laboratory time, i.e. Central European Time (CET). Most likely due to their size (they are at least 30% - 50% the size of an OLSC), they did not use up as much of the nourishment and luciferin

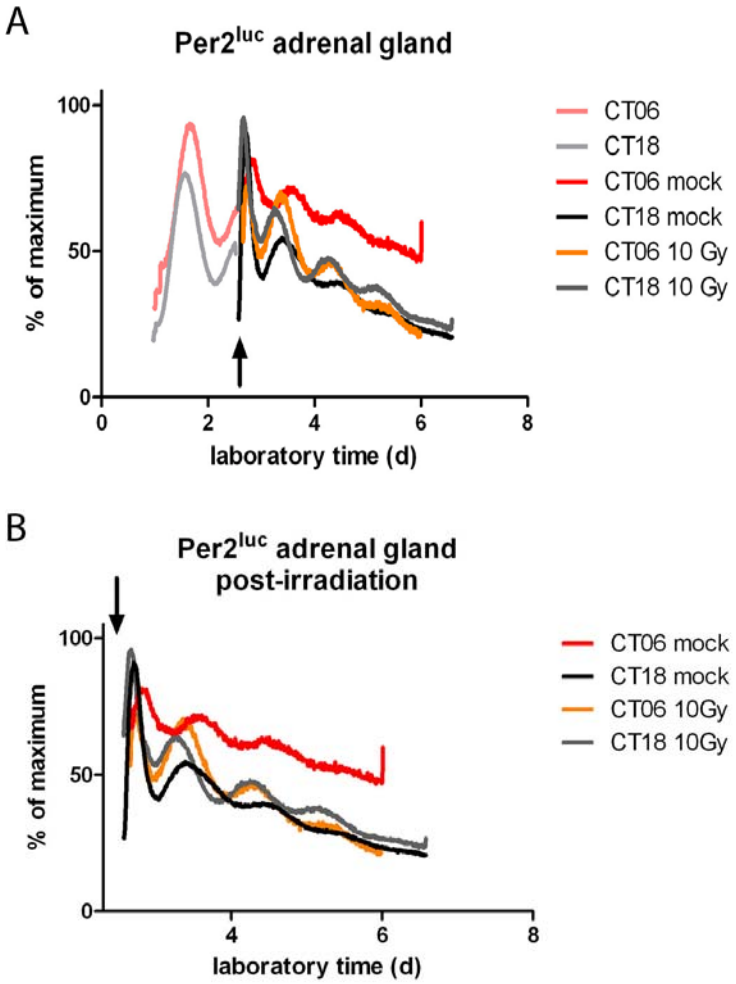

Figure 47 Real time recordings of OAEC recorded before and after the experiment. Mean real time recordings of OAEC prepared at CT06 and CT18. (A) Pre- and post-irradiation recordings oscillate in phase, regardless of the time of death of the donor animal. (B) Mean real time recordings post-irradiation. As compared to mock-irradiated OAEC, irradiated OAEC are phase-shifted by approximately 4h, regardless of the time of death of the donor animal.

per unit time, making it possible to identify four peaks during the time of recording. However, damping of the amplitude was also present in these cultures. Note that the recordings of the OAEC recorded directly after preparation and plotted against CET oscillated in phase. This is in contrast to the results generated for OLSC (Figure 45A). As the animals were entrained to the new 12:12 LD cycle for two weeks prior sacrifice, it is unlikely that their adrenal glands were not entrained to the new cycle. Most probably, the endogenous clock of the adrenal glands was reset during the OAEC preparation, leading to synchronized OAEC (Figure 47). It is therefore meaningless to classify the adrenal glands according the time of death of their donor animals. The classification was kept as a means to link the organs to their donor animals.

The mean real time recordings of mock-irradiated and irradiated OAEC after the experiment are shown in Figure 47B. Real time recordings of irradiated samples were phase-advanced by 4h compared to mock-irradiated OAEC.

Table 6 Minima and maxima of luciferin expression from OAEC. Minima and maxima are given as % of maximum ± the standard error of the mean (SEM). The SEM represents the sampling error of all scored OSC and OEC from two independent experiments. The time of the occurrence of minima and maxima is given in hours of laboratory time.

	CT06				**CT18**			
Before experiment	**h**		**% of max. ± SEM**		**h**		**% of max. ± SEM**	
1. minimum	53,4		52,3 ± 5		51,0		38,7 ± 4	
2. minimum	-		-		-		-	
1. maximum	40,7		93,5 ± 3		37,6		76,9 ± 9	
2. maximum	-		-		-		-	
After experiment	**mock h**	**mock % of max. ± SEM**	**10 Gy h**	**10 Gy % of max. ± SEM**	**mock h**	**10 Gy % of max. ± SEM**	**mock h**	**10 Gy % of max. ± SEM**
1. minimum	78,2	64,9 ± 16	72,2	48,0 ± 12	72,9	40,8 ± 4	71,4	53,4 ± 6
2. minimum	-	-	93,9	40,9 ± 11	-	-	92,2	39,9 ± 2
1. maximum	85,7	71,6 ± 20	80,7	70,5 ± 8	81,9	54,3 ± 1	77,7	65,0 ± 5
2. maximum	-	-	-	-	-	-	101,9	47,8 ± 1

4.9.4 Irradiation with X-rays did not lead to a change in period length

A tissue-specific characteristic to describe the circadian rhythmicity is the period τ of the oscillatory bioluminescence. For the OLSC recorded before irradiation, the data were pooled according to the time of death of the donor animals. Due to synchronization of the circadian rhythms via medium exchange prior to irradiation, post-irradiation data were pooled depending on whether OLSC had been irradiated or not. There was no significant difference between the mean periods of all recorded OLSC ($p=0.76$; ANOVA) (Figure 48A). Thus, radiation did not have an acute effect on circadian period.

The periods of the OAEC prepared at CT06 (Figure 48B) showed a relatively constant mean period τ roughly around 23 h, regardless of whether they were mock-irradiated or irradiated (CT06: $\tau_{06} = (24.2 \pm 1.2)$ h, mock: $\tau_{mock} = (23.5 \pm 1.0)$ h, X-ray: $\tau_x = (22.8 \pm 0.9)$ h). Errors given are the standard error of the mean (SEM). The samples which were harvested from animals killed at CT18 showed a significantly longer period ($\tau_{18} = (26.7 \pm 1.3)$ h) than the OAEC prepared at CT06 ($p<0.0001$; ANOVA). Again, the period was not affected by irradiation with X-rays.

The two real time recordings of the mock-irradiated OPEC which showed a distinct circadian

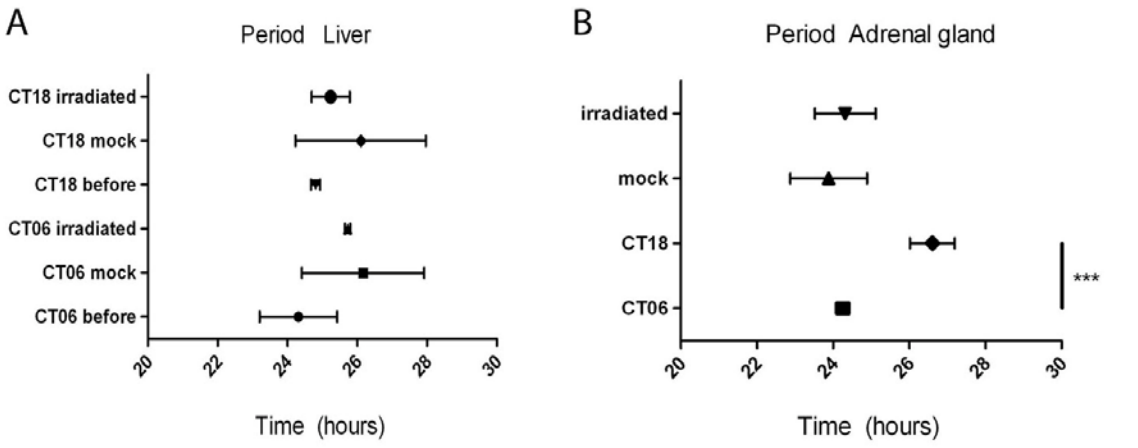

Figure 48 Mean periods for OLSC (A) and OAEC (B). (A) *CT06 before* and *CT18 before* are the mean periods (±SEM) of OLSC recorded directly after slice preparation according to the time of death of the donor animals. *CT06 mock* and *CT18 mock* are the periods of the mock-irradiated OLSC, *CT06 irradiated* and *CT18 irradiated* are the periods of the irradiated OLSC with regard to the time of death of the donor animals. There was no significant difference between the period lengths of OLSC prior to and after the experiment. (B) *CT06* and *CT18* are the mean periods (±SEM) of OAEC recorded directly after OEC preparation according to the time of death of the donor animals. *Mock* and *irradiated* are the mean periods (±SEM) of the mock-irradiated and irradiated OAEC regardless of the time of death of the donor animals. OAEC from donor animals killed at CT18 showed a significantly longer period than all the other OAEC. The SEM values represent the sampling error of all scored OSC and OEC from two independent experiments.

rhythm in bioluminescent activity gave a period of τ_{panc} = (26.0 ± 0.8) h. All other samples were to be considered arrhythmic, so that there were no period data for samples measured directly after OPEC preparation or after irradiation.

4.9.5 Irradiation with X-rays lead to a phase-shift

Phase maps were used to analyze whether radiation has a phase-shifting effect on OLSC and OAEC. Mapped were the time of day of the peaks in bioluminescence between 12 h and 36 h *in vitro* before and after irradiation, respectively.

As can be seen in Figure 49A, the phases of the *Per2*-expression in OLSC prepared from animals killed at CT06 and CT18, respectively, and recorded immediately after slice preparation were shifted 2.5 h at the most for the given experiment. There was a significant difference between the phase of mice killed at CT18 which were recorded for 5 d immediately after slicing and mice killed at CT18 which were recorded for 1 d prior to irradiation. The time shift here was 4 h.

For the determination of phase shifts after irradiation, data from irradiated and mock-irradiated samples were pooled, respectively, regardless of the time of death of the donor animal. This was due to the fact that all samples, regardless of the time *in vitro*, received a medium change prior to the experiment, which reinitiated the circadian clock of the OLSC (see real time data, Figure 45). After 1 div, X-ray irradiation with a dose of 10 Gy lead to a (statistically not significant) phase advance of about 1 h with respect to the mock-irradiated samples. After 7 div, mock-irradiated OLSC showed a peak at CT03.5. X-ray irradiation with a dose of 50 Gy lead to a significant phase advance of about 6 h (ANOVA, $p<0.001$, Newman-Keuls post-test).

Phase maps for OAEC measured immediately after organ culture preparation showed a peak around 23 h (CT06,7div = (23.1 ± 1.5) h; CT18,7div = (22.9 ± 0.6) h; CT06,1div = (23.9 ± 1.8) h). Cultures prepared at CT18 and kept 1 div before irradiation peaked slightly advanced, at CT21.4 ± 0.6 h. After irradiation with 10 Gy, irradiated samples were phase-advanced by about 4 h. There was only one adrenal which was irradiated with 50 Gy and one adrenal that was mock-irradiated in that experiment. Therefore, the data from this irradiation could not be taken into account for the statistical analysis. However, the data fit the irradiation data with 10 Gy very nicely (see Figure 49D).

As there was no periodic data to be gained from irradiated pancreas organ cultures, we must conclude from these experiments that irradiation of pancreas does not lead to a phase-shift, but rather to a complete abolishment of circadian rhythm. For mock-irradiated OPEC, bioluminescent peaks were calculated to be at CT08.4 ± 1.8 h.

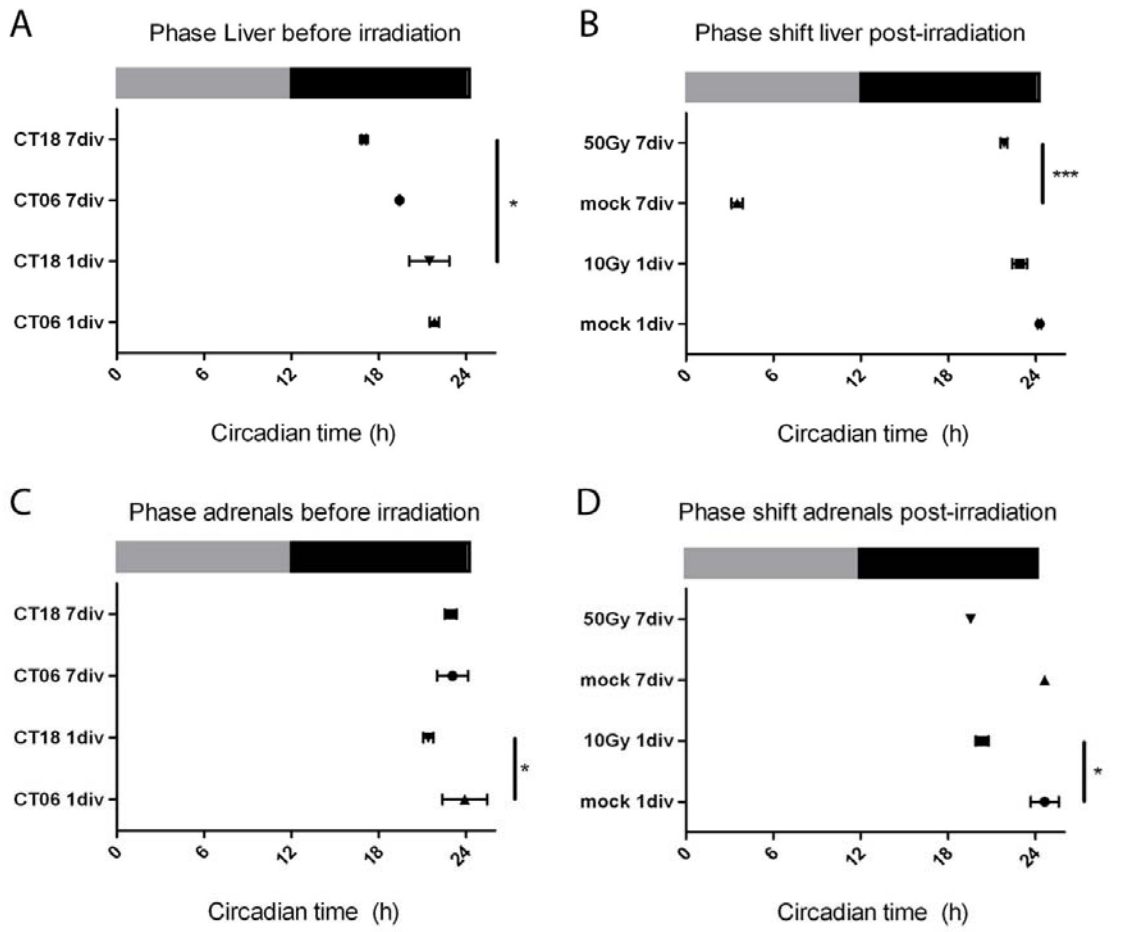

Figure 49 Phase maps for OLSC and OAEC prior to and post-irradiation. Mapped are the mean peaks of bioluminescent activity between 12h and 36h *in vitro*. (A) Phase map for OLSC recorded immediately after slice preparation. *CT067div* and *CT18 7div* showed peaks shifted about 2.5h (~CT19.5 and ~CT17, respectively), the peaks from C*T06 1div* and C*T18 1div* were shifted about 1h (~CT22.5 and ~CT21.25, respectively). (B) Phase map for OLSC recorded after irradiation. *Mock 1div*: CT 0.25; *10Gy 1div*: CT23; *Mock 7div*: CT 3.5; *50Gy 7div*: CT 21.8. Irradiation with 10Gy at 1div lead to a (statistically not significant) phase shift of 1h. Irradiation with 50Gy at 7div lead to a statistically significant phase advance of about 6h. (C) Phase map for OAEC recorded immediately after slice preparation. C*T06 7div* and C*T18 7div* both peaked at CT23, the peaks from *CT06 1div* and *CT18 1div* were shifted about 2.5h (~CT23.9 and ~CT21.4, respectively). (D) Phase map for OAEC recorded after irradiation. *Mock 1div*: CT00.7; *10Gy 1div*: ~CT20.3; *Mock 7div*: CT00.7; *50Gy 7div*: CT 19.5. Irradiation with 10Gy at 1div lead to a phase advance of more than 4h. There were only single data for the irradiation with 50Gy, but they nicely fit the data from the irradiation after 1div and promoted a phase-advance of about 4h.

5 Discussion

The first neoplastic tissue slices to be taken into culture for experimentation were prepared almost 100 years ago in 1923 [Warburg1923]. These first tissue slices were manually prepared with a razor blade at a thickness > 0.3 mm, and were viable only for a short time *in vitro*. As the thickness of prepared slices is of crucial importance for their viability [Parrish1995, Guo2007], advancements in tissue culture were not realized until the early 1980s, when the process of slice preparation at a determined thickness could be automated with the Krumdieck tissue-slicer [Krumdieck1980]. The optimum slice thickness for organotypic slice cultures (OSC) with regard to tissue viability and handling was determined to be between (100-250) µm [Smith1985, Guo2007, Verrill2002]. Since then, especially liver precision-cut tissue slices were mostly used to study drug metabolism [Guo2007, Shigematsu2000] and drug toxicity [Catania2007, Klassen2008, vandeBovenkamp2005]. However, most of these studies were performed with short-term cultures, usually kept *in vitro* for roughly 24 h, up to a maximum of 96 h [Klassen2008, Vickers2004].

The pancreas parenchyma consists of two main, functionally completely different substructures, the endocrine and the exocrine pancreas. Whereas the endocrine pancreas is responsible for the production of hormones such as insulin or glucagon and their release into the bloodstream in order to control blood glucose levels, the exocrine pancreas produces digestive enzymes which are released into the small intestine. These enzymes take part in the digestion of carbohydrates, lipids, and proteins. Since these two parts of the pancreas function so very differently, cell cultures – characteristically preserving only one cell type *in vitro* – usually focus on diseases of either part, i.e. diabetes mellitus or pancreatic cancer [Ulrich2002, Chick1975, Lieber1975, Bachem2008]. Therefore, many organotypic pancreatic explant cultures (OPEC), in which both parts of the pancreas are preserved, are nevertheless evaluated with regard to only one region [Resau1983, Speier2003, vanGeer2009, MeneghelRozzo2004].

In the present thesis, murine organotypic liver slice cultures (OLSC) and murine OPEC were prepared to elucidate the effects of ionizing radiation on living tissue *in vitro*. To this end, OLSC and OPEC were prepared from C3H mice and organotypic healthy liver slice cultures (OHLSC), organotypic neoplastic liver slice cultures (ONLSC), and organotypic transgenic pancreas explant cultures (OTPEC) were prepared from transgenic c-myc/TGF-α mice, respectively. OLSC and OPEC were irradiated with X-rays in order to establish a reference system for radiation side-effects in healthy tissue. OHSLC, ONSLC, and OTPEC

were irradiated with a spread out Bragg peak (SOBP) of ^{12}C. All samples were immunohistochemically stained for biological markers of proliferation, apoptosis, and DNA double-strand breaks (DSBs). OLSC and OHLSC were compared to analyze a possible difference in radiation effect of the two different radiation types.

In radiobiology, standard biological experimental models comprise either animal or human cell lines, cell culture of primary and even stem cells or *in vivo* models. An adequate *in vivo* model – next to rodents – for ionizing radiation-induced side effects, especially in skin, is pig, as its skin is similar to human skin [Zacharias1997, Krämer2000]. The results achieved in this thesis are part of the first efforts to link the advantages of the as yet standard biological modeling systems in radiobiology to the model of OSC: the easy handling and greater amount of samples from one laboratory animal while maintaining the 3D-architecture of a cell's environment and reducing the problem of interindividual differences whilst reducing the number of laboratory animals needed in one experiment [Müller2010, Merz2010, Merz2011].

5.1 Effect of X-rays on OLSC

5.1.1 Proliferation

Proliferation in adult murine liver is very low. Yang et al. [Yang2010] report of very few positive Ki67-labeled cells 24h after partial hepatectomy, which gives an indication of the normal proliferative state of healthy liver. Mori et al. [Mori1999] determine the proliferation rate of OLSC from fetal and neonatal mice to be approximately 30%, however, they only detected positive PCNA signals at the periphery of the slices. The effect of X-rays on murine OLSC is not reported in literature, but the diminishing effect on the number of proliferating cells has been reported extensively for various cell lines [Belyakov1999, Wulf1985, Ofuchi1999, Goldstein1981] and has obviously been proven successful in clinical radiotherapy [Kamada2012, Durante2010, Schulz-Ertner2009, Schulz-Ertner2006].

Next to the deleterious effect of ionizing radiation, studies driven by the observation that the severity of certain side-effects of radiotherapy depend on the timepoint at which radiation is applied [Rahn2011, Shukla2010], the timepoint at which ionizing radiation acts on biological target material may also influence the biological reaction [Becciolini1997, Blank1995, Haus2002, Scheving2000]. Furthermore it has been shown that proliferation (of healthy tissue) is time-dependent [Barbason1987, Miller2007, Sharma2010], the prevailing theory being that the sensitive S-phase of the cell cycle needs to be shielded from harmful exogenous stimuli (such as UV-radiation) [Johnson2010]. Based on these presettings, it is evident that a tissue response to X-ray radiation regarding proliferation is expected to be time-dependent.

For this thesis, OLSC of healthy adult C3H mice were prepared at two different circadian timepoints, the middle of the subjective day (CT06) and the middle of the subjective night (CT18). These were irradiated with X-rays at doses between 2Gy and 10Gy. The results of proliferation response of these OLSC do not show any dose-effect. Proliferation rate in mock-irradiated OLSC is extremely low, below 0.2%, resembling the result from *in vivo* evaluations, for which the proliferation rate in liver was determined to be around 0.5%. Irradiated samples of any dose generally show a lower proliferation rate, which, however, was not statistically significant. The subjective time of day at which the OLSC were irradiated did, however, show a significant response in dose-dependent radiation effect. All observed proliferation rates for samples from mice killed at CT18 are lower than those at CT06.

The absence of a significant dose-effect in these experiments is contrary to results reported in literature [Scott2001]. However, the data do show a tendency for decreasing proliferation after irradiation with X-rays. Ki67 is present throughout the cell cycle, and if the cell cycle is stopped for whatever reason, Ki67 is decomposed immediately [Scholzen2000]. Therefore, X-rays do show an effect on the proliferation rate of OLSC. Yet as the rate is extremely low in a mock-irradiated state, it may take longer for the deleterious effect of X-rays to significantly show. In the current culturing system, this may be masked by the general deterioration of the OLSC, which were fixed 1h and 24h post-irradiation. In addition, Scott et al. have found that the inhibition of proliferation is not due to apoptosis but rather on a cell cycle delay for a time period of 24-96h [Scott2001].

In the liver, Miller et al. [Miller2007] found the largest clusters of rhythmic genes to be expressed at CT06 and CT18 as well as ascertaining the timing of cell division to be gated by the circadian clock. The significant circadian effect detected in OLSC in this thesis are in good agreement with these findings, as proliferation at the middle of the subjective day was significantly higher than at the middle of the subjective night. This circadian effect was detected in spite of a medium change OLSC received prior to irradiation, the medium containing 10% fetal bovine serum. According to Balsalobre et al. [Balsalobre1998], a serum shock induces circadian gene expression in mammalian tissue culture cells. Therefore, in addition to proving a robust rhythm of liver in vitro, these results indicate that C3H OLSC have a robust circadian rhythm which withstands reinitiation by a single medium change.

In addition to following the circadian rhythm dictated by the SCN, the circadian clock of the liver can also be entrained by food [Atwood2011, Stokkan2001, Stephan2002]. C3H melatonin-proficient mice, even if exposed to an inverted light/dark cycle, entrain to the new cycle within a few days [Pfeffer2012], the liver adjusting to this new circadian stimulus

about two days later [Stokkan2001]. All animals used for this thesis were entrained to a new light/dark cycle for at least two weeks prior to sacrifice and had access to food and water *ad libitum*. A stable entrainment even of the inverted mice can be inferred from the proliferation data.

5.1.2 Apoptosis

An increasing apoptosis rate following X-ray irradiation has been reported in literature for various cell types such as e.g. lymphocytes [Boreham1996, Fujikawa2000], T-cells hybridoma [Warters1992], and intestinal epithelial cells [Inagaki-Ohara2002]. Christiansen et al. [Christiansen2004] report of an apoptosis rate of roughly 12% for hepatocytes irradiated with X-rays at a dose of 8 Gy. Tello et al. [Tello2008] report of an increased activity of caspase3 in Kupffer-cells up to 50% 24h post-irradiation with an X-ray dose of 8Gy. In addition, circadian rhythms in the incidence of apoptotic cells have been reported for various tissues [Duncan1983, Ijiri1988, Ijiri1990].

The apoptotic rates determined for OLSC after irradiation with X-rays in this thesis are inconclusive. No dose-dependency could be established, although samples from mice killed at CT06 and fixed 24h post-irradiation show a tendency of linear dose-dependency, i.e. an increasing apoptotic rate with increasing dose. All apoptotic values determined for the different circadian timepoints are roughly around 2% and do not allow for the conclusion of a circadian effect of radiation response.

Apoptotic rates of approximately 2% post-irradiation with X-rays are much lower than previously reported [Christiansen2004]. An increased rate in cleaved caspase3 [Tello2008] after 24h supports the stable apoptotic rate found in mock-irradiated and irradiated OLSC fixed 1h post-irradiation. After (irradiation) damage, it takes several hours for the cell to activate its cell death program, in which caspase3 can be a part of. Additionally, cells do not necessarily have to go into apoptosis via the caspase3 pathway.

This may also be the reason for an absent circadian effect concerning apoptotic rates in OLSC. Reports of different time periods after which apoptosis peaks post-irradiation range from a few hours [Potten1998, Yanagihara1995, Mirkovic1994] up to 168 h [Mirzaie-Joniani2002]. It is therefore likely that cells in OLSC take longer to activate the caspase3 pathway. Thus, fixing the OLSC 24h post-irradiation was not long enough to unmask a circadian effect, as it was not long enough to initiate apoptosis via caspase3. It can be concluded from this data, that apoptosis in OLSC takes longer than 24h to show a discernible effect.

Another possibility for the absence of a dose or circadian effect is that, following irradiation, cells did not die apoptotically but via necrosis, which would not be detected via

a cleaved caspase3 staining. This could be a short-term response, however, as the number of apoptotic cells increases with dose 24h post-irradiation. Necrosis was not considered a dominant effect masking apoptosis results.

5.1.3 DNA double-strand breaks

The target molecule for radiation damage in biological material is the DNA of the cell. DNA damage can either be classified as single-strand breaks (SSBs), double-strand breaks (DSBs), or – the most severe form of DNA damage – clusters of DSBs. Since the late 1990s, it is possible to visualize DNA DSBs located on histone H2AX via immunohistochemistry [Rogakou1998], thus allowing for the documentation of the linear dose-dependency of DNA DSBs in response to irradiation [Ghardi2012, Rübe2008].

Considering the subjective timepoint at which DNA damage occurs, the response to DNA damage has recently been closely linked to the biological clock [Ramsey2011, Khapre2010, Sancar2010, Collis2007]. Of the various ways in which DNA damage can be repaired, only nucleotide excision repair has been reported to be circadian clock controlled. Whether the repair of DSBs is time dependent or not remains to be elucidated. To this end, the number of γH2Ax positively-labeled cells in irradiated samples prepared at the different circadian timepoints CT06 and CT18 was evaluated.

Surprisingly, OLSC did not show any positive γH2Ax-staining even 1 h post-irradiation and at a dose of 10 Gy, regardless of the subjective time of day at which samples were irradiated. Since there is no physical reason why the samples should have not been irradiated and the reaction specificity of the used antibody was verified in OLSC that had been irradiated with X-rays at a dose of 50 Gy, it must be concluded that any radiation-induced DNA DSBs were immediately repaired in the OLSC. Murray et al. [Murray1984] report of liver to be the fastest normal tissue to repair DNA damage after *in vivo* X-ray irradiation with doses between 10 Gy and 12.5 Gy, however still showing elevated values of unrepaired DNA lesions after 2 h compared to control values. According to Rübe et al. [Rübe2008], increased levels of γH2Ax-foci can be detected up to 24 h in murine brain, lung, heart, and intestine after *in vivo* X-ray irradiation of 2 Gy. A possible explanation of the absent DNA DSB detection could be that 24 h after OLSC preparation, the tissue is still acclimatizing to culturing conditions and repair mechanisms are activated due to the mechanical trauma of slicing. Irradiation with even 10 Gy of X-rays does not seem to pose a significant additional damage. However, after 7 div, the OLSC have had time enough to acclimate to culturing conditions and the remaining viable cells show a definitive DNA DSB rate after X-ray irradiation of 50 Gy. This indicates the need for still optimizing culturing conditions for OLSC from adult donor animals so as to keep OLSC viable in culture for a prolonged

period of time to exclude masking of any effects due to acclimatization to culture, even though OLSC have successfully been used in several short-term studies [Olinga1997, Catania2007, Guo2007, vandeBovenkamp2005]. The rate of X-ray-induced DNA DSBs in OLSC should systematically be analyzed depending on the time *in vitro* and on the time post-irradiation, starting at earlier timepoints than 1 h.

5.2 Effect of ^{12}C radiation on healthy and neoplastic transgenic liver OSC

Tissue-dependent differences in response to radiation-induced DNA damage have been reported by various authors and as early as 1936 [Murray1984, Meyn1983, Lawrence1936, Urano1984, Roeske1990]. Usually, however, this comparison is based on *in vitro* irradiated tumor cell lines compared to *in vivo* irradiation of healthy organs or implanted, non-*in vivo* induced tumors irradiated with the experimental animal. The ideal experimental design for comparing healthy to neoplastic tissue would be freshly resected human surgical specimens, as described in [vanGeer2009]. As these human tissue specimens are limited, especially for preliminary studies, the transgenic tumor-inducing mouse model poses a valuable alternative to elucidate the effects of radiation-induced DNA damage in healthy and neoplastic tissue.

In this thesis, the effects of ^{12}C-radiation on normal and neoplastic tissue of the same organ under the same experimental conditions were analyzed. To this end, OHLSC and ONLSC were prepared separately and subsequently co-cultured and thus irradiated in identical conditions, allowing the direct comparison of radiation-induced effects.

5.2.1 Proliferation

Proliferation in OHLSC was determined at approximately 0.5 % for most samples. No dose- or fixation time effect could be established. The proliferation rate for all samples irradiated at the middle of the subjective day (CT06) was significantly higher than for the samples irradiated at the middle of the subjective night (CT18).

Compared to the proliferation rate of OHLSC, the proliferation rate for ONLSC is about four-fold, generally approximately 2 %. Individual values show an increased proliferation rate up to almost 10 %. No dose-effect could be established, however, the proliferation result for samples irradiated at CT06 and fixed 24 h post-irradiation show an almost (non-significant) linear dose-dependent increase. The fixing timepoint was not determined

significant, and although the proliferation rate resembled the results from the OHLSC with regard to a circadian effect, this was also not significant.

The increased proliferation rate in ONLSC compared to OHLSC was expected and proves this culturing method a successful model in the study of comparing healthy vs. neoplastic tissue from one animal. However, proliferation rates detected here are much lower than for a variety of solid tumors, which have been detected to be between 30%-50% [Hall2004]. A possible explanation for this lower proliferation rate could be the general culturing conditions of the liver OSC, which cause them to deteriorate irrespective of additional external radiation-induced damage. The absent dose-effect on the other hand is rather unexpected. Numerous authors report of the enhanced relative biological effectiveness (RBE) for heavy ions compared to X-rays, not just concerning proliferation, but with regard to other methods of DNA damage detection as well, for example chromosome aberration, PCC, clonogenic survival, or DNA DSBs [Belyakov1999, Ofuchi1999, Skarsgard1967, George2003, Okayasu2012, Tobias1982, Urano1984]. In addition, the increase in proliferation seen for ONLSC irradiated at CT06 and fixed 1 h post-irradiation seems rather illogical. However, this radiation response has been reported before [Takahashi2004, Szczepanski1975, Potmesil1980, Hermens1969]. Takahashi et al. [Takahashi2004] irradiated human salivary gland tumor cells and determined their proliferation rate via an immunohistochemical Ki67 staining. The proliferation rate prior to irradiation is reported to be approximately 35%, which increased up to roughly 56% 5 d after a single irradiation of 15 Gy with X-rays. After this peak, the proliferation rate decreased to the original value prior to irradiation after 9 div. Based on their results, Takahashi et al. agree with Nakano [Nakano1991] that radiation most likely stimulates quiescent cells to enter the cell cycle.

Even though not statistically significant for ONLSC, both tissue types show a slightly higher proliferation rate at the middle of the subjective day (CT06) than at the middle of the subjective night (CT18). This allows for the hypothesis of a circadian influenced proliferation rate, not just in OHLSC, as could be expected concluding from various articles verifying circadian rhythmicity in isolated liver [Yoo2004, Davidson2006], but also for the ONLSC. Reports on neoplastic tissue are rather inconclusive, many articles verifying circadian oscillations in neoplastic tissue and cell lines [Williams2008, Davidson2006, Smaaland1995, Klevecz1987b], others falsifying it [Bernebei1992]. The proliferation results of this thesis do not document a circadian rhythm in ONLSC, but they do justify a more detailed inspection of this issue.

5.2.2 Apoptosis

Radiation-induced apoptosis has been reported by numerous authors in various biological model systems of (tumor) cell lines and *in vivo* irradiations [Boreham1996, Li1998, Warters1992, Schwartz1995, Tong2000, Inagaki-Ohara2002, Mirzaie-Joniani2002, Tsuchida1998, Nowak2006, Marshman2001, O'Brien2005]. Many document a dose-dependency [Fujikawa2000, Limoli2004, Guida2005, Takahashi2001, Yanagihara1995, Mirkovic1994, Michelin2004], some elucidate the effect time of day has at which irradiation occurs [Duncan1983, Ruifrok1988, Ijiri1990] and some report on the timescale needed for apoptosis to initiate [Radford1994, Shinomiya2001, Potten1998, Meijer1998, Gobé1998, Mirkovic1994, Michelin2004]. Most of these studies were conducted with X-rays, but Fujikawa et al. report of experiments with fission neutrons, Guida et al. used high-LET iron ions, Tsuchida et al. high-LET carbon ions and Meijer et al. high-LET nitrogen ions. In comparison to results achieved with reference X-rays, these authors report of an increased RBE for particles to induce apoptosis, although Tsuchida et al. report of detecting apoptosis only at distinct timepoints post-irradiation.

The apoptotic rate in OHLSC was determined between 2-10 %. A significant dose effect was established for OHLSC irradiated at CT18, fixed 24h post-irradiation. OHLSC prepared at both circadian timepoints and fixed 1h post-irradiation show a linear dose-dependency. No fixation time effect was established, but the subjective circadian timepoint of irradiation was evaluated as significant.

Apoptotic rates for ONLSC are higher than in OHLSC, they are roughly at 10-20%. Analysis of the apoptotic rate at *CT18,1h* suggests a linear dose-dependency. The apoptotic rate, however, decreases with increasing dose for these ONLSC. This at first glance illogical observation of less cell death at a higher radiation dose may be explained by hypothesizing an increase in necrosis at higher doses, causing a decrease in caspase3-positive cells. No fixation time of circadian effect was established.

Although reported by many authors, apoptotic rates in OHLSC and ONLSC were not conclusively determined to be dose dependent. Some report of elevated apoptosis rates only a few hours post-irradiation [Potten1998, Yanagihara1995, Mirkovic1994], others report of apoptosis reaching its peak 48 h post-irradiation [Guida2005, Meijer1998], some even later [Boreham1996, Mirzaie-Joniani2002]. As no elevated levels of apoptosis were detected up to 24 h post-irradiation in OHLSC or ONLSC, this indicates that increased apoptosis levels are – if at all – expected to appear later than 24 h post-irradiation. The apoptotic pathway via caspase3 was analyzed in this thesis – it is also possible that cells go into apoptosis via a caspase-free pathway. Additional methods of detection are needed to supply more insight into the DNA damage response of the OHLSC and ONLSC after irradiation.

Liver tends to keep its circadian rhythm *in vitro* [Yoo2004]. As for proliferation, a distinct circadian response with regard to apoptosis can be detected in OHLSC. This is in agreement with other reports of a circadian effect in apoptotic response to radiation [Duncan1983, Ruifrok1988, Ijiri1990] and indicates that OHLSC maintin a circadian rhythm *in vitro*. An absence of a circadian effect in ONLSC for apoptosis – just as for proliferation – suggests arrhythmic neoplastic tissue (*in vitro*).

5.2.3 DNA DSBs

Heavy ions are known for a higher induction of DNA DSBs than photons [Leatherbarrow2006, Ibañez2009, Okayasu2012], which by now can quantitatively be easily determined via γH2Ax-labeled foci [Desai2005, Kuo2008, Rogakou1998, Ghardi2012, Rübe2008]. If observed over a timeperiod post-irradiation, the formation of γH2Ax-foci can give information about the damage potential of the radiation used. In addition, the disappearing rate of foci, associated with the dephosphorylation of repaired DSBs, gives further information about the repair capacity of the specific biological model system [Nazarov2003, Antonelli2005, Kato2008]. Last but not least, the labelling of γH2Ax-foci has become a reliable and widespread detector for the bystander effect [Hu2006, Yang2005, Yang2007], which describes the observed cell death of unirradiated cells in the surrounding areas of irradiated cells.

Karlsson et al. and Mahrhofer et al. [Karlsson2004, Mahrhofer2006] have reported of the different radiosensitivities of different mammalian tissues and cell lines as assessed via γH2Ax-foci following radiation-induced DNA DSBs. In this thesis, the radiosensitivity of OHLSC and ONLSC differ 1 h post-irradiation, values of OHLSC at approximately 2 %, the values of ONLSC ranging up to 20%. As the co-cultured OHLSC and ONLSC were exposed to identical irradiation conditions, this indicates tissue-specific differences in radiosensitivity and repair capacity. The rate of positively labelled DNA DSBs 24 h post-irradiaton compared to 1 h post-irradiation is also tissue dependent. Whereas there is no significant difference in fixation time for OHLSC, DSB rates in ONLSC differ significantly 1 h and 24 h post-irradiation. However, this radiosensitivity does not just seem dependent on tissue type, but also on the subjective time of day at which the OHLSC and ONLSC were irradiated. The rate of DNA DSBs in OHLSC is generally higher at the middle of the subjective night (CT18), resulting in a significant circadian effect. In ONLSC prepared at CT06, DSB rates are rather high 24h post-irradiation, whereas DSB rates in ONLSC prepared at CT18 decrease significantly 24h post-irradiation. No dose-effect for OHLSC was established. A linear dose-dependency with regard to DNS DSBs was verified for ONLSC prepared at CT06 and CT18, fixed at 24h and 1h, respectively.

The OHLSC and ONLSC show an increased number of DNA DSBs not only in irradiated samples, but also in mock-irradiated samples. Positively labelled γH2Ax cells are more abundant in ONLSC than in OHLSC, an observation in accordance with Mahrhofer [Mahrhofer2006], who reports of a significantly higher background level of γH2Ax-foci in malignant than in non-malignant cell lines. Han et al. [Han2006] have found numerous radiation-unrelated γH2Ax-foci after exposure to ionizing radiation, MacPhail et al. [MacPhail2003] have associated elevated γH2Ax-foci to the position of the individual cell in the cell cycle, concluding that γH2Ax-foci occur increasingly in the S- and G2-phase. As the proliferation rate, especially of OHLSC, tested via Ki67 immunohistochemistry and Ki67 being present during the whole cell cycle, is very low, it is unlikely that the elevated γH2Ax values in mock-irradiated OHLSC are due to an increased number of cells in the S- or G2-phase of the cell cycle. These elevated levels of γH2Ax-foci can so far not be explained.

It has been shown by Hendry [Hendry1975] that the radiosensitivity and hence, repair capacity, of a cell is dependent on its current position in the cell cycle. The core clock gene *mPer2* has been reported to influence radiosensitivity and response to DNA damage [Zhang2008, Fu2002]. Miller et al. [Miller2007] have shown that the cell cycle is gated by the circadian rhythm of an organism or organ. Statistical analysis of the OHLSC used in this thesis support the theory of time-dependent radiosensitivity of liver, the tissue being more radiosensitive at the middle of the subjective night (CT18). This is in agreement with Pizzarello et al. [Pizzarello1964], who, already in 1964, detected that mice are more radiosensitive to whole body X-ray irradiation at *zeitgeber* time (ZT) 19 than at any other time of day.

5.3 Comparison X-rays to ^{12}C

In almost all publications comparing the DNA damage effects of heavy ions to photons, a linear energy transfer (LET)-dependent increased RBE is reported for heavy ions [Ando2009, Tomizawa2000]. The RBE compares the doses of photons and heavy ions needed to result in a certain biological effect. Elevated RBE values have been reported for clonogenic survival [Belyakov1999, Ofuchi1999, Skarsgard1967, Paganetti2002, Suzuki2000a, Elsässer2010], premature chromosome condensation PCC [Ofuchi1999, George2003], micronuclei formation [Belyakov1999], apoptosis [Belykov1999, Takahashi1998], DNA DSBs [Okayasu2012] and various other biological effects [Tobias1982, Leith1982, Urano1984].

In this thesis, the RBE for carbon ions with regard to inhibition of proliferation and induction of apoptosis was not determined. RBE is determined for different radiation types

based on a certain biological effect in a specific biological model system. The X-ray irradiations for this thesis were carried out with OLSC prepared from healthy C3H mice. For the ^{12}C-irradiations, it was possible to prepare OHLSC and ONLSC from double transgenic mice with an induced liver tumor. As it was further possible to prepare OHLSC and ONLSC separately, this section discusses the proliferation and apoptosis determined in OLSC and OHLSC after X-ray- and ^{12}C-irradiation. As there were no γH2Ax-foci detected in OLSC, this effect cannot be compared. It should be noted, however, that this points to a high repair capacity of C3H liver tissue, and emphasizes the fact that RBE of different radiation types can only be determined for the same biological model system.

In order to determine whether a comparison of the OLSC and OHLSC was meaningful, the proliferation and apoptosis rates of the mock-irradiated samples were compared. If any significant differences were established for these values, any further statistical comparison of the dose effects would be rendered mute due to the different culturing responses of the tissues. The mock-irradiated samples did show significant differences for both proliferation and apoptosis. This indicates that the biological systems are significantly different per se and should not be compared with regard to radiation type effectiveness. Following, only a discussion of the radiation response of the different tissues is given.

Comparing proliferation rates for X-rays and ^{12}C, proliferation rates for ^{12}C are surprisingly higher than those determined for X-ray doses. This manifests an incompatibility to compare the radiation effects of different radiation types in different biological systems. Both OHLSC and ONLSC were irradiated with an SOBP, and carbon ions in the Bragg peak region have repeatedly been reported to have an increased RBE [Ando2005, Ofuchi1999, Goldstein1981]. Therefore, it is unlikely that the enhanced proliferation rate of the ^{12}C-irradiations demonstrates a decreased effectiveness of carbon ions, but rather stems from the different genetic background of the donor animals.

Apoptosis rates induced by X-ray and ^{12}C-irradiation did not differ significantly. For doses of 5 Gy and 10 Gy, ^{12}C-induced apoptosis rates were a little higher. Initiation of apoptosis has been reported to start after various timepoints post-irradiation, ranging from a few hours [Potten1998, Yanagihara1995, Mirkovic1994] to several days [Boreham1996, Mirzaie-Joniani2002] depending on the tissue type. The current results indicate that X-rays and ^{12}C-ions in an SOBP are equally effective in inducing apoptosis. But to ascertain this, clearly liver OSC made of one donor animal type, preferably the double transgenic mouse, should be kept *in vitro* longer after irradiation.

5.4 OSC of murine liver and OEC of murine pancreas stay viable and functional in vitro

5.4.1 Liver

Cultivating OSC or organotypic explant cultures (OEC) poses high demands on culturing conditions, as the degeneration of blood vessels and the remoteness of cells in the center of the slice from oxygen supply may cause rapid deterioration of the whole OSC. Therefore, various viability tests need to be performed parallel to the actual experiment, so as to exclude masking culturing effects as opposed to true experimental effects. For the liver, a few common tests are morphological assessment via histological stainings [Olinga1997, Verrill2002], enzyme (GLDH, GPT, GLT) leakage [Vickers2004, Klassen2008, vandeBovenkamp2005, Guo2007], and/or production of ATP, albumin or α-fetoprotein [Vickers2004, Klassen2008, Mori1999].

Another indirect viability test is the recording of bioluminometric activity in OLSC prepared from transgenic reporter mice which harbor an intrinsic biomolecular reporter system of the endogenous clock. The expression of several core clock genes in certain mice has been transgenically manufactured to couple with the expression of luciferase (*Per2* - Yoo2004; *Per1* – Stokkan2001, Abe2002, Yamazaki2002; *Bmal1* - Robles2010). OSC and OEC of various tissues such as suprachiasmatic nuclei (SCN), liver, lung, kidney, adrenal gland, heart, or muscle [Dibner2010] of these transgenic mice allow the real time observation of *Per1* and *Per2* expression, respectively, via bioluminometry, a stable rhythm indicating intact functioning clockwork in the OLSC or OPEC cells.

In this thesis, the viability of OLSC was determined via histomorphological assessment of cryosections prepared from the tissue slices post-fixation as well as via real time bioluminometric recordings of transgenic $Per2^{luc}$ mice. The morphological assessment via an HE staining revealed the preservation of the tissue architecture in OLSC, with the central veins well identifiable and homogeneous size of the hepatocyte nuclei. In the outer edge of the OLSC a more intense staining than in the central part was present, indicating a possible deterioration of the inner OLSC with a beginning necrosis. Verrill et al. [Verrill, 2002] kept OLSC of neonatal rat and mouse as well as from humans in the same culturing system as was used in this thesis. OLSC show a gradient of hepatocyte viability in the center, with a live cap of hepatocytes under the capillary fluid layer and a layer of hypoxic tissue next to the membrane. In the experiments with adult mouse tissue, Verrill et al. found hepatocytes to die within 2-3 d with a mean hepatocyte viability of 2 % after 7 days *in vitro* (div). The OLSC in this thesis were therefore irradiated after approximately 24 h *in vitro*, so as not to mask any radiation-effect by the general deterioration of the OLSC.

Positive immunohistochemical stainings were also limited to this outer edge of the OLSC in this work, supporting the hypothesis of deterioration inside the OLSC. This is in agreement with the work of Mori et al. [Mori, 1999], who cultivated fetal mouse liver and identified PCNA-positive cells only at the periphery of the OLSC. The percentage of PCNA-positive cells is given at 33 % during the first week *in vitro* and increased up to 59 % after three weeks in culture. The proliferation rates of the adult OLSC used in this thesis are far lower than that, never reaching relative frequencies above 5 %. Even the mean number of positively BrdU-labeled hepatocytes of Bmal1-wt mice, BrdU having been incorporated into the cells over a time course of 3 d, was determined to be only at roughly 0.5 %. The apparent differences of the donor animals are the genotype and age. As the liver is known to have a rather low proliferation rate, it is suspected that the difference in proliferation rates *in vitro* of these data sets originate in the age of the donor animals – Mori et al. used livers of E14 mice, whereas C3H livers in this thesis were from mice aged 3-6 months.

In general, animal models will always have certain limitations when simulating situation in humans. Therefore, the aim of the work with these tissue slices must be to evaluate any effects in actual human tissue acquired in biopsies. For the meantime, biological models should be optimized with regard to the physiological situation in humans. Verril et al. [Verrill, 2002] show that the hepatocyte viability of their neonatal rat OLSC resembled the viability of adult human liver tissue up to a time of 10 div. Verrill does not remark on the comparability of further markers such as proliferation or morphological changes between rat and human OLSC.

The liver has been shown to oscillate in a circadian fashion *in vitro* and *in vivo* after SCN lesion [Yoo, 2004], indicating a functioning and self-sustained cellular circadian clock. Yoo et al. have found liver OEC of intact and SCN-lesioned mice to display a stable luminescent circadian rhythm for up to 20 div. Experiments of OLSC from *Per2*^{luc} mice in this thesis show a distinct circadian rhythm up to 4 div. After this time, the signal is too damped to elicit any further oscillation. However, this dampening is most likely due to depletion of nourishment and luciferin, as the medium of these OLSC was not changed over the course of the recording. Supporting this hypothesis are the real time recordings of additional OLSC, which had been kept in standard culturing conditions for 7 d, had been irradiated and then recorded for bioluminescence. These OLSC displayed a clear circadian rhythm as well, indicating functioning, viable cells in liver tissue for up to 12 div. This is in accordance with the previously mentioned data of Yoo et al. [Yoo, 2004] and indicates viable hepatocytes in spite of certain central necrosis and positive immunohistochemical labeling at the periphery of the OLSC.

The c-myc/TGF-α double transgenic mouse was generated specifically for the study of an animal oncogene-induced hepatic carcinogenesis model [Murakami1993, Sandgren1993]. To this end, transgenic mice expressing *c-myc* under the control of the mouse albumin enhancer/promoter were crossed to a transgenic mouse which was carrier of a fusioned mouse metallothionein (MT) 1 promoter/human TGF-α cDNA gene. Linking the expression of the oncogene *c-myc* to the albumin enhancer/promoter directs *c-myc* to the liver, coupling the expression of TGF-α to the MT promoter makes the expression of TGF-α easily inducible by adding Zn^{2+} ($ZnSO_4$, $ZnCl_2$) to the drinking water [Sandgren1990, Murakami1993]. This coexpression of *c-myc* and TGF-α causes an accelerated neoplastic development of liver than the expression of only one of these genes [Murakami1993, Sandgren1993]. Sandgren et al. [Sandgren1993] report of double transgenic mice having multiple pronounced hepatic tumors and a life span of a little less than 40 weeks. Littermates expressing only *c-myc* and sacrificed at the same age displayed no neoplastic development. Furthermore, Santoni-Rugio et al. [Santoni-Rugio1996] rate this animal model an appropriate model for the study of human hepatocarcinogenesis as *c-myc* and TGF-α are simultaneously present in pre-malignant human liver diseases as well.

Histological assessment of double transgenic neoplastic livers presented hyperplastic foci, adenomas and solid or trabecular carcinomas [Sandgren1993, Murakami1993]. Characteristic for neoplastic developed tissue are dysplastic hepatocytes which vary noticeably in size and shape.

For this thesis, c-myc/TGF-α double transgenic mice were kept at a 12:12 LD cycle until sacrifice. $ZnCl_2$ was added to their drinking water at four weeks of age, directly after weaning. After 6 months, MRIs were performed regularly to check for developing liver neoplasms. If mice had detected neoplasms ~1 cm^3 in size, they were sacrificed. Of all 15 double transgenic mice sacrificed in the scope of this thesis, only one mouse did not have a macroscopic tumor. All double transgenic mice were killed at 6-8 months of age. In accordance with [Sandgren1993, Murakami1993], isolation of the liver presented an enlarged organ with multiple neoplastic nodes, which could easily be distinguished macroscopically from the surrounding healthy transgenic liver tissue.

For culturing, 8 mm-cores were stamped from either apparent neoplastic tissue or apparent healthy transgenic tissue for co-culturing. Histological stainings of these OHLSC and ONLSC show characteristic gross structures of the different tissue types. The OHLSC presented clearly identifiable central veins with hepatocytes radiating outwards. The macroscopically identified neoplastic tissue showed no signs of structured liver tissue architecture as ONLSC, but rather a disordered, uncontrolled cell proliferation. Furthermore, homogeneously distributed throughout the neoplastic tissue were cell nuclei of

various shape and size, according to [Murakami1993, Sandgren1993] an unmistakable sign of neoplastic tissue development. It should be noted that cell nuclei of different size were also found in OHLSC, indicating dysplastic cells, but to a much lesser degree than in evidently ONLSC. This points to beginning neoplastic development in macroscopically healthy tissue, which is in accordance with [Santoni-Rugio1996]. Santoni-Rugio et al. give a detailed histological report of c-myc/TGF-α liver neoplasms and the adjacent non-tumorous parenchyma, which presents oval-like cells. Oval cells are intra-hepatic precursor cells [Fausto2003], which are considered to play a role in liver neoplasms [Lowes1999]. This was an important finding for the comparison of the effect of X-rays and ^{12}C in liver. Different ionizing radiation types were not only analyzed in different mouse strains, but also in healthy liver of one mouse displaying beginning neoplastic cellular changes. Therefore, before comparing an effect of the different radiation types, biological markers were first compared in mock-irradiated samples of the different mice. Any significant differences detected in these samples would render a further comparison of the irradiated samples mute, as a radiation-effect could not be attributed unambiguously to the radiation type.

In addition to the histological assessment, proliferation rates were another method to distinguish between neoplastic and apparent non-tumorous double transgenic liver. To this end, cryosections of mock-irradiated OHLSC and ONLSC were stained with a Ki67 antibody for proliferating cells and counterstained with Hoechst. The differences in proliferation rate were highly significant ($p < 0.0001$). Surprising to this rather comprehensible result, Kao et al. [Kao1996] report of a reduced growth capacity of double transgenic c-myc/TGF-α hepatocytes *in vitro*. The authors prepared hepatocyte primary cell cultures of 10-week-old c-myc/TGF-α mice and evaluated the DNA content at various timepoints up to 6 days *in vitro*, coming to the conclusion that proliferation rates of control mice were 1.5-fold higher than those of c-myc/TGF-α hepatocytes. Despite of this, the co-culturing of OHLSC and ONLSC was considered successful and differences to [Kao1996] are considered to result from the different biological models *in vitro* and the different ages of the donor animals.

Kao et al. [Kao1996] also report of a higher apoptosis rate in double transgenic hepatocyte cell culture (~4 %) compared to control hepatocyte cell culture (~1 %). The apoptotic rates observed for OHLSC and ONLSC in this thesis have been observed as much higher, ~15 % for mock-irradiated OHLSC and ~30 % for mock-irradiated ONLSC. Again, this discrepancy of data is considered to result from the different biological models *in vitro* and the different ages of the donor animals.

5.4.2 Pancreas

To test the viability of OPEC *in vitro*, histomorphologic assessments are deployed as well as tests for enzyme reactivity, for example amylase [Speier2003, vanGeer2009, Resau1983]. Resau et al. prepared OPEC from adult Syrian hamsters and were able to keep acinar and ductal cells viable *in vitro* for up to 70 d. However, endocrine cells were only viable for the first week *in vitro*. Speier et al. and van Geer et al. prepared pancreas OSC of adult NMRI mice and neoplastic and non-neoplastic human tissue, respectively. Speier et al. report of viable endocrine cells for at least 24 h, with a well preserved three-dimensional architecture of the tissue in which the acinar branches could easily be distinguished from the Langerhans islets. Van Geer et al. kept human pancreatic OSC *in vitro* for up to 6 d, reporting of moderate to good morphology for at least 3 div. In addition to the histomorphological assessment, van Geer et al. evaluated the amylase activity in the medium. They conclude that pancreas OSC remain functional at least up to 2 div.

In this thesis, OPEC from C3H mice and OTPEC from double transgenic c-myc/TGF-α mice were isolated and kept in a membrane-based liquid-air interface culturing system after having been manually cut into OEC of ~1 mm^3 in size. Histological stainings of OPEC showed good retainment of the 3D-architecture up to 8 div, with Langerhans islets and acini readily distinguishable. This is in accordance with data generated by the authors mentioned above. However, insulin-immunohistochemical staining reveals a homogeneous distribution of insulin throughout the OPEC, indicating an unspecific background staining, and testing of amylase and lipase activity in the supernatants of the samples reveal a significant enzyme leakage.

Autolysis of murine OPEC *in vitro* was not confirmed by Speier et al. [Speier2003] or Jones [Jones1967], although Jones does point out that the release of amylase initiates autolysis and concedes that his results of mouse OPEC failing to go into autolysis is difficult to interpret. As the oldest C3H mice of which Jones prepared OPEC were 26 weeks old and thus comparable in age to the mice used in this thesis, it is most likely that differences in the culturing procedure account for the amylase increase in the present data. Despite the enzyme leakage, however, typical morphological characteristics remained intact.

In addition to enzyme leakage, another sign for the deteriorating state of OPEC *in vitro* is the complete failure to produce any kind of positive signal in immunohistochemical staining for proliferative cells. Sections of OPEC from 18 mice were stained for Ki67 antigen with simultaneous staining of a positive control for Ki67 to rule out protocol mistakes. However, in none of these sections was any positive signal detected. To analyze the antibody reactivity with pancreatic tissue and the proliferative status *in vivo*, cryosections of perfused Bmal1-wt pancreata were stained for BrdU and Ki67 and post-fixed C3H pancreata were

stained solely for Ki67. Bmal1-wt pancreas was stained for Ki67 to evaluate colocalization with BrdU. Positively BrdU- and/or Ki67-labeled cells were observed in both pancreatic tissues, homogeneously distributed in acini and Langerhans islets. This suggests that the culturing conditions are the cause for the complete lack of proliferative cells *in vitro*. Meneghel-Rozzo et al. [Meneghel-Rozzo2004] analyzed the proliferative capacity of pancreas OSC *in vitro* of fetal and postnatal (up to post-natal day 3 (P3)) mice and concluded that glucagon- and insulin-positive cells of the endocrine pancreas retain their proliferative capacity *in vitro*. The discrepancy could be explained by the age of the donor animals as well as different culturing media used.

Indicating deteriorating OPEC quality furthermore are the real time recordings of the *Per2*^{luc} OPEC. Several publications confirm circadian oscillations of the pancreas, especially the endocrine pancreas [Mühlbauer2009, Mühlbauer2004, Peschke1998]. Recently, real time bioluminometric recordings of *Bmal1*^{luc} OPEC over a time period of several days support these previous findings [Sadacca2011]. Bioluminescent real time recordings of OPEC for 5 d immediately after preparation in this thesis, however, did not show a circadian rhythm. At most, they displayed one peak with a sharp fall off in photon count thereafter for the remaining recording time. The samples did not receive fresh medium during the recording time and were thus exposed to their own digestive enzymes for 5 d. It is thus likely that the enzyme leakage in these samples lead to a deterioration and subsequent autolysis of the tissue. These samples, which only showed one bioluminescent activity peak, were considered arrhythmic in accordance with [Abe2002].

The pancreata of double transgenic c-myc/TGF-α mice were cultivated to analyze the pancreas reaction to ^{12}C-irradiation. Already during preparation of OPEC, differences of the transgenic pancreas compared to the pancreas of healthy C3H mice were evident. During the organ isolation from the organism, healthy unperfused pancreas was soft with the ability to stretch and unraveled easily in solution. Transgenic pancreas, on the other hand, was firm and compact, remaining so in solution, which is in accordance with Bockmann et al. [Bockmann1992].

Histological staining of these OTPEC presented extensively fibrotic tissue with small areas of duct-like structures. Published literature does not specifically report on the pancreas of the doube transgenic c-myc/TGF-α mouse in which the *c-myc* gene expression is linked to the mouse albumin enhancer/promoter and thus directed to the liver. Yet the role of MT-TGF-α in single-transgenic mice has been elaborated on. Sandgren et al. [Sandgren1990, Sandgren1993] ascribe MT-TGF-α a proliferation-inducing effect in acinar cells and fibroblasts, focally altered acinar cell differentiation, and fibroplasia. However, no

neoplasms were reported due to MT-TGF-α alone. Bockmann et al. [Bockmann1992] describe the redifferentiation of acinar cells to produce tubular complexes with some resembling ductal cells, which is in accordance with the histological assessment of the double transgenic pancreatic tissue analyzed in this thesis. In the case of *c-myc* single transgenic mice, in which *c-myc* is linked to the elastase-1 promoter which directs *c-myc* expression to pancreatic acinar cells [Sandgren1991], mice develop acinar cell adenomas and carcinomas between 2 and 7 months of age. The effect of the double transgenic fusion of MT-TGF-α and *Ela-1-myc* on pancreas is reported in [Sandgren1993]. Double transgenic mice display an accelerated tumor growth and tumors have a generally more malignant appearance compared to tumors induced by *c-myc* alone.

In light of these transgenic variants, it can be concluded that the pancreata of the double transgenic *c-myc*/TGF-α mice in which the liver is the target for the enhanced expression of *c-myc*, display an extensive fibrosis and redifferentiated acinar cells. This does not, however, suffice as a tumor model. OTPEC were thus not evaluated for the effect of ^{12}C-irradiation.

5.5 Ionizing radiation leads to a phase-shift in circadian rhythm

Circadian rhythms have been detected for various tissues such as SCN, liver, heart, skeletal muscle, and kidney [Yamazaki2000, Yamamoto2004]. The results for OLSC and OAEC of *Per2*^{luc} mice show that they retain their circadian function in a membrane-based culture system with a liquid-air interface [Verrill2002]. For as much as 12 div, these tissue cultures show a distinct rhythmic circadian expression of the *Per2*-reporter luciferase. Most of the recorded OLSC show three peaks in bioluminescence over a timeperiod of 5 d, with the recording started directly after slice/explant preparation. When the real time recordings are displayed vs. the circadian time (CT), it becomes evident that the culturing procedure does not reset the biological clock of the liver tissue. Other OLSC, which had been kept under standard culturing conditions for 7 d prior to irradiation, show a continued oscillation even after X-ray irradiation with a dose of 50 Gy, also for 4 d post-irradiation. During the culturing process of 7 d, these tissue samples had been subject to three medium changes, a process which reset the circadian clocks of these samples. At the time of irradiation, these samples had been in phase set to the time of the last medium change. A seemingly dose-dependent phase-advance of the irradiated samples is detected. For an X-ray dose of 50 Gy, a phase-advance of approximately 6 h was observed, for a dose of 10 Gy, the phase-advance observed was about 1 h. This is in accordance with the data of [Oklejewicz2008] concerning the phase-advance, albeit not its magnitude. Oklejewicz et al. subjected live animals and rat-1

fibroblasts to γ–radiation of a ^{137}Cs-source at doses ranging from 0.5 Gy to 12 Gy. They have reported dose-dependent phase-advances of up to 4 h for doses of 10 Gy and 12 Gy.

The period lengths of the recorded OLSC were unaffected by the irradiation with X-rays. A significantly longer period was only observed for OLSC which had been cultured for 7 d and were then mock-irradiated. The period of these samples was 29.1 h as opposed to 24.3 h of the irradiated OLSC.

The OAEC showed a very robust circadian rhythm in culture, which is in accordance with data published by [Andrews1964, Andrews1971, Oster2006]. However, when displaying the real time data from the adrenal gland vs. the time scale of the mouse circadian time (CT), a phase shift occurs between OAEC from animals killed at different timepoints (CT06 and CT18). The time axis was therefore adjusted to the time of culturing, leading to real time data which was in phase. It can be concluded that – as the culturing procedure for OLSC and OAEC was the same except for the slice preparation – the mere fact of removing the adrenal gland from the organism and taking it into culture reinitiates the endogenous clock of the adrenal caused by an intrinsic factor. Balsalobre et al. [Balsalobre2000] have reported that glucocorticoids have the ability to induce circadian gene expression in organs such as liver, kidney, and heart and thus change the phase of these organs. Therefore, it can be presumed that during the removal of the adrenal gland from the organism, glucocorticoids and possibly other phase-resetting substances are released uncontrollably from the adrenal gland, making it subject to its own rhythm-influencing factors.

Irradiating the OAEC leads to a phase-advance just as we have detected in OLSC. However, the phase-advance for OAEC is 4 h at the most, even after a dose of 50 Gy, whereas for OLSC, a phase-advance of 6 h was detected. This gives rise to questions whether a phase-advance is tissue-specific, (linearly) dose-dependent, and whether there is a maximal phase-shift which can be caused by radiation. Of these questions, the present data only allow to presume a tissue-specific radiation-induced phase-advance.

Of the 26 OPEC recorded for bioluminescent activity in all, only two OPEC showed a discernible circadian oscillation. The remaining 24 OPEC showed – if at all – a clearly distinguishable peak at the very beginning of culturing, the amplitude of which was damped too much during the remaining recording time to make out an oscillation to be used for post-processing. These OPEC were therefore regarded as arrhythmic in accordance with other reports of arrhythmic OEC [Abe2002]. Curiously, the two OPEC which produced a distinguishable rhythm were OPEC which had been kept under standard culturing conditions for 7 d, received a medium change every day, and were then mock-irradiated. It can be concluded from this result that (1) OPEC are capable of rhythmic oscillation and

(2) OPEC retain their ability to function rhythmically after several days in culture, which is in agreement with [Sadacca2011].

Several reports on the rhythmic expression of insulin [Peschke1998] and glutathione [Neuschwander-Tetri1996] as well as *mPer1* and *mPer2* [Mühlbauer2004] support the theory of the pancreas as another organ which harbors a biological clock. Studies separating the endocrine pancreas, i.e. the Langerhans islets, from the exocrine pancreas, the acini, enforce the hypothesis that both parts of the pancreas show a distinct circadian rhythm [Mühlbauer2004, Völkl1983, Maouyo1993, Peschke1998, Neuschwander-Tetri1996]. These data give rise to the question why most of the bioluminometrically recorded OPEC of the present thesis have to be considered arrhythmic. Presumably, an important factor is the culturing condition itself. Removing the pancreas from the donor animal and cutting it into smaller pieces fit for culturing is only possible via mechanically destroying the intact parenchyma of the tissue, leading to a release of various digestive enzymes, resulting in the autolysis of the tissue. To this end, the amount of α-amylase and lipase in the samples supernatants were analyzed (Figure 34). The amount of α-amylase and lipase is given in U/(l·h) (assuming the simplified situation of a constant discharge of enzymes into the medium). After 1 div, the amount of α-amylase is increased about 4700-fold for CT06 and roughly 80 000-fold for CT18. Lipase is increased 15-fold for CT06 and 340-fold for CT18. The relative amount of α-amylase in the supernatants is significantly higher than lipase. However, the data show that directly after slicing, the OPEC release a considerable amount of digestive enzymes. There is also a significant difference between the two CT timepoints, the amount of enzymes released during the subjective day (CT06) is significantly higher than that released during the subjective night (CT18).

The OPEC recorded immediately after preparation for 5 d were exposed to their own digestive enzymes for the entire recording time, as there were no medium changes after the beginning of recording. On the other hand, the samples which were kept in standard culturing conditions for 7 d received a medium change every day and were washed with prewarmed HBSS. It can be suspected that any digestive enzymes released into the medium and tissue as a consequence of the preparation trauma were removed during this process, protecting the tissue from further autolysis damage and allowing it to function according to its endogenous clock. After this successful culturing, irradiating OPEC with a dose of 50 Gy caused further damage to the tissue so as to abolish any circadian rhythm of the cells.

5.6 Clinical relevance

Organotypic tissue slice cultures pose a novel model system in radiobiological research with the potential of an important link between the standard biological system of monotypic cell culture and *in vivo* experiments. OSC allow the elucidation of radiation response in the original 3D environment of a cell [Blakely1992] whilst reducing the number of experimental animals needed for statistically significant testing. Probably the most meaningful fact about this system is that OSC can be prepared from human biopsy specimens. This would allow for the study of tissue radiation response in a more physiological state of normal and possibly neoplastic human tissue without species or interindividual differences.

OLSC from double transgenic mice with an inducible liver tumor pose an ideal substitute for human tissue for preliminary studies, as they allow for the separate co-culturing of healthy (OHLSC) and neoplastic tissue (ONLSC) which will be subject to identical experimental conditions. Various transgenic mouse strains with inducible tumor allow for the expansion of this animal model to various other tissues, such as pancreas [Sandgren, 1991].

Radiation response studies via immunohistochemistry in this thesis were not distinctly conclusive as to a superior DNA damage and apoptosis induction by ^{12}C as well as inhibition of proliferation as other reported biological systems. However, bioluminometric studies have shown that OLSC remain functional even after 7div, and have distinctly documented the maintenance of a circadian oscillation after irradiation with X-rays as well as supporting a previously reported phase-advance due to irradiation [Oklejewicz2008]. ^{12}C time-dependent irradiation data give a first clue about the extent of side-effects: in OHLSC, proliferation was higher, apoptosis and DNA DSBs were lower at the middle of the subjective day (CT06) than at the middle of the subjective night (CT18). This suggests that during the day, a higher number of proliferating cells may speak for a higher repair capacity, and thus less negative side-effects due to irradiation.

Further optimization of culturing methods of adult tissue could make the cultivation of human biopsy specimens possible over a longer period of time. This would allow for the more detailed study of radiation effects with regard to general radiotherapy conditions, for example possible effects of fractionated irradiation compared to single irradiation [Koike2002], as well as individual patient treatment.

6 Summary

6.1 Background

Cancer is the second leading cause of death in Germany, after cardiovascular diseases. Two tumor types with a very poor prognosis are liver and pancreas cancer, despite continuing improvements in therapeutic regimens. Cancer therapies comprise surgery, chemo- and/or radiotherapy or a combination of these three regimens. In most cases radiotherapy is performed conventionally, i.e. with X-rays. However, in the last 20 years, radiotherapy with ions, especially with ^{12}C, has gained increased attention and in 2009, the carbon therapy developed at the GSI (Helmholtzzentrum für Schwerionenforschung, Germany), unique with its active beam shaping technology, was successfully implemented into clinical routine at the HIT (Heidelberger Ionen-Therapiezentrum) in Heidelberg, Germany.

X-rays are high-energy photons. At therapy-relevant energies (up to a few MeV), they interact with matter via photoeffect, Compton effect, and pair production. These types of interaction result in an exponential decrease of dose in matter. ^{12}C-ions on the other hand are massive atomic nuclei, which interact mainly via inelastic collisions with the target material. At high energies, the ions collide sporadically with the target material. At these rare events, however, a lot of energy is transferred into the target material. ^{12}C-ions are slowed down after each collision, subsequently leading to more frequent collisions. Thus, the ions transfer most of their energy in a short range at the very end of their track, in the so-called Bragg-peak. The resulting depth-dose profile is in contrast to the exponentially decreasing depth-dose profile of X-rays and is therefore called inverse depth-dose profile. Because of this inverse depth-dose profile, ions are well-suited to treat tumors located in deep parts of the body. Due to the lower dose in the entrance channel, the surrounding tissue is spared, leading to less pronounced side-effects.

Ions interact with target material not only via elastic and inelastic collisions, but also via fragmentation. Not only the incoming ions, but also the nuclei of the target material fragment. Therefore, as the range the ions have passed in the target material increases, the number of fragments also increases and the number of original ions decreases. The fragments have their own energy-dependent depth-dose profiles, which superimpose

that of the original ions. As lighter ions have a greater range, these fragments lead to a characteristic tail of lower dose behind the Bragg-peak of the original ions.

For the irradiation of a patient, exact data are needed to determine the number of ions and fragments and the applied dose at any given depth in the target. This can only be measured exemplarily with the help of a phantom experimental setup. This setup consists of a water target of variable thickness, behind which ionization chambers measure the energy of detected particles. These data can then be used to generate a patient treatment plan by calculating the applied dose in the tumor volume as well as the surrounding tissue. For this, special simulation programs are used.

In these programs, two procedures have been established for the underlying modes of calculation: deterministic and Monte-Carlo (MC)-calculations. Deterministic programs are based on equations for energy loss, which are derived from experimental data tables. These equations allow calculating the applied dose in a patient. MC-programs on the other hand are based on measured cross sections, indicating the interaction probability of an ion with the surrounding target material. In addition to the transferred energy, these programs allow the calculation of the produced fragments as well as other physical processes (e.g. positron emission).

However, before ions are applied in patient treatment, their apparent advantages deduced from their physical properties have to be tested in biological material. There are two primary biological test systems in radiation research: cell lines or primary cell cultures (so-called *in vitro* cultures) or laboratory animals (*in vivo* experiments). Primary cell cultures are prepared directly from fresh tissue, cell lines develop from primary cell cultures due to genetic mutations during cell division and can be kept in culture for several decades. In both cases, cells of one specific cell type are cultured, usually as a monolayer. They are characterized by restricted (primary cell culture) or non-restricted (so-called immortal cell lines) proliferation.

Cell lines are advantageous because they can be handled rather easily. They can be grown without limitation and can be stored frozen. In addition, cell cultures can be prepared from human cells. This reduces experimental uncertainties due to species-specific differences.

However, studies based on such cell cultures also have disadvantages. The whole culture comprises only one cell type. Native tissue, however, consists of a variety of different cell types, an extracellular matrix, and an immune system. Moreover, cell cultures usually grow as a monolayer and thus the native three-dimensional

environment of the cells is reduced to two dimensions, meaning the loss of information of a whole dimension. In conclusion, cell cultures can be handled rather easily, but they represent a very simplified biological testing system.

The most complex experimental model is the laboratory animal. The animal model has the advantage of keeping cells in their natural environment at the time of the experiment. Targeted genetic modifications allow the generation of a variety of mouse models with specific properties. Disadvantages of the animal model include 1) the large number of animals needed per experiment, 2) species-specific results that may not be transferred directly to humans as well as 3) interindividual variation.

An intermediate model which combines advantages of cell cultures and whole animal models are the so-called organotypic slice cultures. These are tissue slices which can be prepared from various organs of an animal and are subsequently taken into culture. In these slice cultures, the different cell types of an organ remain in their original three-dimensional tissue architecture and the extracellular matrix is preserved. Furthermore, multiple slices can be made from one organ. This greatly reduces the number of required animals and different experimental parameters can be analyzed without interindividual variation. In addition, slice cultures can be prepared from human material obtained during surgery and, thus, putative species-specific differences can be eliminated. Pathological tissue can be used to study diseases and develop therapeutic strategies, healthy tissue serves as a physiological model to study side-effects and investigate elementary molecular processes.

Radiation therapies are often accompanied by manifold acute as well as long-term side-effects (e.g. fatigue, nausea, diarrhea, skin irritation). In serious cases, these side effects may interrupt the therapy. Minimizing side-effects is extremely important for the success of radiotherapy. It is therefore mandatory to keep the applied dose in healthy tissue as low as possible. As stated above, this can be achieved via ion irradiation. A further option to reduce radiation-induced side-effects could be to apply radiation at a timepoint at which healthy tissue is less vulnerable to radiation effects. Studies have shown that a well selected timepoint of irradiation can positively influence the extent of radiation-induced side-effects. These time-dependent differences in radiosensitivity of healthy tissue may be due to the circadian molecular clock which resides in all tissues and is coordinated by a master clock in the brain (suprachiasmatic nucleus) which itself is entrained to the environmental day-night rhythm.

The crucial point of this consideration is that normal tissue retains the normal rhythm of the circadian molecular clock, whereas tumor tissue has apparently lost circadian rhythmicity. Considerations about the best suited timepoint for therapy may help to reduce side-effects and thus to make therapy more tolerable for the patient.

6.2 Goals

The first goal of this thesis was to compare the depth-dose profile of the extended Bragg-peak generated for the irradiation of the biological samples with ^{12}C by means of the GSI simulation program TRiP98 with the depth-dose profiles generated by three other simulation programs (ATIMA, MCHIT, TRIM). The second goal was to assess the extent of side-effects caused by ionizing radiation. To this end the effects of ionizing radiation on proliferation (cell division), apoptosis (programmed cell death), and DNA double-strand breaks were analysed in organotypic slice cultures of murine liver and organotypic explant cultures of murine pancreata in order. In addition, these parameters were investigated in neoplastic murine liver tissue following ^{12}C-irradiation. The effects of ionizing radiation on the molecular clockwork were examined in liver slice cultures and explant cultures of pancreas and adrenal glands prepared from transgenic $Per2^{luc}$-mice. The tissues of these animals allow the „online“-recording of the expression of *Per2*, an important clock gene, for several days.

6.3 Materials and methods

Four programs, ATIMA, MCHIT, TRIM, and TRiP98, were used to simulate the dose deposition from ^{12}C-ions in the biological samples. The experimental setup used was consistent with the actual experimental setup for slice irradiation behind the exit window of the beam line. The biological samples, slice and explant cultures, were modeled as water targets and irradiated with an extended Bragg-peak at doses of 2 Gy, 5 Gy, or 10 Gy. In the simulations, the linear energy transfer (LET) of ^{12}C-ions was calculated for a total of 26 different energies. The individual Bragg-peaks were superimposed in a post-processing step to generate the depth-dose profile of the extended Bragg-peak which is characterized by a constant dose over a certain range. In

addition to this depth-dose profile, the number of fragments was calculated with the help of MCHIT.

For irradiation experiments, slice cultures were prepared from three different mouse types. For reference experiments with X-rays, liver and pancreas were prepared from C3H-wildtype (wt) mice. These samples were used to analyze ionizing radiation side-effects in healthy tissue. For ^{12}C-irradiation, the opportunity arose to investigate transgenic c-myc/TGF-α mice with an inducible liver tumor. Liver slice cultures from these animals comprised both healthy (OHLSC – organotypic healthy liver slice cultures) and neoplastic (ONLSC – organotypic neoplastic liver slice cultures) areas. In order to investigate the effects of ionizing radiation on the endogenous clock, organotypic liver slice cultures and explant cultures of pancreas and adrenal glands were prepared from transgenic Per2^{luc}-mice. Per2^{luc}-mice express the enzyme luciferase under the control of the *Per2* promoter, an important part of the circadian clock. These cultures were irradiated with X-rays.

To analyze a possible time-dependent tissue reaction to radiation slice and explant cultures from all mouse strains investigated were prepared at two different timepoints of the day: at the middle of the subjective day and at the middle of the subjective night.

After slice and explant culture preparation, samples were kept in a membrane-based culturing system with a liquid-air interface for several days. Samples were irradiated at different doses 24 h after preparation. Mock-irradiated samples served as controls. The samples were fixed either 1 h or 24 h post-irradiation and processed for immunohistochemistry. Proliferation (cell division, marker: Ki67), apoptosis (programmed cell death, marker: caspase3), and DNA double-strand breaks (marker: γH2Ax) were determined by use of a confocal laser scanning microscope and an automated image evaluation software (Volocity).

6.4 Results and discussion

The parameters for the ^{12}C-irradiation of the liver slice and pancreas explant cultures were determined with the GSI simulation program TRiP98. The resulting depth-dose profile, according to which the biological samples were irradiated, served as reference for the results generated by three other programs (ATIMA, MCHIT, TRIM). ATIMA and TRIM are general programs for the calculation of the stopping power of ions in matter. They can reproduce the depth-dose profile generated by TRiP98 only

inadequately. ATIMA calculates a linearly increasing depth-dose profile mainly due to lack of fragmentation. In principle, TRIM calculates a similar depth-dose profile. However, due to the discretely implemented ripple filter (a structural element in the beam line for artificial beam broadening) and internal binning, the depth-dose profile calculated with TRIM shows significant deviations from the characteristic depth-dose profile. The depth-dose profile calculated with MCHIT, which was developed specifically for the simulation of ions interacting with matter in medical applications, is in good agreement with the reference curve. Except for a slightly higher mean dose (0.1Gy), the depth-dose profile could be reproduced accurately.

With regard to proliferation, apoptosis, and DNA double-strand breaks, no clear-cut results could be obtained from pancreas explant cultures. On the other hand, distinct day-night differences were found in healthy liver slice cultures irrespective of whether they were irradiated or not: the proliferation rate was significantly higher at the middle of the subjective day than at the middle of the subjective night while the rates for apoptosis and DNA double-strand breaks were significantly higher at the middle of the subjective night. At both timepoints the parameters investigated did not show significant differences between control slices and slices irradiated with increasing doses. Neoplastic liver tissue differed from healthy liver tissue in two important aspects: proliferation, apoptosis and DNA double-strand breaks did not show a day-night difference and the number of DNA double-strand breaks increased dose-dependently.

The effects of ionizing radiation on the circadian clockwork were analyzed in tissue samples of transgenic $Per2^{luc}$-mice allowing the real-time recording of the circadian rhythm of the molecular clockwork via measurement of the luciferase-activity in liver and other tissues. As could be shown in liver slice cultures and explant cultures of pancreas and adrenal glands, these samples maintain their circadian rhythm in culture. Ionizing radiation was found to cause a dose-dependent phase-advance of the circadian clockwork without changing the period length.

6.5 Conclusion

The results from the dose-simulations of ^{12}C-ions in water show that deterministic and MC-programs lead to almost identical results. MC-programs can simultaneously calculate the production of fragments. At the current state of computer technology, MC-programs are not yet suitable for use in clinical routine due to the fact that calculations

are very time-consuming. However, it can be assumed that with further advances in computing power, these programs can also be used for therapy planning in clinical routine.

In this thesis, for the first time organotypic slice cultures were exposed to ionizing radiation with the goal of analyzing the effect on proliferation, apoptosis, and DNA double-strand break rate. The slice culture model yields reproducible results with regard to these parameters. It is suited as a test model for the study of tissue response to ionizing radiation and offers an attractive addition to the models of cell culture and laboratory animals. The results of the tissue slice analysis after irradiation with doses of up to 10 Gy indicate a dose-independent high repair capacity of healthy liver tissue. In tumor tissue, however, the DNA double-strand break rate increases dose-dependently. This suggests an impaired repair capacity of neoplastic tissue. The time-dependent tissue response of healthy liver raises the possibility that radiation-induced side effects may be further reduced if the treatment is performed at the most appropriate timepoint. The results provide an important basis for further experiments, in which the efficacy of conventional X-rays and ion beams on neoplastic tissue should be compared. The experimentally acquired know-how and findings constitute a good foundation to expedite the future development of organotypic slice cultures from human tissue samples.

Bibliography

[Abe2002] Abe M , Herzog ED, Yamazaki S, Straume M, Tei H, Sakaki Y, Menaker M, Block GD „Circadian rhythms in isolated brain regions“ J Neurosci. 2002;22(1):350-6

[Ando2005] Ando K, Koike S, Uzawa A, Takai N, Fukawa T, Furusawa Y, Aoki M, Miyato Y "Biological gain of carbon-ion radiotherapy for the early response of tumor growth delay and against early response of skin reaction in mice" J Radiat Res. 2005 Mar;46(1):51-7

[Ando2009] Ando K, Kase Y "Biological characteristics of carbon-ion therapy" Int J Radiat Biol. 2009 Sep;85(9):715-28

[Andrews1964] Andrews RV, Folk GE Jr “Circadian metabolic patterns in cultured hamster adrenal glands” Comparative Biochemistry and Physiology 1964;11:393-409

[Andrews1971] Andrews RV „Circadian rhythms in adrenal organ cultures“ Gegenbaurs Morphologisches Jahrbuch 1971;117:89-98

[Antonelli2005] Antonelli F, Belli M, Cuttone G, Dini V, Esposito G, Simone G, Sorrentino E, Tabocchini MA "Induction and repair of DNA double-strand breaks in human cells: dephosphorylation of histone H2AX and its inhibition by calyculin A" Radiat Res. 2005 Oct;164(4 Pt 2):514-7

[Aschoff1971] Aschoff J, Fatranská M, Giedke H, Doerr P, Stamm D, Wisser H „Human circadian rhythms in continuous darkness: entrainment by social cues“Science. 1971 Jan 15;171(3967):213-5

[Ask2005] Ask A, Johansson B, Glimelius B „The potential of proton beam radiation therapy in gastrointestinal cancer“ Acta Oncol. 2005;44(8):896-903

[ATIMA] http://web-docs.gsi.de/~weick/atima/

[Atwood2011] Atwood A, DeConde R, Wang SS, Mockler TC, Sabir JS, Ideker T, Kay SA „Cell-autonomous circadian clock of hepatocytes drives rhythms in transcription and polyamine synthesis“ Proc Natl Acad Sci 2011;108(45):18560-5

[Bachem2008] Bachem MG, Zhou S, Buck K, Schneiderhan W, Siech M „Pancreatic stellate cells--role in pancreas cancer“ Langenbecks Arch Surg. 2008;393(6):891-900

[Balsalobre1998] Balsalobre A, Damiola F, Schibler U „A serum shock induces circadian gene expression in mammalian tissue culture cells“ Cell 1998;93(6):929-37

[Balsalobre2000] Balsalobre A, Brown SA, Marcacci L, Tronche F, Kellendonk C, Reichardt HM, Schütz G, Schibler U „Resetting of Circadian Time in Peripheral Tissues by Glucocorticoid Signaling“ Science 2000;289:2344-7

[Barbason1987] Barbason H, Herens C, Mormont MC, Bouzahzah B „Circadian synchronization of hepatocyte proliferation in young rats: the role played by adrenal hormones“ Cell Tissue Kinet 1987;20(1):57-67

[Barbason1998] Barbason H, Herens C, Robaye B, Milis G, Sulon J, Bouzahzah B, VanCantfort J „Importance of cell kinetics rhythmicity fort he control of cell proliferation and carcinogenesis in rat liver (review)“ In Vivo 1998 Nov-Dec;9(6):539-48

[Barkas1963] Barkas HW, Nuclear Research Emulsions, Vol. I, Academic Press New York and London, 1963

[Becciolini1997] Becciolini A, Balzi M, Fabbrica D, Potten CS "The effects of irradiation at different times of the day on rat intestinal goblet cells" Cell Prolif. 1997 Mar-Apr;30(3-4):161-70

[Becker-Weimann2004] Becker-Weimann S, Wolf J, Herzel H, Kramer A „Modeling feedback loops of the mammalian circadian oscillator“Biophys J. 2004 Nov;87(5):3023-34

[Belli1998] Belli M, Cera F, Cherubini R, Dalla Vecchia M, Haque AM, Ianzini F, Moschini G, Sapora O, Simone G, Tabocchini MA, Tiveron P „RBE-LET relationships for cell inactivation and mutation induced by low energy protons in V79 cells: further results at the LNL facility“ Int J Radiat Biol. 1998 Oct;74(4):501-9

[Belyakov1999] Belyakov OV, Prise KM, Trott KR, Michael BD "Delayed lethality, apoptosis and micronucleus formation in human fibroblasts irradiated with X-rays or alpha-particles" Int J Radiat Biol. 1999 Aug;75(8):985-93

[Bernabei1992] Bernabei PA, Balzi M, Saccardi R, Becciolini A, Ferrini PR „Time-dependent sensitivity of rat CFU-GM to total body irradiation“ Haematologica. 1992 Jan-Feb;77(1):21-4

[Bernard2007] Bernard S, Gonze D, Cajavec B, Herzel H, Kramer A „Synchronization-induced rhythmicity of circadian oscillators in the suprachiasmatic nucleus“ PLoS Comput Biol. 2007 Apr 13;3(4):e68

[Berthou1989] Berthou F, Ratanasavanh D, Riche C, Picart D, Voirin T, Guillouzo A “Comparison of caffeine metabolism by slices, microsomes and hepatocyte cultures from adult human liver” Xenobiotica. 1989 Apr;19(4):401-17

[Bethe1930] Bethe H „Zur Theorie des Durchgangs schneller Korpuskularstrahlen durch Materie“ Ann Phys 1930;397:325-400

[Bienvenu1993] Bienvenu T, Pons G, Rey E, Thiroux G, Olive “Caffeine metabolism in liver slices during postnatal development in rats” Drug Metab Dispos. 1993 Jan-Feb;21(1):178-80

[Blakely1979] Blakely EA, Tobias CA, Yang TC, Smith KC, Lyman JT „Inactivation of human kidney cells by high-energy monoenergetic heavy-ion beams“ Radiat Res. 1979 Oct;80(1):122-60

[Blakely1992] Blakely EA "Cell inactivation by heavy charged particles" Radiat Environ Biophys. 1992;31(3):181-96

[Blank1995] Blank MA, Gushchin VA, Halberg F, Portela A, Cornélissen G "X-irradiation chronosensitivity and circadian rhythmic proliferation in healthy and sarcoma-carrying rats' bone marrow" In Vivo 1995;9(4):395-400

[Bloch1933a] Bloch F „Bremsvermögen von Atomen mit mehreren Elektronen“ Z Phys A: Hadrons Nucl 1933;81:363-376

[Bloch1933b] Bloch F „Zur Bremsung rasch bewegter Teilchen beim Durchgang durch Materie“ Ann Phys 1933;408:285-320

[Bockmann1992] Bockman DE, Merlino G „Cytological changes in the pancreas of transgenic mice overexpressing transforming growth factor alpha“ Gastroenterology 1992;103(6):1883-92

[Boreham1996] Boreham DR, Gale KL, Maves SR, Walker JA, Morrison DP "Radiation-induced apoptosis in human lymphocytes: potential as a biological dosimeter" Health Phys. 1996 Nov;71(5):685-91

[Bragg1905] Bragg WH, Kleemann R „On the □-Particles of Radium and Their Loss of Range in Passing Through Various Atoms and Molecules“ Phil Mag 1905;10:318-340

[Buhr2010] Buhr ED, Yoo SH, Takahashi JS “Temperature as a universal resetting cue for mammalian circadian oscillators” Science 2010;330:379-385

[Catania2007] Catania JM, Pershing AM, Gandolfi AJ „Precision-cut tissue chips as an in vitro toxicology system“ Toxicol In Vitro. 2007;21(5):956-61

[Ceha2000] Ceha HM, van Tienhoven G, Gouma DJ, Veenhof CH, Schneider CJ, Rauws EA, Phoa SS, González González D “Feasibility and efficacy of high dose conformal radiotherapy for patients with locally advanced pancreatic carcinoma” Cancer. 2000 Dec 1;89(11):2222-9

[Chen1954] Chen JM “The cultivation in fluid medium of organised liver, pancreas and other tissues of foetal rats” Exp Cell Res. 1954 Nov;7(2):518-29

[Chick1975] Chick WL, Like AA, Lauris V „Beta cell culture on synthetic capillaries: an artificial endocrine pancreas“ Science 1975;187(4179):847-9

[Christiansen2004] Christiansen H, Saile B, Neubauer-Saile K, Tippelt S, Rave-Fränk M, Hermann RM, Dudas J, Hess CF, Schmidberger H, Ramadori G "Irradiation leads to susceptibility of hepatocytes to TNF-alpha mediated apoptosis" Radiother Oncol. 2004 Sep;72(3):291-6

[Collis2007] Collis SJ, Boulton SJ „Emerging links between the biological clock and the DNA damage response“ Chromosoma 2007;116(4):331-9

[Conners1989] Conners S, Rankin DR, Krumdieck CL, Brendel K “Interactive toxicity of cocaine with phenobarbital, morphine and ethanol in organ cultured human and rat liver slices” Proc West Pharmacol Soc. 1989;32:205-8

[Connors1990] Connors S, Rankin DR, Gandolfi AJ, Krumdieck CL, Koep LJ, Brendel K “Cocaine hepatotoxicity in cultured liver slices: a species comparison” Toxicology. 1990 Apr 17;61(2):171-83

[Crane2001] Crane C, Janjan N, Evans D, Wolff R, Ballo M, Milas L, Mason K, Charnsangavej C, Pisters P, Lee J, Lenzi R, Vauthey J, Wong A, Phan T, Nguyen Q, Abbruzzese J “Toxicity and Efficacy of Concurrent Gemcitabine and Radiotherapy for Locally Advanced Pancreatic Cancer” Int J Gastrointest Cancer. 2001;29(1):9-18

[Damiola2000] Damiola F, Le Minh N, Preitner N, Kornmann B, Fleury-Olela F, Schibler U “Restricted feeding uncouples circadian oscillators in peripheral tissues from the central pacemaker in the suprachiasmatic nucleus” Genes Dev 2000;14:2950-2961

[Davidson2006] Davidson AJ, Straume M, Block GD, Menaker M „Daily timed meals dissociate circadian rhythms in hepatoma and healthy host liver“ Int J Cancer. 2006 Apr 1;118(7):1623-7

[deGraaf2002] de Graaf IA, Geerlinks A, Koster HJ „Incubation at 37 degrees C prior to cryopreservation decreases viability of liver slices after cryopreservation by rapid freezing“Cryobiology. 2002 Aug;45(1):1-9

[deGraaf2010] de Graaf IA, Olinga P, de Jager MH, Merema MT, de Kanter R, van de Kerkhof EG, Groothuis GM „Preparation and incubation of precisiion-cut liver and intestinal slices for application in drug metabolism and toxicity studies“Nat Protoc. 2010 Sep;5(9):1540-51

[deKanter2002] De Kanter R, De Jager MH, Draaisma AL, Jurva JU, Olinga P, Meijer DK, Groothuis GM „Drug-metabolizing activity of human and rat liver, lung, kidney and intestine slices“ Xenobiotica. 2002 May;32(5):349-62

[Desai2005] Desai N, Davis E, O'Neill P, Durante M, Cucinotta FA, Wu H "Immunofluorescence detection of clustered gamma-H2AX foci induced by HZE-particle radiation" Radiat Res. 2005 Oct;164(4 Pt 2):518-22

[Dibner2010] Dibner C, Schibler U, Albrecht U „The Mammalian Circadian Timing System: Organization and Coordination of Central and Peripheral Clocks“ Annu Rev Physiol. 2010;72:517-49

[Duncan1983] Duncan AM, Ronen A, Blakey DH "Diurnal variation in the response of gamma-ray-induced apoptosis in the mouse intestinal epithelium" Cancer Lett 1983;21(2):163-6

[Durante2010] Durante M, Loeffler JS „Charged particles in radiation oncology“ Nat Rev Clin Oncol. 2010 Jan;7(1):37-43

[Edgar2004] Ben-Josef E, Shields AF, Vaishampayan U, Vaitkevicius V, El-Rayes BF, McDermott P, Burmeister J, Bossenberger T, Philip PA “Intensity-modulated radiotherapy (IMRT) and concurrent capecitabine for pancreatic cancer” Int J Radiat Oncol Biol Phys. 2004 Jun 1;59(2):454-9

[Eickhoff1999] Eickhoff H, Haberer T, Kraft G, Krause U, Richter M, Steiner R, Debus J „The GSI Cancer Therapy Project“ Strahlenther Onkol. 1999 Jun;175 Suppl 2:21-4

[Elayat1995] Elayat AA, el-Naggar MM, Tahir M „An immunocytochemical and morphometric study of the rat pancreatic islets“ J Anat. 1995 Jun;186 (Pt 3):629-37

[Elsässer2010] Elsässer T, Weyrather WK, Friedrich T, Durante M, Iancu G, Krämer M, Kragl G, Brons S, Winter M, Weber KJ, Scholz M "Quantification of the relative biological effectiveness for ion beam radiotherapy: direct experimental comparison of proton and carbon ion beams and a novel approach for treatment planning" Int J Radiat Oncol Biol Phys. 2010 Nov 15;78(4):1177-83

[Fausto2003] Fausto N, Campbell JS „The role of hepatocytes and oval cells in liver regeneration and repopulation“ Mech Dev. 2003;120(1):117-30

[Filipski2003] Filipski E, King VM, Li X, Granda TG, Mormont MC, Claustrat B, Hastings MH, Lévi F „Disruption of circadian coordination accelerates malignant growth in mice“ Pathol Biol (Paris). 2003 Jun;51(4):216-9

[Filipski2009a] Filipski E, Subramanian P, Carrière J, Guettier C, Barbason H, Lévi F „Circadian disruption accelerates liver carcinogenesis in mice“ Mutat Res. 2009 Nov-Dec;680(1-2):95-105

[Filipski2009b] Filipski E, Lévi F „Circadian disruption in experimental cancer processes“ Integr Cancer Ther. 2009 Dec;8(4):298-302

[Fu2002] Fu L, Pelicano H, Liu J, Huang P, Lee C "The circadian gene Period2 plays an important role in tumor suppression and DNA damage response in vivo" Cell. 2002 Oct 4;111(1):41-50

[Fujikawa2000] Fujikawa K, Hasegawa Y, Matsuzawa S, Fukunaga A, Itoh T, Kondo S "Dose and dose-rate effects of X rays and fission neutrons on lymphocyte apoptosis in p53(+/+) and p53(-/-) mice" J Radiat Res. 2000 Jun;41(2):113-27

[Furusawa2000] Furusawa Y, Fukutsu K, Aoki M, Itsukaichi H, Eguchi-Kasai K, Ohara H, Yatagai F, Kanai T, Ando K „Inactivation of aerobic and hypoxic cells from three different cell lines by accelerated (3)He-, (12)C- and (20)Ne-ion beams“ Radiat Res. 2000 Nov;154(5):485-96

[Gähwiler1997] Gähwiler BH, Capogna M, Debanne D, McKinney RA, Thompson SM „Organotypic slice cultures: a technique has come of age” Trends Neurosci. 1997 Oct;20(10):471-7

[GasentBlesa2008] Gasent Blesa JM, Dawson LA „Options for radiotherapy in the treatment of liver metastases“ Clin Transl Oncol. 2008 Oct;10(10):638-45

[Geier2005] Geier F, Becker-Weimann S, Kramer A, Herzel H „Entrainment in a model of the mammalian circadian oscillator“ J Biol Rhythms. 2005 Feb;20(1):83-93

[George2003] George K, Durante M, Willingham V, Wu H, Yang TC, Cucinotta FA "Biological effectiveness of accelerated particles for the induction of chromosome damage measured in metaphase and interphase human lymphocytes" Radiat Res. 2003 Oct;160(4):425-35

[Gery2006] Gery S, Komatsu N, Baldjyan L, Yu A, Koo D, Koeffler HP „The circadian gene per1 plays an important role in cell growth and DNA damage control in human cancer cells“ Mol Cell. 2006 May 5;22(3):375-82

[Ghardi2012] Ghardi M, Moreels M, Chatelain B, Chatelain C, Baatout S „Radiation-induced double strand breaks and subsequent apoptotic DNA fragmentation in human peripheral blood mononuclear cells“ Int J Mol Med 2012;29(5):769-80

[Gobé1998] Gobé GC, Axelsen RA, Harmon BV, Allan DJ "Cell death by apoptosis following X-irradiation of the foetal and neonatal rat kidney" Int J Radiat Biol. 1988 Oct;54(4):567-76

[Goldstein1981] Goldstein LS, Phillips TL, Fu KK, Ross GY, Kane LJ "Biological effects of accelerated heavy ions. I. Single doses in normal tissue, tumors, and cells in vitro" Radiat Res. 1981 Jun;86(3):529-41

[Greco2004] Greco C, Catalano G, Di Grazia A, Orecchia R „Radiotherapy of liver malignancies. From whole liver irradiation to stereotactic hypofractionated radiotherapy“ Tumori. 2004 Jan-Feb;90(1):73-9

[Guida2005] Guida P, Vazquez ME, Otto S "Cytotoxic effects of low- and high-LET radiation on human neuronal progenitor cells: induction of apoptosis and TP53 gene expression" Radiat Res. 2005 Oct;164(4 Pt 2):545-51

[Gunzert-Marx2004] Gunzert-Marx, K Nachweis leichter Fragmente aus Schwerionenreaktionen mit einem BaF_2-Teleskop-Detektor Dissertation, TU Darmstadt, Fachbereich Physik, 2004

[Guo2007] Guo Y, Wang H, Zhang C „Establishment of rat precision-cut fibrotic liver slice technique and its application in verapamil metabolism“ Clinical and Experimental Pharmacology and Physiology 2007, 34:406-413

[Haberer1993] Haberer Th, Becher W, Schardt D, Kraft G „Magnetic scanning system for heavy ion therapy“ Nucl. Instr. Meth. Phys. Res. A 1993;330(1-2):296-305

[Hall2004] Hall EJ, Giaccia, AJ „Radiation for the Radiobiologist“ Lippincott Williams & Wilkins, Philadelphia, 2006

[Han2006] Han J, Hendzel MJ, Allalunis-Turner J "Quantitative analysis reveals asynchronous and more than DSB-associated histone H2AX phosphorylation after exposure to ionizing radiation" Radiat Res. 2006 Mar;165(3):283-92

[Haus2002] Haus E "Chronobiology of the mammalian response to ionizing radiation. Potential applications in oncology" Chronobiol Int 2002;19(1):77-100

[Hawkins2006] Hawkins MA, Dawson LA „Radiation therapy for hepatocellular carcinoma: from palliation to cure“ Cancer. 2006 Apr 15;106(8):1653-63

[Hendry1975] Hendry JH "Diurnal variations in radiosensitivity of mouse intestine" Br J Radiol. 1975 Apr;48(568):312-4

[Hermens1969] Hermens AF, Barendsen GW „Changes of cell proliferation characteristics in a rat rhabdomyosarcoma before and after x-irradiation“ Eur J Cancer 1969;5(2):173-89

[Hu2006] Hu B, Wu L, Han W, Zhang L, Chen S, Xu A, Hei TK, Yu Z "The time and spatial effects of bystander response in mammalian cells induced by low dose radiation" Carcinogenesis. 2006 Feb;27(2):245-51

[Hua2006] Hua H, Wang Y, Wan C, Liu Y, Zhu B, Yang C, Wang X, Wang Z, Cornelissen-Guillaume G, Halberg F „Circadian gene mPer2 overexpression induces cancer cell apoptosis“ Cancer Sci. 2006 Jul;97(7):589-96

[Ibañez2009] Ibañez IL, Bracalente C, Molinari BL, Palmieri MA, Policastro L, Kreiner AJ, Burlón AA, Valda A, Navalesi D, Davidson J, Davidson M, Vázquez M, Ozafrán M, Durán H "Induction and rejoining of DNA double strand breaks assessed by H2AX phosphorylation in melanoma cells irradiated with proton and lithium beams" Int J Radiat Oncol Biol Phys. 2009 Jul 15;74(4):1226-35

[Ijiri1988] Ijiri K, Potten CS "Circadian rhythms in the incidence of apoptotic cells and number of clonogenic cells in intestinal crypts after radiation using normal and reversed light conditions" Int J Radiat Biol Relat Stud Phys Chem Med 1988;53(5):717-27

[Ijiri1990] Ijiri K, Potten CS "The circadian rhythm for the number and sensitivity of radiation-induced apoptosis in the crypts of mouse small intestine" Int J Radiat Biol 1990;58(1):165-75

[Inagaki-Ohara2002] Inagaki-Ohara K, Takamura N, Yada S, Alnadjim Z, Liu E, Yu X, Yoshida H, Lin T "Radiation-induced crypt intestinal epithelial cell apoptosis in vivo involves both caspase-3-dependent and -independent pathways" Dig Dis Sci. 2002 Dec;47(12):2823-30

[Johnson2010] Johnson CH „Circadian clocks and cell division: what's the pacemaker?“ Cell Cycle. 2010 Oct 1;9(19):3864-73

[Jones1967] Jones RO „Factors affecting the survival of organ cultures of the mammalian pancreas“ Exp Cell Res. 1967;47(1):403-7

[JungHynes2010] Jung-Hynes B, Huang W, Reiter RJ, Ahmad N “Melatonin resynchronizes dysregulated circadian rhythm circuitry in human prostate cancer cells” J Pineal Res. 2010 Aug;49(1):60-8

[Kamada2012] Kamada T „Clinical evidence of particle beam therapy (carbon)“ Int J Clin Oncol. 2012 Apr;17(2):85-8

[Kao1996] Kao CY, Factor VM, Thorgeirsson SS „Reduced growth capacity of hepatocytes from c-myc and c-myc/TGF-alpha transgenic mice in primary culture“ Biochem Biophys Res Commun 1996;222(1):64-70

[Karlsson2004] Karlsson KH, Stenerlöw B "Focus formation of DNA repair proteins in normal and repair-deficient cells irradiated with high-LET ions" Radiat Res. 2004 May;161(5):517-27

[Kato2008] Kato TA, Okayasu R, Bedford JS "Comparison of the induction and disappearance of DNA double strand breaks and gamma-H2AX foci after irradiation of chromosomes in G1-phase or in condensed metaphase cells" Mutat Res. 2008 Mar 1;639(1-2):108-12

[Kauffmann2006] Kauffmann GW, Moser E, Sauer R “Radiologie” Urban & Fischer 2006, 3rd edition, p. 332-333

[Khapre2010] Khapre RV, Samsa WE, Kondratov RV „Circadian regulation of cell cycle: Molecular connections between aging and the circadian clock“ Ann Med 2010;42(6):404-15

[Khvostunov2010] Khvostunov IK, Nikjoo H, Uehara S, Hoshi M “The consideration of biological effectiveness of low energy protons using biophysical modeling of the effects induced by exposure of V79 cells” Radiats Biol Radioecol. 2010 Jan-Feb;50(1):81-9

[Klassen2008] Klassen LW, Thiele GM, Duryee MJ, Schaffert CS, DeVeney AL, Hunter CD, Olinga P, Tuma DJ „An in vitro method of alcoholic liver injury using precision-cut liver slices from rats“ Biochem Pharmacol. 2008;76(3):426-36

[Klevecz1987b] Klevecz RR, Shymko RM, Blumenfeld D, Braly PS „Circadian gating of S phase in human ovarian cancer“ Cancer Res. 1987 Dec 1;47(23):6267-71

[Klevecz1987a] Klevecz RR, Braly PS „Circadian and ultradian rhythms of proliferation in human ovarian cancer“ Chronobiol Int 1987;4(4)513-23

[Koike2002] Koike S, Ando K, Oohira C, Fukawa T, Lee R, Takai N, Monobe M, Furusawa Y, Aoki M, Yamada S, Shimizu W, Nojima K, Majima H "Relative biological effectiveness of 290 MeV/u carbon ions for the growth delay of a radioresistant murine fibrosarcoma" J Radiat Res. 2002 Sep;43(3):247-55

[Kokubo2000] Kokubo M, Nishimura Y, Shibamoto Y, Sasai K, Kanamori S, Hosotani R, Imamura M, Hiraoka M “Analysis of the clinical benefit of intraoperative radiotherapy in patients undergoing macroscopically curative resection for pancreatic cancer” Int J Radiat Oncol Biol Phys. 2000 Nov 1;48(4):1081-7

[Kornmann2007] Kornmann B, Schaad O, Bujard H, Takahashi JS, Schibler U “System-driven and iscillator-dependent circadian transcription in mice with a conditionally active liver clock” PloS Biol 2007; 5:e34

[Kraft2000] Kraft G “Tumor Therapy with Heavy Charged Particles” Prog Part Nucl Phys 2000;45:473-544

[Krämer2000a] Krämer M, Jäkel O, Haberer T, Kraft G, Schardt D, Weber U „Treatment planning for heavy-ion radiotherapy: physical beam model and dose optimization“ Phys Med Biol. 2000;45:3299-3317

[Krämer2000b] Krämer M, Scholz M „Treatment planning for heavy-ion radiotherapy: calculation and optimization of biologically effective dose“ Phys Med Biol. 2000;45(11):3319-30

[Krämer2006] Krämer M, Scholz M “Rapid calculation of biological effects in ion radiotherapy” Phys Med Biol. 2006;51:1959-70

[Krishnan2008] Krishnan S, Dawson LA, Seong J, Akine Y, Beddar S, Briere TM, Crane CH, Mornex F „Radiotherapy for hepatocellular carcinoma: an overview“ Ann Surg Oncol. 2008 Apr;15(4):1015-24

[Krumdieck1980] Krumdieck CL, dos Santos JE, Ho KJ „A new instrument for the rapid preparation of tissue slices“ Anal Biochem 1980, 104(1):118-123

[Kuo2008] Kuo LJ, Yang LX "Gamma-H2AX - a novel biomarker for DNA double-strand breaks" In Vivo. 2008 May-Jun;22(3):305-9

[Lawrence1936] Lawrence JH, Aebersold PC, Lawrence EO, „Comparative Effects of X-Rays and Neutrons on Normal and Tumor Tissue“ Proc Natl Acad Sci U S A 1936; 22(9): 543–557.

[Leatherbarrow2006] Leatherbarrow EL, Harper JV, Cucinotta FA, O'Neill P "Induction and quantification of gamma-H2AX foci following low and high LET-irradiation" Int J Radiat Biol. 2006 Feb;82(2):111-8

[Leith1982] Leith JT, McDonald M, Howard J "Residual skin damage in rats 1 year after exposure to X rays or accelerated heavy ions" Radiat Res. 1982 Jan;89(1):209-13

[Li1998] Li WX, Franklin WA "Radiation- and heat-induced apoptosis in PC-3 prostate cancer cells" Radiat Res. 1998 Aug;150(2):190-4

[Li2004] Li D, Xie K, Wolff R, Abbruzzese JL „Pancreatic cancer“ Lancet. 2004 Mar 27;363(9414):1049-57

[Lieber1975] Lieber M, Mazzetta J, Nelson-Rees W, Kaplan M, Todaro G „Establishment of a continuous tumor-cell line (panc-1) from a human carcinoma of the exocrine pancreas“ Int J Cancer. 1975;15(5):741-7

[Limoli2004] Limoli CL, Giedzinski E, Rola R, Otsuka S, Palmer TD, Fike JR "Radiation response of neural precursor cells: linking cellular sensitivity to cell cycle checkpoints, apoptosis and oxidative stress" Radiat Res. 2004 Jan;161(1):17-27

[Lockhart2005] Lockhart AC, Rothenberg ML, Berlin JD “Treatment for pancreatic cancer: current therapy and continued progress” Gastroenterology. 2005 May;128(6):1642-54

[Lowes1999] Lowes KN, Brennan BA, Yeoh GC, Olynyk JK „Oval Cell Numbers in Human Chronic Liver Diseases Are Directly Related to Disease Severity“ Am J Pathol. 1999 February; 154(2): 537–541

[MacPhail2003] MacPhail SH, Banáth JP, Yu Y, Chu E, Olive PL "Cell cycle-dependent expression of phosphorylated histone H2AX: reduced expression in unirradiated but not X-irradiated G1-phase cells" Radiat Res. 2003 Jun;159(6):759-67

[Mahrhofer2006] Mahrhofer H, Bürger S, Oppitz U, Flentje M, Djuzenova CS „Radiation induced DNA-damage and damage repair inhuman tumor- and fibroblast cell lines assessed by phosphorylated histone gamma-H2AX“ Int J Radiat Oncol Biol Phys 2006 Feb 1;64(2):573-80

[Maouyo1993] Maouyo D, Sarfati P, Guan D, Morisset J, Adelson JW „Circadian rhythm of exocrine pancreatic secretion in rats: major and minor cycles“Am J Physiol.230 1993 Apr;264(4 Pt 1):G792-800

[Marshman2001] Marshman E, Ottewell PD, Potten CS, Watson AJ "Caspase activation during spontaneous and radiation-induced apoptosis in the murine intestine" J Pathol. 2001 Oct;195(3):285-92

[Martin2000] Martin H, Sarsat JP, Lerche-Langrand C, Housset C, Balladur P, Toutain H, Albaladejo V „Morphological and biochemical integrity of human liver slices in long-term culture: effects of oxygen tension“Cell Biol Toxicol. 2002;18(2):73-85

[Martin2002] Martin H, Bournique B, Sarsat JP, Albaladejo V, Lerche-Langrand C „Cryopreserved rat liver slices: a critical evaluation of cell viability, histological integrity, and drug-metabolizing enzymes“Cryobiology. 2000 Sep;41(2):135-44

[Matsuzaki1999] Matsuzaki Y „Powerful radiotherapy for hepatocellular carcinoma“ J Gastroenterol Hepatol. 1999 Oct;14(10):941-5

[Mayahara2005] Mayahara H, Oda Y, Kawaguchi A, Kagawa K, Murakami M, Hishikawa Y, Igaki H, Tokuuye K, Abe M „A case of hepatocellular carcinoma initially treated by carbon ions, followed by protons for marginal recurrence with portal thrombus“ Radiat Med. 2005 Nov;23(7):513-9

[Mazzaccoli2010] Mazzoccoli G, Vendemiale G, De Cata A, Carughi S, Tarquini R “Altered time structure of neuro-endocrine-immune system function in lung cancer patients” BMC Cancer. 2010 Jun 21;10:314

[Meijer1998] Meijer AE, Kronqvist US, Lewensohn R, Harms-Ringdahl M "RBE for the induction of apoptosis in human peripheral lymphocytes exposed in vitro to high-LET radiation generated by accelerated nitrogen ions" Int J Radiat Biol. 1998 Feb;73(2):169-77

[MeneghelRozzo2004] Meneghel-Rozzo T, Rozzo A, Poppi L, Rupnik M „In vivo and in vitro development of mouse pancreatic beta-cells in organotypic slices“ Cell Tissue Res 2004;316(3):295-303.

[Merz2010] Merz F, M Müller, G Taucher-Scholz, F Rödel, H Stöcker, K Schopow, L Laprell, F Dehghani, M Durante, I Bechmann „Tissue slice cultures from humans or rodents: a new tool to evaluate biological effects of heavy ions“ Radiat Environ Biophys 2010;49(3):457-462

[Merz2011] Merz F, Bechmann I „Irradiation of human tumor tissue cultures: optimizing ion radiation therapy“ Future Oncol. 2011;7(4):489-91

[Meyn1983] Meyn RE, Jenkins WT "Variation in normal and tumor tissue sensitivity of mice to ionizing radiation-induced DNA strand breaks in vivo" Cancer Res 1983;43(12 Pt 1):5668-73

[Michelin2004] Michelin S, del Rosario Perez M, Dubner D, Gisone P "Increased activity and involvement of caspase-3 in radiation-induced apoptosis in neural cells precursors from developing rat brain" Neurotoxicology. 2004 Mar;25(3):387-98

[Miller2007] Miller BH, McDearmon EL, Panda S, Hayes KR, Zhang J, Andrews JL, Antoch MP, Walker JR, Esser KA, Hogenesch JB, Takahashi JS „Circadian and CLOCK-controlled regulation of the mouse transcriptome and cell proliferation“ Proc Natl Acad Sci U S A 2007;104(9):3342-7

[Minsky1961] Minsky, M. Microscopy apparatus, US patent 3013467, 1961

[Minsky1988] Minsky BD, Hilaris B, Fuks Z „The role of radiation therapy in the control of pain from pancreatic carcinoma“ J Pain Symptom Manage. 1988 Fall;3(4):199-205

[Mirkovic1994] Mirkovic N, Meyn RE, Hunter NR, Milas L "Radiation-induced apoptosis in a murine lymphoma in vivo" Radiother Oncol. 1994 Oct;33(1):11-6

[Mirzaie-Joniani2002] Mirzaie-Joniani H, Eriksson D, Sheikholvaezin A, Johansson A, Löfroth PO, Johansson L, Stigbrand T "Apoptosis induced by low-dose and low-dose-rate radiation" Cancer. 2002 Feb 15;94(4 Suppl):1210-4

[Mishustin2010] Mishustin I, Pshenichnov I, Greiner W „Modelling heavy-ion energy deposition in extended media“ Eur. Phys. J. D 2012;60:109-114

[Molière1948] Molière G „Theorie der Streuung schneller geladener Teilchen II, Mehrfach- und Vielfachstreuung“ Z Naturforschung 1948;3A:78-97

[Moore1972] Moore RY, Eichler VB „Loss of a circadian adrenal corticosterone rhythm following suprachiasmatic lesions in the rat“Brain Res. 1972 Jul 13;42(1):201-6

[Mori1999] Mori T, Iwai M, Harada Y, Tanaka S, Muramatsu A, Okanoue T, Kashima K, Fushiki S „Parenchymal cells proliferate and differentiate in an organotypic slice culture of the neonatal liver“ Anat Embryol (Berl). 1999;199(4):319-27

[Mühlbauer2004] Mühlbauer E, Wolgast S, Finckh U, Peschke D, Peschke E „Indication of circadian oscillations in the rat pancreas“ FEBS Lett. 2004 ;564(1-2):91-6

[Mühlbauer2009] Mühlbauer E, Gross E, Labucay K, Wolgast S, Peschke E „Loss of melatonin signalling and its impact on circadian rhythms in mouse organs regulating blood glucose“ Eur J Pharmacol. 2009;606(1-3):61-71

[Müller2010] Müller M, Durante M, Stöcker H, Merz F, Bechmann I „Modeling radiation effects at the tissue level“ Eur Phys J D 2010;60:171-176

[Murakami1993] Murakami H, Sanderson ND, Nagy P, Marino PA, Merlino G, Thorgeirsson SS „Transgenic mouse model for synergistic effects of nuclear oncogenes and growth factors in tumorigenesis: interaction of c-myc and transforming growth factor alpha in hepatic oncogenesis“ Cancer Res. 1993;53(8):1719-23

[Murray1984] Murray D, Jenkins WT, Meyn RE "The efficiency of DNA strand-break repair in two fibrosarcoma tumors and in normal tissues of mice irradiated in vivo with X rays" Radiat Res 1984;100(1):171-81s

[Nader2010] Nader N, Chrousos GP, Kino T „Interactions of the circadian CLOCK system and the HPA axis“Trends Endocrinol Metab. 2010 May;21(5):277-86

[Nakano1991] Nakano T, Oka K „Transition of Ki-67 index of uterine cervical tumors during radiation therapy. Immunohistochemical study“ Cancer 1991;68(3):517-23

[Nazarov2003] Nazarov IB, Smirnova AN, Krutilina RI, Svetlova MP, Solovjeva LV, Nikiforov AA, Oei SL, Zalenskaya IA, Yau PM, Bradbury EM, Tomilin NV "Dephosphorylation of histone gamma-H2AX during repair of DNA double-strand breaks in mammalian cells and its inhibition by calyculin A" Radiat Res. 2003 Sep;160(3):309-17

[Neoptolemos2004] Neoptolemos JP, Stocken DD, Friess H, Bassi C, Dunn JA, Hickey H, Beger H, Fernandez-Cruz L, Dervenis C, Lacaine F, Falconi M, Pederzoli P, Pap A, Spooner D, Kerr DJ, Büchler MW; European Study Group for Pancreatic Cancer "A randomized trial of chemoradiotherapy and chemotherapy after resection of pancreatic cancer" N Engl J Med. 2004 Mar 18;350(12):1200-10

[Neuschwader-Tetri1996] Neuschwander-Tetri BA, Rozin T „Diurnal variability of cysteine and glutathione content in the pancreas and liver of the mouse" Comp Biochem Physiol B Biochem Mol Biol 1996 May;114(1):91-5

[Newhauser2011] Newhauser WD, Durante M "Assessing the risk of second malignancies after modern radiotherapy" Nat Rev Cancer. 2011 Jun;11(6):438-48

[Nikaido2007] Nikaido SS, Johnson CH "Daily and circadian variation in survival from ultraviolet radiation in Chlamydomonas reinhardtii" Photochem Photobiol. 2007 Jun;71(6):758-65

[Nikjoo1994] Nikjoo H, O'Neill P, Terrissol M, Goodhead DT "Modelling of radiation-induced DNA damage: the early physical and chemical event" Int J Radiat Biol. 1994 Nov;66(5):453-7

[Nikjoo1999] Nikjoo H, O'Neill P, Terrissol M, Goodhead DT "Quantitative modelling of DNA damage using Monte Carlo track structure method" Radiat Environ Biophys. 1999 May;38(1):31-8

[Nowak2006] Nowak E, Etienne O, Millet P, Lages CS, Mathieu C, Mouthon MA, Boussin FD "Radiation-induced H2AX phosphorylation and neural precursor apoptosis in the developing brain of mice" Radiat Res. 2006 Feb;165(2):155-64

[O'Brien 2005] O'Brien TJ, Létuvé S, Haston CK "Radiation-induced strain differences in mouse alveolar inflammatory cell apoptosis" Can J Physiol Pharmacol. 2005 Jan;83(1):117-22

[Ofuchi1999] Ofuchi T, Suzuki M, Kase Y, Ando K, Isono K, Ochiai T "Chromosome breakage and cell lethality in human hepatoma cells irradiated with X rays and carbon-ion beams" J Radiat Res. 1999 Jun;40(2):125-33

[Oh2010] Oh EY, Yang X, Friedman A, Ansell CM, Du-Quiton J, Quiton DF, Wood PA, Hrushesky WJ "Circadian transcription profile of mouse breast cancer under light-dark and dark-dark conditions" Cancer Genomics Proteomics. 2010 Nov-Dec;7(6):311-22

[Okayasu2012] Okayasu R "Repair of DNA damage induced by accelerated heavy ions--a mini review" Int J Cancer. 2012 Mar 1;130(5):991-1000

[Oklejewicz2008] Oklejewicz M, Destici E, Tamanini F, Hut RA, Janssens R, van der Horst GT „Phase resetting of the mammalian circadian clock by DNA damage" Curr Biol. 2008 Feb 26;18(4):286-91

[Olinga1997] Olinga P, Groen K, Hof IH, De Kanter R, Koster HJ, Leeman WR, Rutten AA, Van Twillert K, Groothuis GM „Comparison of five incubation systems for rat liver slices using functional and viability parameters" J Pharmacol Toxicol Methods 1997;38(2):59-69

[Olinga1998] Olinga P, Merema MT, Hof IH, De Jager MH, De Jong KP, Slooff MJ, Meijer DK, Groothuis GM „Effect of cold and warm ischaemia on drug metabolism in isolated hepatocytes and slices from human and monkey liver"Xenobiotica. 1998 Apr;28(4):349-60

[Olinga2001a] Olinga P, Hof IH, Merema MT, Smit M, de Jager MH, Swart PJ, Slooff MJ, Meijer DK, Groothuis GM „The applicability of rat and human liver slices to the

study of mechanisms of hepatic drug uptake“ J Pharmacol Toxicol Methods. 2001 Jan-Feb;45(1):55-63

[Olinga2001b] Olinga P, Merema MT, de Jager MH, Derks F, Melgert BN, Moshage H, Slooff MJ, Meijer DK, Poelstra K, Groothuis GM „Rat liver slices as a tool to study LPS-induced inflammatory response in the liver“ J Hepatol. 2001 Aug;35(2):187-94

[Oster2006] Oster H, Damerow S, Kiessling S, Jakubcakova V, Abraham D, Tian J, Hoffmann MW, Eichele G „The circadian rhythm of glucocorticoids is regulated by a gating mechanism residing in the adrenal cortical clock“ Cell Metab. 2006 Aug;4(2):163-73

[Paganetti2002] Paganetti H, Niemierko A, Ancukiewicz M, Gerweck LE, Goitein M, Loeffler JS, Suit HD "Relative biological effectiveness (RBE) values for proton beam therapy" Int J Radiat Oncol Biol Phys. 2002 Jun 1;53(2):407-21

[Parrish1995] Parrish AR, Gandolfi AJ, Brendel K „Precision-cut tissue slices: applications in pharmacology and toxicology“ Life Sci. 1995;57(21):1887-901

[Parrish1998] Parrish AR, Fisher R, Bral CM, Burghardt RC, Gandolfi AJ, Brendel K, Ramos KS „Benzo(a)pyrene-induced alterations in growth-related gene expression and signaling in precision-cut adult rat liver and kidney slices“Toxicol Appl Pharmacol. 1998 Oct;152(2):302-8

[Pendergast2010] Pendergast JS, Yeom M, Reyes BA, Ohmiya Y, Yamazaki S “Disconnected circadian and cell cycles in a tumor-driven cell line” Commun Integr Biol. 2010 Nov;3(6):536-9

[Peschke1998] Peschke E, Peschke D „Evidence for a circadian rhythm of insulin release from perifused rat pancreatic islets“ Diabetologia. 1998;41(9):1085-92

[Pizzarello1964] Pizzarello DJ, Isaak D, Chua KE, Rhyne AL "Circadian Rhythmicity in the Sensitivity of two Strains of Mice to Whole-Body Radiation" Science. 1964 Jul 17;145(3629):286-91

[Pfeffer, 2012] Pfeffer M, Rauch A, Korf HW, von Gall C. (2012). The endogenous melatonin (MT) signal facilitates reentrainment of the circadian system to light-induced phase advances by acting upon MT2 receptors. *Chronobiol Int.* 29(4):415-429.

[Potmesil1980] Potmesil M, Goldfeder A „Cell kinetics of irradiated experimental tumors: cell transition from the non-proliferating to the proliferating pool“ Cell Tissue Kinet 1980;13(5):563-70

[Potten1998] Potten CS, Grant HK "The relationship between ionizing radiation-induced apoptosis and stem cells in the small and large intestine" Br J Cancer. 1998 Oct;78(8):993-1003

[Pshenichnov2005] Pshenichnov I, Mishustin I, Greiner W „Neutrons from fragmentation of light nuclei in tissue-like media: a study with the GEANT4 toolkit“ Phys Med Biol. 2005 Dec 7;50(23):5493-507

[Pshenichnov2007] Pshenichnov I, Larionov A, Mishustin I, Greiner W “PET monitoring of cancer therapy with ^{3}He and ^{12}C beams: a study with the GEANT4 toolkit” Phys. Med. Biol. 2007;52:7295–7312

[Pshenichnov2008] Pshenichnov I, Mishustin I, Greiner W “Comparative study of depth-dose distributions for beams of light and heavy nuclei in tissue-like media” Nucl. Instr. Meth. Phys. Res. B 2008;266:1094-1098

[Pshenichnov2010] Pshenichnov I, Botvina A, Mishustin I, Greiner W „Nuclear fragmentation reactions in extended media studied with GEANT4 toolkit“Nucl. Instr. Meth. Phys. Res. B 2010;268:604-615

[Radford1994] Radford IR, Murphy TK "Radiation response of mouse lymphoid and myeloid cell lines. Part III. Different signals can lead to apoptosis and may influence

sensitivity to killing by DNA double-strand breakage" Int J Radiat Biol. 1994 Feb;65(2):229-39

[Rahn2011] Rahn DA 3rd, Ray DK, Schlesinger DJ, Steiner L, Sheehan JP, O'Quigley JM, Rich T "Gamma Knife Radiosurgery for Brain Metastasis of Nonsmall Cell Lung Cancer: Is There a Difference in Outcome Between Morning and Afternoon Treatment?", Cancer 2011 Jan 15;117(2):414-20

[Ralph1990] Ralph MR, Foster RG, Davis FC, Menaker M „Transplanted suprachiasmatic nucleus determines circadian period" Science 1990 Feb 23;247(4945):975-8

[Ramsey2011] Ramsey MR, Ellisen LW „Circadian function in cancer: regulating the DNA damage response" Proc Natl Acad Sci U S A 2011;108(26):10379-80

[Reppert2001] Reppert SM, Weaver DR „Molecular analysis of mammalian circadian rhythms"Annu Rev Physiol. 2001;63:647-76

[Resau1983] Resau JH, Hudson EA, Jones RT „Organ explant culture of adult Syrian golden hamster pancreas" In Vitro 1983;19(4):315-25

[RKI2012] „Krebs in Deutschland 2007/2008." 8th edition, Robert Koch-Institut (Hrsg) und die Gesellschaft der epidemiologischen Krebsregister in Deutschland e.V. (Hrsg). Berlin, 2012

[Robles2010] Robles MS, Boyault C, Knutti D, Padmanabhan K, Weitz CJ „Identification of RACK1 and protein kinase Calpha as integral components of the mammalian circadian clock" Science. 2010;327(5964):463-6

[Roeske1990] Roeske JC, Chen GT, Atcher RW, Pelizzari CA, Rotmensch J, Haraf D, Montag A, Weichselbaum RR „Modeling of dose to tumor and normal tissue from intraperitoneal radioimmunotherapy with alpha and beta emitters " Int J Radiat Oncol Biol Phys 1990;19(6):1539-48

[Rogakou1998] Rogakou EP, Pilch DR, Orr AH, Ivanova VS, Bonner WM „DNA double-stranded breaks induce histone H2AX phosphorylation on serine 139“ J Biol Chem 1998;273(10):5858-68

[Rübe2008] Rübe CE, Grudzenski S, Kühne M, Dong X, Rief N, Löbrich M, Rübe C "DNA double-strand break repair of blood lymphocytes and normal tissues analysed in a preclinical mouse model: implications for radiosensitivity testing" Clin Cancer Res 2008;14(20):6546-55

[Ruifrok1998] Ruifrok AC, Weil MM, Thames HD, Mason KA "Diurnal variations in the expression of radiation-induced apoptosis" Radiat Res. 1998 Apr;149(4):360-5

[Rypka2006] Rypka M, Cervenková K, Uherková L, Poczatková H, Florschutz AV, Veselý J „A novel simplified ultra-rapid freezing technique for cryopreservation of tissue slices“ Cryobiology. 2006 Apr;52(2):193-9

[Sadacca2011] Sadacca LA, Lamia KA, deLemos AS, Blum B, Weitz CJ „An intrinsic circadian clock of the pancreas is required for normal insulin release and glucose homeostasis in mice“ Diabetologia. 2011;54(1):120-4

[Sancar2010] Sancar A, Lindsey-Boltz LA, Kang TH, Reardon JT, Lee JH, Ozturk N „Circadian clock control of the cellular response to DNA damage“ FEBS Lett 2010;584(12):2618-25

[Sandgren1990] Sandgren EP, Luetteke NC, Palmiter RD, Brinster RL, Lee DC „Overexpression of TGF alpha in transgenic mice: induction of epithelial hyperplasia, pancreatic metaplasia, and carcinoma of the breast“ Cell 1990;61(6):1121-35

[Sandgren1991] Sandgren EP, Quaife CJ, Paulovich AG, Palmiter RD, Brinster RL „Pancreatic tumor pathogenesis reflects the causative genetic lesion“ Proc Natl Acad Sci U S A. 1991;88(1):93-7

[Sandgren1993] Sandgren EP, Luetteke NC, Qiu TH, Palmiter RD, Brinster RL, Lee DC „Transforming growth factor alpha dramatically enhances oncogene-induced

carcinogenesis in transgenic mouse pancreas and liver“ Mol Cell Biol. 1993;13(1):320-30

[Santoni-Rugio1996] Santoni-Rugiu E, Nagy P, Jensen MR, Factor VM, Thorgeirsson SS „Evolution of neoplastic development in the liver of transgenic mice co-expressing c-myc and transforming growth factor-alpha“ Am J Pathol. 1996;149(2):407-28

[Scheving2000] Scheving LA „Biological clocks and the digestive system“ Gastroenterology 2000;119(2):536-49

[Schibler2003] Schibler U, Ripperger J, Brown SA „Peripheral circadian oscillators in mammals: time and food“J Biol Rhythms. 2003 Jun;18(3):250-60

[Scholz1996a] Scholz M “Calculation of RBE for normal tissue complications based on charged particle track structure” Bull. Cancer/Radiother 1996;83(suppl 1):505-45

[Scholz1996b] Scholz M, Kraft G “Track structure and the calculation of biological effects of heavy charged partices” Adv Space Res. 1996;18:5-14

[Scholz1997] Scholz M, Kellerer A M, Kraft-Weyrather W, Kraft G “Computation of cell survival in heavy ion beams for therapy – the model and its approximation” Rad Environ Biophys. 1997; 36:59-66

[Scholzen2000] Scholzen T, Gerdes J. „The Ki-67 protein: from the known and the unknown” J Cell Physiol. 2000 Mar;182(3):311-22. Review.

[Schulz-Ertner2006] Schulz-Ertner D, Jäkel O, Schlegel W „Radiation therapy with charged particles“ Semin Radiat Oncol. 2006 Oct;16(4):249-59

[Schulz-Ertner2009] Schulz-Ertner D „The clinical experience with particle therapy in adults“ Cancer J. 2009 Jul-Aug;15(4):306-11

[Schwartz1995] Schwartz JL, Jordan R, Sedita BA, Swenningson MJ, Banáth JP, Olive PL "Different sensitivity to cell killing and chromosome mutation induction by gamma

rays in two human lymphoblastoid cell lines derived from a single donor: possible role of apoptosis" Mutagenesis. 1995 May;10(3):227-33

[Scott2001] Scott NA, Crocker IR, Yin Q, Sorescu D, Wilcox JN, Griendling KK "Inhibition of vascular cell growth by X-ray irradiation: comparison with gamma radiation and mechanism of action" Int J Radiat Oncol Biol Phys. 2001 Jun 1;50(2):485-93

[Sharma2010] Sharma S, Haldar C, Chaube SK, Laxmi T, Singh SS „Long-term melatonin administration attenuates low-LET gamma-radiation-induced lymphatic tissue injury during the reproductively active and inactive phases of Indian palm squirrels (Funambulus pennanti)“ Br J Radiol 2010;83(986):137-51

[Shigematsu2000] Shigematsu A, Motoji N, Momose Y, Iida A, Higashi N „Viability of liver slices exhibiting absorption, metabolism, and elimination of substrates in culture medium“ Exp Mol Pathol. 2000;69(2):119-43

[Shinchi2002] Shinchi H, Takao S, Noma H, Matsuo Y, Mataki Y, Mori S, Aikou T “Length and quality of survival after external-beam radiotherapy with concurrent continuous 5-fluorouracil infusion for locally unresectable pancreatic cancer” Int J Radiat Oncol Biol Phys. 2002 May 1;53(1):146-50

[Shinomiya 2001] Shinomiya N "New concepts in radiation-induced apoptosis: 'premitotic apoptosis' and 'postmitotic apoptosis'" J Cell Mol Med. 2001 Jul-Sep;5(3):240-53

[Shukla2010] Shukla P, Gupta D, Bisht SS, Pant MC, Bhatt ML, Gupta R, Srivastava K, Gupta S, Dhawan A, Mishra D, Negi MP “Circadian Variation in Radiation-Induced Intestinal Mucositis in Patients With Cervical Carcinoma” Cancer 2010 Apr 15;116(8):2031-5

[Shukla2011] Shukla P, Gupta D, Munshi A, Agarwal JP “Cetuximab and cancers of the head and neck: tapping the circadian rhythm” Med Hypotheses. 2011 Sep;77(3):336-8

[Skarsgard1967] Skarsgard LD, Kihlman BA, Parker L, Pujara CM, Richardson S "Survival, chromosome abnormalities, and recovery in heavy-ion and x-irradiated mammalian cells" Radiat Res Suppl. 1967;7:208-21

[Smaaland1995] Smaaland R, Laerum OD, Abrahamsen JF „Circadian cell kinetics in humans. Aspects related to cancer chemotherapy“ In Vivo. 1995 Nov-Dec;9(6):529-37

[Smith1985] Smith PF, Gandolfi AJ, Krumdieck CL, Putnam CW, Zukoski CF 3rd, Davis WM, Brendel K „Dynamic organ culture of precision liver slices for in vitro toxicology“ Life Sci. 1985;36(14):1367-75

[Sommerer2009] Sommerer F, Cerutti F, Parodi K, Ferrari A, Enghardt W, Aiginger H „In-beam PET monitoring of mono-energetic (16)O and (12)C beams: experiments and FLUKA simulations for homogeneous targets“ Phys Med Biol. 2009 Jul 7;54(13):3979-96

[Son2011] Son GH, Chung S, Kim K „The adrenal peripheral clock: glucocorticoid and the circadian timing system“Front Neuroendocrinol. 2011 Oct;32(4):451-65

[Speier2003] Speier S, Rupnik M „A novel approach to in situ characterization of pancreatic beta-cells“ Pflugers Arch 2003;446(5):553-8

[Speier2005] Speier S, Yang SB, Sroka K, Rose T, Rupnik M “KATP-channels in beta-cells in tissue slices are directly modulated by millimolar ATP” Mol Cell Endocrinol. 2005 Jan 31;230(1-2):51-8

[Collis2007] Collis SJ, Boulton SJ “Emerging links between the biological clock and the DNA damage response” Chromosoma 2007;116:331-339

[StatBund2010] Statistisches Bundesamt „Todesursachenstatistik – Todesursachenstatistik in Deutschland“ 2011 Sept; downloaded from https://www.destatis.de/DE/Publikationen/Thematisch/Gesundheit/Todesursachen/Todesursachen.html

[Stephan1972] Stephan FK, Zucker I „Circadian rhythms in drinking behavior and locomotor activity of rats are eliminated by hypothalamic lesions“Proc Natl Acad Sci U S A. 1972 Jun;69(6):1583-6

[Stephan2002] Stephan FK „The "other" circadian system: food as a Zeitgeber“ J Biol Rhythms 2002;17(4):284-92

[Stokkan2001] Stokkan KA, Yamazaki1 S, Tei H, Sakaki Y, Menaker M „Entrainment of the Circadian Clock in the Liver by Feeding“ Science 2001;291(5503):490-493

[Suzuki2000b] Suzuki M, Kase Y, Kanai T, Ando K „Correlation between cell killing and residual chromatin breaks measured by PCC in six human cell lines irradiated with different radiation types“ Int J Radiat Biol. 2000 Sep;76(9):1189-96

[Suzuki2000a] Suzuki M, Kase Y, Yamaguchi H, Kanai T, Ando K "Relative biological effectiveness for cell-killing effect on various human cell lines irradiated with heavy-ion medical accelerator in Chiba (HIMAC) carbon-ion beams" Int J Radiat Oncol Biol Phys. 2000 Aug 1;48(1):241-50

[Szczepanski1975] Szczepanski L, Trott K-R „Post-irradiation proliferation kinetics of a serially transplanted murine adenocarcinoma“ Br J Radiol 1975;48(567):200-8

[‘tHart2005] 't Hart NA, van der Plaats A, Faber A, Leuvenink HG, Olinga P, Wiersema-Buist J, Verkerke GJ, Rakhorst G, Ploeg RJ „Oxygenation during hypothermic rat liver preservation: an in vitro slices study to demonstrate beneficial or toxic oxygenation effects“Liver Transpl. 2005 Nov;11(11):1403-11

[Takahashi1998] Takahashi T, Mitsuhashi N, Furuta M, Hasegawa M, Ohno T, Saito Y, Sakurai H, Nakano T, Niibe H "Apoptosis induced by heavy ion (carbon) irradiation of two human tumours with different radiosensitivities in vivo: relative biological effectiveness (RBE) of carbon beam" Anticancer Res. 1998 Jan-Feb;18(1A):253-6

[Takahashi2001] Takahashi A, Ohnishi K, Asakawa I, Kondo N, Nakagawa H, Yonezawa M, Tachibana A, Matsumoto H, Ohnishi T "Radiation response of apoptosis

in C57BL/6N mouse spleen after whole-body irradiation" Int J Radiat Biol. 2001 Sep;77(9):939-45

[Takahashi2004] Takahashi T, Nakano T, Oka K, Ando K „Transitional increase in growth fraction estimated by Ki-67 index after irradiation to human tumor in xenograft“ Anticancer Res 2004;24(1):107-10

[Taniguchi2009] Taniguchi H, Fernández AF, Setién F, Ropero S, Ballestar E, Villanueva A, Yamamoto H, Imai K, Shinomura Y, Esteller M “Epigenetic inactivation of the circadian clock gene BMAL1 in hematologic malignancies” Cancer Res. 2009 Nov 1;69(21):8447-54

[Tello2008] Tello K, Christiansen H, Gürleyen H, Dudas J, Rave-Fränk M, Hess CF, Ramadori G, Saile B „Irradiation leads to apoptosis of Kupffer cells by a Hsp27-dependant pathway followed by release of TNF-alpha“ Radiat Environ Biophys 2008;47(3):389-97

[Tobias1982] Tobias CA, Blakely EA, Alpen EL, Castro JR, Ainsworth EJ, Curtis SB, Ngo FQ, Rodriguez A, Roots RJ, Tenforde T, Yang TC "Molecular and cellular radiobiology of heavy ions" Int J Radiat Oncol Biol Phys. 1982 Dec;8(12):2109-20

[Tong2000] Tong X, Liu B, Dong Y, Sun Z "Cleavage of ATM during radiation-induced apoptosis: caspase-3-like apoptotic protease as a candidate" Int J Radiat Biol. 2000 Oct;76(10):1387-95

[Tse2008] Tse RV, Guha C, Dawson LA „Conformal radiotherapy for hepatocellular carcinoma“ Crit Rev Oncol Hematol. 2008 Aug;67(2):113-23

[Tsuchida1998] Tsuchida Y, Tsuboi K, Ohyama H, Ohno T, Nose T, Ando K "Cell death induced by high-linear-energy transfer carbon beams in human glioblastoma cell lines" Brain Tumor Pathol. 1998;15(2):71-6

[Tsuruoka2005] Tsuruoka C, Suzuki M, Kanai T, Fujitaka K „LET and ion species dependence for cell killing in normal human skin fibroblasts“ Radiat Res. 2005 May;163(5):494-500

[Ulrich2002] Ulrich AB, Schmied BM, Standop J, Schneider MB, Pour PM „Pancreatic cell lines: a review“ Pancreas. 2002;24(2):111-20

[Urano1984] Urano M, Verhey LJ, Goitein M, Tepper JE, Suit HD, Mendiondo O, Gragoudas ES, Koehler A „Relative biological effectiveness of modulated proton beams in various murine tissue“ Int J Radiat Oncol Biol Phys 1984;10(4):509-14

[vandeBovenkamp2005] van de Bovenkamp M, Groothuis GM, Draaisma AL, Merema MT, Bezuijen JI, van Gils MJ, Meijer DK, Friedman SL, Olinga P „Precision-cut liver slices as a new model to study toxicity-induced hepatic stellate cell activation in a physiologic milieu“ Toxicol Sci. 2005;85(1):632-8

[vanGeer2009] van Geer MA, Kuhlmann KF, Bakker CT, ten Kate FJ, Oude Elferink RP, Bosma PJ „Ex-vivo evaluation of gene therapy vectors in human pancreatic (cancer) tissue slices“ World J Gastroenterol 2009 ;15(11):1359-66

[vanMidwoud2010] van Midwoud PM, Merema MT, Verpoorte E, Groothuis GM „A microfluidic approach for in vitro assessment of interorgan interactions in drug metabolism using intestinal and liver slices“Lab Chip. 2010 Oct 21;10(20):2778-86

[vanMidwoud2011] van Midwoud PM, Janssen J, Merema MT, de Graaf IA, Groothuis GM, Verpoorte E „On-line HPLC analysis system for metabolism and inhibition studies in precision-cut liver slices“Anal Chem. 2011 Jan 1;83(1):84-91

[Verrill2002] Verrill C, Davies J, Millward-Sadler H, Sundstrom L, Sheron N „Organotypic liver culture in a fluid-air interface using slices of neonatal rat and adult human tissue--a model of fibrosis in vitro.“ J Pharmacol Toxicol Methods. 2002;48(2):103-10

[Vickers2004] Vickers AE, Saulnier M, Cruz E, Merema MT, Rose K, Bentley P, Olinga P „Organ slice viability extended for pathway characterization: an in vitro model to investigate fibrosis“ Toxicol Sci. 2004;82(2):534-44

[Vickers2009] Vickers AE “Tissue slices for the evaluation of metabolism-based toxicity with the example of diclofenac” Chem Biol Interact. 2009 Apr 15;179(1):9-16

[Völkl1983] Völkl A, Poort C “Circadian rhythm of protein synthesis activity in the exocrine pancreas of fed and starved rats” J Cell Sci.237 1983 May;61:467-73

[vonGall2000] von Gall C, Weaver DR, Kock M, Korf HW, Stehle JH „Melatonin limits transciptional impact of phosphoCREB in the mouse SCN via the Mel1a receptor“ Neuroreport. 2000 Jun 26;11(9):1803-7

[Wanebo2000] Wanebo HJ, Glicksman AS, Vezeridis MP, Clark J, Tibbetts L, Koness RJ, Levy A “Preoperative chemotherapy, radiotherapy, and surgical resection of locally advanced pancreatic cancer” Arch Surg. 2000 Jan;135(1):81-7

[Warburg1923] Warburg, 0 „Versuche an überlebendem Carcinomgewebe“ Biochemische Zeitschrift 1923, 142:17-333

[Warszawski1981] Warszawski D, Ben-Zvi Z, Gorodischer R “Caffeine metabolism in liver slices during postnatal development in the rat” Biochem Pharmacol. 1981 Dec 1;30(23):3145-50

[Warters1992] Warters RL "Radiation-induced apoptosis in a murine T-cell hybridoma" Cancer Res. 1992 Feb 15;52(4):883-90

[Weber1999] Weber U, Kraft G “Design and construction of a ripple filter for a smoothed depth dose distribution in conformal particle therapy” Phys Med Biol 1999;44:2765-75

[Weyrather1999] Weyrather WK, Ritter S, Scholz M, Kraft G „RBE for carbon track-segment irradiation in cell lines of differing repair capacity“ Int J Radiat Biol. 1999 Nov;75(11):1357-6

[Williams2008] Williams JR, Zhang Y, Zhou H, Gridley DS, Koch CJ, Slater JM, Little JB „Overview of radiosensitivity of human tumor cells to low-dose-rate irradiation“ Int J Radiat Oncol Biol Phys 2008;72(3):909-17

[Wilson1946] Wilson RR „Radiological use of fast protons“ Radiology. 1946 Nov;47(5):487-91

[Winkelmann2008] Winkelmann T, Cee R, Haberer T, Naas B, Peters A, Scheloske S, Spädtke P, Tinschert K „Electron cyclotron resonance ion source experience at the Heidelberg Ion Beam Therapy Center“ Rev Sci Instrum. 2008 Feb;79(2 Pt 2):02A331

[Winkelmann2012] Winkelmann T, Cee R, Haberer T, Naas B, Peters A „Test bench to commission a third ion source beam line and a newly designed extraction system“ Rev Sci Instrum. 2012 Feb;83(2):02B904

[Wulf1985] Wulf H, Kraft-Weyrather W, Miltenburger HG, Blakely EA, Tobias CA, Kraft G "Heavy-ion effects on mammalian cells: inactivation measurements with different cell lines" Radiat Res Suppl 1985;8:S122-34

[Xia2010] Xia HC, Niu ZF, Ma H, Cao SZ, Hao SC, Liu ZT, Wang F “Deregulated expression of the Per1 and Per2 in human gliomas” Can J Neurol Sci. 2010 May;37(3):365-70

[Yamamoto2004] Yamamoto T, Nakahata Y, Soma H, Akashi M, Mamine T, Takumi T „Transcriptional oscillation of canonical clock genes in mouse peripheral tissues“ BMC Mol Biol 2004;5:18

[Yamazaki2000] Yamazaki S, Numano R, Abe M, Hida A, Takahashi R, Ueda M, Block GD, Sakaki Y, Menaker M, Tei H „Resetting central and peripheral circadian oscillators in transgenic rats“ Science 2000;288:682-85

[Yamazaki2002]Yamazaki S, Straume M, Tei H, Sakaki Y, Menaker M, Block GD „Effects of aging on central and peripheral mammalian clocks“ Proc Natl Acad Sci U S A. 2002;99(16):10801-6

[Yamazaki2009] Yamazaki S, Yoshikawa T, Biscoe EW, Numano R, Gallaspy LM, Soulsby S, Papadimas E, Pezuk P, Doyle SE, Tei H, Sakaki Y, Block GD, Menaker M „Ontogeny of circadian organization in the rat“J Biol Rhythms. 2009 Feb;24(1):55-63

[Yanagihara1995] Yanagihara K, Nii M, Numoto M, Kamiya K, Tauchi H, Sawada S, Seito T "Radiation-induced apoptotic cell death in human gastric epithelial tumour cells; correlation between mitotic death and apoptosis" Int J Radiat Biol. 1995 Jun;67(6):677-85

[Yang2005] Yang H, Asaad N, Held KD "Medium-mediated intercellular communication is involved in bystander responses of X-ray-irradiated normal human fibroblasts" Oncogene. 2005 Mar 17;24(12):2096-103

[Yang2007] Yang H, Anzenberg V, Held KD "The time dependence of bystander responses induced by iron-ion radiation in normal human skin fibroblasts" Radiat Res. 2007 Sep;168(3):292-8

[Yang2010] Yang X, Guo M, Wan YJ „Deregulation of growth factor, circadian clock, and cell cycle signaling in regenerating hepatocyte RXRalpha-deficient mouse livers“ Am J Pathol 2010;176(2):733-43

[Yang2011] Yang MY, Yang WC, Lin PM, Hsu JF, Hsiao HH, Liu YC, Tsai HJ, Chang CS, Lin SF “Altered expression of circadian clock genes in human chronic myeloid leukemia” J Biol Rhythms. 2011 Apr;26(2):136-48

[Yoo2004]Yoo SH, Yamazaki S, Lowrey PL, Shimomura K, Ko CH, Buhr ED, Siepka SM, Hong HK, Oh WJ, Yoo OJ, Menaker M, Takahashi JS „PERIOD2::LUCIFERASE real-time reporting of circadian dynamics reveals persistent circadian oscillations in mouse peripheral tissues“ Proc Natl Acad Sci U S A. 2004; 101(15): 5339–5346

[Zacharias1997] Zacharias T, Dörr W, Enghardt W, Haberer T, Krämer M, Kumpf R, Röthig H, Scholz M, Weber U, Kraft G, Herrmann T „Acute response of pig skin to irradiation with 12C-ions or 200 kV X-rays“ Acta Oncol. 1997;36(6):637-42

[Zhang2008] Zhang J, Zhu B, Liu Y, Jiang Z, Wang Y, Li Y, Hua H, Wang Z „High expression of circadian gene mPer2 diminishes radiosensitivity of tumor cells“ Cancer Biother Radiopharm. 2008 Oct;23(5):561-70

[Ziegler1985] Ziegler J F, Biersack J P, Littmark U “The Stopping and Range of Ions in Solids” Vol. 1, Pergamon Press, 1985

[Ziegler2008] Ziegler J F, Biersack J P, Ziegler M D “SRIM – The Stopping and Range of Ions in Matter” SRIM Co., 2008

Glossary

C3H wildtype mouse	Melatonin-proficient, inbred mouse strain
Circadian clock (endogenous clock)	Specific cells located in a certain part of the brain (suprachiasmatic nuclei), which are entrained to a 24h daily cycle by light entering the eyes. These cells function as the master clock which orchestrates the daily rhythm in all peripheral clocks, located in almost all other tissues. In the absence of an external zeitgeber, the master clock retains the synchronization of all peripheral tissues to a circadian rhythm.
Circadian molecular clock	A translational/transcriptional feedback loop, which is present at cellular level and causes single cells to follow a circadian rhythm. This loop regulates the expression and synthesis of core clock genes and proteins. One loop takes about 24h to complete.
c-myc	A regulator gene, which controls the expression of other genes.
c-myc/TGF-α mouse model	Double-transgenic mouse model, in which the transgenes c-myc and TGF-α are co-expressed. Via these transgenes, hepato-cellular carcinoma can be induced in these mice.
Hepatocellular carcinoma (HCC)	Type of liver cancer
Neoplasm	Tumor
Organotypic explant culture (OEC)	Tissue culture of an organ that has been cut into small, irregular-shaped pieces.
Organotypic healthy liver slice culture (OHLSC)	Tissue culture of the healthy part of the liver from c-myc/TGF-α mice.
Organotypic liver slice culture (OLSC)	Liver tissue culture of a defined thickness, in this thesis from C3H-wildtype mice.
Organotypic neoplastic liver slice culture (ONLSC)	Tissue culture of the neoplastic part of the liver from c-myc/TGF-α mice.

Organotypic pancreas explant culture (OPEC)	Pancreas tissue culture of C3H-wildtype mice.
Organotypic slice culture (OSC)	Tissue culture of an organ of a defined thickness.
Organotypic transgenic pancreas explant culture (OTPEC)	Pancreas tissue culture of c-myc/TGF-α mice.
Per2	Clock gene, important part of the molecular endogenous clock.
$Per2^{luc}$ mouse model	Transgenic mice, in which the expression of luciferase is linked to the *Per2* promoter.
Promoter	A part of DNA located close to a gene, which initiates the transcription of that gene.
Transcription	The process of copying a certain DNA segment into RNA for future protein synthesis.
Transforming growth factor α (TGF-α)	Gene, whose expression is upregulated in certain human cancer types.
Transgene	A gene which has been transferred from one organism to another.
Translation	Protein synthesis
Zeitgeber	External stimulus (usually light), which sets the endogenous clock.

List of Abbreviations

ANOVA	Analysis of variance
BrdU	5-bromo-2-deoxyuridine
Cas3	Caspase3
CCG	Clock controlled genes
DMEM	Dulbecco's Modified Eagle Medium
DNA	Deoxyribonucleic acid
DSB	Double-strand break
FIAS	Frankfurt Insitute for Advanced Studies
GSI	Helmholtzzentrum für Schwerionenforschung GmbH
HBSS	Hank's Balanced Salt Solution
HCC	Hepatocellular carcinoma
HE	Hematoxylin and eosin
LET	Linear energy transfer
OEC	Organotypic explant culture
OHLSC	Organotypic healthy liver slice culture
OLSC	Organotypic liver slice culture
ONLSC	Organotypic neoplastic liver slice culture
OPEC	Organotypic pancreas explant culture
OSC	Organotypic slice culture
OTPEC	Organotypic transgenic pancreas explant culture
PBS	Phosphate buffered saline
PFA	Paraformaldehyde
PMMA	Polymethyl methacrylate

SCN	Suprachiasmatic nuclei
SIS	Schwerionen Synchrotron (heavy ion synchrotron at GSI)
SOBP	Spread-out Bragg peak
TGF-α	Transforming growth factor α
UNILAC	Universal linear accelerator, linear accelerator at GSI